Universität Potsdam
Institut für Erd- und Umweltwissenschaften
und
Helmholtz-Zentrum Potsdam
Deutsches GeoForschungsZentrum GFZ
Sektion 5.2 - Klimadynamik und Landschaftsentwicklung

Holocene climate and environmental variability in NE Germany inferred from annually laminated lake sediments

Kumulative Dissertation

zur Erlangung des akademischen Grades
"doctor rerum naturalium" (Dr. rer. nat.)
in der Wissenschaftsdisziplin Geologie/ Paläoklimatologie

eingereicht in der
Mathematisch-Naturwissenschaftlichen Fakultät
der Universität Potsdam

von

Nadine Dräger

Potsdam, 22. Juni 2016

Published online at the
Institutional Repository of the University of Potsdam:
URN urn:nbn:de:kobv:517-opus4-103037
http://nbn-resolving.de/urn:nbn:de:kobv:517-opus4-103037

Erklärung

Hiermit erkläre ich gemäß §12 Abs. 1 Nr. 7 der Promotionsordnung der Mathematisch-Naturwissenschaftlichen Fakultät der Universität Potsdam, dass ich die von mir vorgelegte Dissertation mit dem Titel

„Holocene climate and environmental variability in NE Germany inferred from annually laminated lake sediments"

selbständig angefertigt, benutzte Quellen und Hilfsmittel vollständig angegeben und wörtliche und sinngemäße Zitate als solche gekennzeichnet habe sowie Tabellen, Karten und Abbildungen, die anderen Werken in Wortlaut oder dem Sinn nach entnommen sind, in jedem Einzelfall als Entlehnung kenntlich gemacht habe. Diese Dissertation wurde noch keiner anderen Fakultät oder Hochschule zur Prüfung vorgelegt und ist, abgesehen von unten angegebenen Teilpublikationen, noch nicht veröffentlicht worden. Ich erkläre, dass ich solche Veröffentlichung vor Abschluss des Promotionsverfahrens nicht vornehmen werde. Die Bestimmungen der Promotionsordnung sind mir bekannt.

Teilveröffentlichungen:

- Dräger, N., Brauer, A., Theuerkauf M., Szeroczyńska, K., Wulf, S., Tjallingii, R., Plessen, B., Kienel, U., Lorenz, S., submitted: **Varve micro-facies and varve preservation record of climate change and human impact for the last 6000 years at Lake Tiefer See (NE Germany).** *The Holocene, in Review*
- Wulf, S., Dräger, N., Ott, F., Serb, J., Appelt, O., Guðmundsdóttir, E., van den Boogard, C., Słowiński, M., Błaszkiewicz, M., Brauer, A., 2016: **Holocene tephrostratigraphy of varved sediment records from Lakes Tiefer See (NE Germany) and Czechowskie (N Poland).** *Quaternary Science Reviews 132*: 1-14
- Dräger, N., Plessen, B., Kienel, U., Groß-Schmölders, M., Ramisch, A., Brauer, A., submitted: **Varying controls on δ^{13}C of sedimentary organic matter in the partially varved sediment record of Lake Tiefer See (NE Germany) over the last 6000 years.** *Quaternary Science Reviews, submitted*
- Dräger, N., Brauer, A., Brademann, B., Tjallingii, R., Słowiński, M., Błaszkiewicz, M., Schlaak, N., 2016: **Spontaneous self-combustion of organic-rich lateglacial lake sediments after freeze-drying** *Journal of Paleolimnology 55*: 185-194

Ort, Datum, Unterschrift (Nadine Dräger)

Abstract

Understanding the role of natural climate variability under the pressure of human-induced changes of climate and landscapes, is crucial to improve future projections and adaption strategies. This doctoral thesis aims to reconstruct Holocene climate and environmental changes in NE Germany based on annually laminated lake sediments. The work contributes to the ICLEA project (Integrated CLimate and Landscape Evolution Analyses). ICLEA intends to compare multiple high-resolution proxy records with independent chronologies from the N central European lowlands, in order to disentangle the impact of climate change and human land use on landscape development during the Lateglacial and Holocene. In this respect, two study sites in NE Germany are investigated in this doctoral project, Lake Tiefer See and palaeolake Wukenfurche. While both sediment records are studied with a combination of high-resolution sediment microfacies and geochemical analyses (*e.g.* μ-XRF, carbon geochemistry and stable isotopes), detailed proxy understanding mainly focused on the continuous 7.7 m long sediment core from Lake Tiefer See covering the last ~6000 years. Three main objectives are pursued at Lake Tiefer See: (1) to perform a reliable and independent chronology, (2) to establish microfacies and geochemical proxies as indicators for climate and environmental changes, and (3) to trace the effects of climate variability and human activity on sediment deposition.

Addressing the first aim, a reliable chronology of Lake Tiefer See is compiled by using a multiple-dating concept. Varve counting and tephra findings form the chronological framework for the last ~6000 years. The good agreement with independent radiocarbon dates of terrestrial plant remains verifies the robustness of the age model. The resulting reliable and independent chronology of Lake Tiefer See and, additionally, the identification of nine tephras provide a valuable base for detailed comparison and synchronization of the Lake Tiefer See data set with other climate records.

The sediment profile of Lake Tiefer See exhibits striking alternations between well-varved and non-varved sediment intervals. The combination of microfacies, geochemical and microfossil (*i.e.* Cladocera and diatom) analyses indicates that these changes of varve preservation are caused by variations of lake circulation in Lake Tiefer See. An exception is the well-varved sediment deposited since AD 1924, which is mainly influenced by human-induced lake eutrophication. Well-varved intervals before the 20^{th} century are considered to reflect phases of reduced lake circulation and, consequently, stronger anoxic conditions. Instead, non-varved intervals indicate increased lake circulation in Lake Tiefer See, leading to more oxygenated conditions at the lake ground. Furthermore, lake circulation is not only influencing sediment deposition, but

also geochemical processes in the lake. As, for example, the proxy meaning of $\delta^{13}C_{OM}$ varies in time in response to changes of the oxygen regime in the lake hypolinion. During reduced lake circulation and stronger anoxic conditions $\delta^{13}C_{OM}$ is influenced by microbial carbon cycling. In contrast, organic matter degradation controls $\delta^{13}C_{OM}$ during phases of intensified lake circulation and more oxygenated conditions.

The varve preservation indicates an increasing trend of lake circulation at Lake Tiefer See after ~4000 cal a BP. This trend is superimposed by decadal to centennial scale variability of lake circulation intensity. Comparison to other records in Central Europe suggests that the long-term trend is probably related to gradual changes in Northern Hemisphere orbital forcing, which induced colder and windier conditions in Central Europe and, therefore, reinforced lake circulation. Decadal to centennial scale periods of increased lake circulation coincide with settlement phases at Lake Tiefer See, as inferred from pollen data of the same sediment record. Deforestation reduced the wind shelter of the lake, which probably increased the sensitivity of lake circulation to wind stress. However, results of this thesis also suggest that several of these phases of increased lake circulation are additionally reinforced by climate changes. A first indication is provided by the comparison to the Baltic Sea record, which shows striking correspondence between major non-varved intervals at Lake Tiefer See and bioturbated sediments in the Baltic Sea. Furthermore, a preliminary comparison to the ICLEA study site Lake Czechowskie (N central Poland) shows a coincidence of at least three phases of increased lake circulation in both lakes, which concur with periods of known climate changes (2.8 ka event, 'Migration Period' and 'Little Ice Age'). These results suggest an additional over-regional climate forcing also on short term increased of lake circulation in Lake Tiefer See.

In summary, the results of this thesis suggest that lake circulation at Lake Tiefer See is driven by a combination of long-term and short-term climate changes as well as of anthropogenic deforestation phases. Furthermore, the lake circulation drives geochemical cycles in the lake affecting the meaning of proxy data. Therefore, the work presented here expands the knowledge of climate and environmental variability in NE Germany. Furthermore, the integration of the Lake Tiefer See multi-proxy record in a regional comparison with another ICLEA side, Lake Czechowskie, enabled to better decipher climate changes and human impact on the lake system. These first results suggest a huge potential for further detailed regional comparisons to better understand palaeoclimate dynamics in N central Europe.

Zusammenfassung

Es ist von großer Bedeutung die natürliche Klimavariabilität unter dem Einfluss menschlich verursachter Klimaänderungen zu verstehen, um Zukunftsprognosen und Adaptionsstrategien zu verbessern. Die Hauptzielsetzung der vorliegenden Doktorarbeit ist die Rekonstruktion von Klima- und Umweltveränderungen während des Holozäns in NO Deutschland anhand von jährlich geschichteten Seesedimenten. Diese Arbeit ist ein Beitrag zum ICLEA Projekt (integrierte Klima- und Landschaftsentwicklungsanalyse). ICLEA strebt den Vergleich von mehreren hochaufgelösten Proxy-Archiven aus dem Nord-zentral europäischen Tiefland an, um Einflüsse von Mensch und Klima auf die Landschaftsentwicklung auseinander zu dividieren. Demnach werden in diesem Doktorprojekt zwei Gebiete untersucht: der Tiefe See und der verlandete See Wukenfurche. Während beide Sedimentarchive mit einer Kombination aus hochaufgelösten sedimentmikrofaziellen und geochemischen Methoden untersucht werden, konzentriert sich die detaillierte Untersuchung der Proxy-Bedeutung auf den kontinuierlichen 7,7 m langen Sedimentkern vom Tiefer See, der die letzten 6000 Jahre abdeckt. Drei Hauptziele werden am Tiefen See verfolgt: (1) das Erstellen einer robusten und unabhängigen Chronologie (2) das Etablieren von mikrofaziellen und geochemischen Proxies als Indikatoren für Klima- und Landschaftsveränderungen und (3) das Ableiten von Klimaveränderungen und menschlichem Einfluss auf die Sedimentablagerung.

Zum Erreichen des ersten Zieles wurde eine robuste Chronologie mit Hilfe eines multiplen Datierungsansatzes erstellt. Das Zusammenführen der Warvenzählung und Tephra-Funden bildet dabei das Gerüst für die Chronologie der letzten 6000 Jahre, deren Stabilität durch die gute Übereinstimmung mit unabhängigen Radiokarbondatierungen bestätigt wird. Diese robuste und unabhängige Chronologie und die zusätzlichen neun Tephra-Funde bieten die Basis für den detaillierten Vergleich und die Synchronisation des Tiefen See Datensatzes mit anderen Klimaarchiven.

Das Sedimentprofil vom Tiefen See zeigt markante Wechsel zwischen gut warvierten und nicht warvierten Sedimentabschnitten auf. Die kombinierte Untersuchung der Mikrofazies, der Geochemie und von Mikrofossilien (d.h. Cladoceren und Diatomeen) zeigte, dass diese Veränderungen der Warvenerhaltung auf Änderungen der Seezirkulation zurückzuführen sind. Ausgenommen ist der rezente warvierte Abschnitt ab AD 1924, der hauptsächlich durch menschlich verursachte Seeeutrophierung beeinflusst ist. Warvierte Abschnitte vor dem 20. Jahrhundert sind durch verringerte Seezirkulation und die damit verbundenen stärkeren anoxischen Bedingungen

im See hervorgerufen worden. Die Ablagerung von nicht warvierten Sedimenten weist auf stärkere Seezirkulation und sauerstoffreichere Bedingungen am Seegrund hin.

Die Seezirkulation beeinflusst zusätzlich zum Sedimentmuster auch geochemische Prozesse im See. Zum Beispiel verändert sich die Proxy-Bedeutung der stabilen Kohlenstoffisotope von organischem Material ($\delta^{13}C_{OM}$) in Reaktion auf das veränderte Sauerstoffregime. Während geringer Seezirkulation und stärkeren anoxischen Bedingungen werden stark negative $\delta^{13}C_{OM}$ Werte durch mikrobielle Aktivität hervorgerufen. Im Gegensatz verursachen Phasen mit verstärkter Seezirkulation positivere $\delta^{13}C_{OM}$ Werte, was vermutlich auf stärkeren Abbau von organischem Material im sauerstoffangereicherten Milieu am Seegrund zurückzuführen ist.

Die Warvenerhaltung zeigt einen ansteigenden Trend der Seezirkulation im Tiefen See nach ungefähr 4000 Jahre vor heute an. Dieser Trend ist überlagert mit kurzzeitigen Seezirkulationsveränderungen auf dekadischen Zeitskalen. Der Vergleich mit anderen Archiven in Zentral-Europa lässt darauf schließen, dass der Langzeittrend wahrscheinlich auf graduelle Veränderungen der orbitalen Parameter zurückzuführen ist, was kühlere und windigere Bedingungen in Zentral-Europa hervorgerufen hatte und damit die Seezirkulation im Tiefen See verstärkt hat. Die kurzzeitigen Phasen von verstärkter Seezirkulation fallen mit Siedlungsperioden am Tiefen See zusammen, die mit Pollendaten vom selben Sedimentkern rekonstruiert wurden. Die Waldrodung verringerte den Windschutz des Sees, was möglicherweise zu einer erhöhten Sensitivität der Seezirkulation zu Windstress geführt hat. Ein erster Vergleich des Tiefen Sees zu dem ICLEA Untersuchungsgebiet des Czechowskie See zeigt, dass in beiden Seen drei gemeinsame Phasen verstärkter Seezirkulation auftreten, die auch mit bekannten Zeiten veränderter Klimabedingungen zusammenfallen (2.8 ka event, Migrationsperiode und die Kleine Eiszeit). Diese Ergebnisse zeigen, dass die Seezirkulation von einer Kombination aus Klimaveränderung auf langen und kurzen Zeitskalen und der Abholzung des Menschen angetrieben wird.

Zusammengefasst erweitert die hier vorliegende Arbeit das Wissen von Klima und Umweltveränderungen in NO Deutschland. Zudem wird gezeigt, dass ein regionaler Vergleich verschiedener Untersuchungsgebieten mit unabhängigen Chronologien ein verbessertes Auseinanderhalten von Klimaeinflüssen und menschlichen Einflüssen auf die Seesysteme ermöglicht. Damit kann er verbessertes Verständnis der Paläoklimadynamik in Zentral-Europa gewonnen werden.

Acknowledgements

My first thanks go to my supervisor Achim Brauer. Achim, you introduced me to the fascinating world of varved sediments about six years ago, when I carried out my first internship in science at the GFZ Potsdam. In all these years your deep knowledge and trust in my work inspired me to go on with science. I am very thank full for all your help and effort! Further deeply thanks go to my former and current office mates Sabine, Michał, Mateusz and Florian for providing a pleasant work space. You were always open for urgent discussions. Thank you all for that! Furthermore, I would like to thank two external reviewers for evaluating my thesis.

Many thanks go to all scientists involved in the ICLEA project. The meetings and workshops and constant exchange of knowledge improved the developing of ideas. I especially thank Mirosław Błaszkiewicz, Markus Schwab, Theresa Blume, Martin Wilmking, Reinhard Lampe, Martin Theuerkauf, Sebastian Lorenz, Ulrike Kienel, Thomas Hübener, Allan Buras, Ingo Heidbüchel, and Izabela Zawiska, Milena Obremska, Monika Lutynska and Elisabeth Dietze for all the fruitfull discussions.

Furthermore, my thanks go to everybody from GFZ Section 5.2 for all the support, discussions and inspiration. I would like to thank Christine Gerschke for the help in all administrative issues, Andreas Hendrich for helping with figure design and Matthias Köppl for helping with computer issues. Thanks to the lab team Gaby Arnold, Dieter Berger and Brian Brademann who prepared hundreds of thin sections and Birgit Plessen, Sylvia Pinkerneil and Petra Meier for the patients and analyzing thousands of samples for this thesis. Thank you all for the warm working atmosphere.

Finally, a big thank you goes to Janina, David and my family who supported me in all situations during the past years, especially at the end!

Table of Contents

List of Figures

List of Tables

1 Introduction

1.1 Varved lake sediments as palaeoclimate archives – benefits and challenges

The future of the Earth's climate system is one of the greatest problems faced by society today. The Earth has entered a new mode, the 'Anthropocene', distinguished by a superposition of anthropogenic forcing and natural climate variability, which has the potential to trigger global changes beyond the Holocene and even Quaternary baseline (Waters et al., 2016). Predicting the future of the Earth's climate and the consequences for landscape development, however, is complex and controversial, because of both the spatially and temporally multi-scale character and complexity of interactions of the different forcing mechanisms. In particular, the role of natural climate variability induced by, for example, solar activity, volcanic eruptions and orbital forcing on future climate development is still an uncertain variable (Masson-Delmotte et al., 2013). Geological archives provide climatic information before the instrumental record, especially annually laminated archives, such as ice-cores (*e.g.* Dansgaard et al., 1993; Johnson et al., 1992; Rasmussen et al., 2006), tree-rings (*e.g.* Briffa et al., 1990; Büntgen et al., 2011; Luterbacher et al., 2016), and varved sediments (*e.g.* Brauer et al., 2008; Francus et al., 2002; O'Sullivan, 1983) give the advantage of studying both high and low frequency climate variability during the past.

Lake sediment archives are of particular significance, as the lake system itself and the corresponding catchment often react in multiple aspects on changing climate and environmental conditions (*i.e.* physically, chemically and biologically). Lake responses are commonly recorded in the deposited sediments, which can be read from the archive by obtaining proxy data. Annually laminated (varved) lake sediments provide these information in seasonal layers, revealing unprecedented details of the past climate and environmental characteristics. Furthermore, varved lake sediments offer a fundamental base for establishing robust and reliable chronologies and for determining duration and abruptness of, for example, rapid climate changes (Brauer et al., 2008; Martin-Puertas et al., 2012b). Reliable and independent chronologies represent a crucial point in palaeoclimate reconstruction, particularly to enable comparisons between different records and to detect regional lead and lags of changes (Brauer et al., 2014). In this respect, the combination of varve counting with other chronological methods (*e.g.* tephrochronology and radiocarbon dating) allows validating the varve chronologies and minimizing the internal errors. Finding tephras in varved records

might not only serve as an independent dating tool, but also give the potential for synchronizingindividual climate records regionally and even globally by age equivalence (*e.g.* Lane et al., 2013; Wulf et al., 2013).

Reconstructing climate and environmental conditions from varved lake sediments is, however, quite challenging, as the processes which influence lacustrine proxies are usually not straightforward because of two main reasons. Firstly, proxies are mostly influenced by several processes, which are often difficult to unravel (Batterbee et al., 2012). A classical example for this is the long debated issue about disentangling climate and human influences on lake sediment archives (Dearing, 2006). Since the establishment of first agricultural societies in Europe in the mid Holocene (~6000 cal. a BP), humans have substantially altered the landscape (Behre, 1988; Kaplan et al., 2009). Successive cycles of deforestation, abandonment, and afforestation caused variations of, for example, the sediment influx, the lake biota and the lake productivity (*e.g.* Dreibrodt and Wiethold, 2015; Feeser et al., 2016). These processes induced by human impact overlap and interact with climate forcing on the lake system during the past ~6000 years and challenge to extract the importance of climate change out of the sedimentary record. Palaeoclimate studies commonly address the challenge of disentangling different controlling factors on the proxies by applying multi-proxy approaches. These commonly include concurrent analyses of, for example, sediment facies, mineralogy, stable isotope and bulk geochemistry and microfossils (*e.g.* pollen, diatoms, Cladocera, chironomids) (Birks and Birks, 2006; Koutsodendris et al., 2015; Striewski et al., 2009). In particular, pollen analysis potentially allows to identify deforestation phases associated with human settlement periods in the catchment of the lake, which often serves as a base for disentangling climate and human impact on the lake ecosystem (Gaillard et al., 2008; Kalis et al., 2003). A further tool to disentangle the more local changes (*i.e.* human impact) from climate changes on lakes is based on a regional integration of several proxy records. While local changes may only be recorded in individual records, over-regional climatic changes should be traceable as a common signal in all integrated records (Olsen et al., 2013). These high resolution comparisons not only allow to disentangle climate and human impact on lake system, but might also provide very valuable information about different regional manifestations of climate change resulting from, for example, the location with respect to oceanic and climate influences, the geological setting and vegetation development (Lane et al., 2013; Olsen et al., 2013).

The second challenge is related to stationarity of proxy interpretations through time. In contrast to the problem of disentangling human and climate impact, proxy

stationarity is not strongly investigated, because of its difficulties in testing. Only a few studies showed the impact of changing lake and/or climate conditions on the proxy sensitivity through time by utilising multi-proxy approaches (Martin-Puertas et al., 2012a; Amann et al., 2014). However, the proxy stationarity is an important issue in palaeoclimate reconstructions and needs to be more sufficiently discussed in lake sediment studies.

1.2 The ICLEA project – Integrated CLimate and Landscape Evolution Analyses

The ICLEA project (Virtual Institute of the Helmholtz Association) presents a novel concept of bridging time-scales and mainly addresses the challenges of palaeoclimate reconstructions as stated above. ICLEA is funded by the Helmholtz Association and concentrates expertises from the Helmholtz Center Potsdam GFZ German Research Center for Geosciences, Ernst Moritz Arndt University Greifswald, the Brandenburg University of Technology Cottbus-Senftenberg and the Polish Academy of Sciences (PAN). The long-term mission of ICLEA is to provide a substantiated data base for sustainable environmental management based on a profound process understanding at all relevant time scales (www.iclea.de). In particular, the objectives of ICLEA are:

A) To integrate instrumental monitoring data, remote sensing information and model-understanding with proxy data analyses for a comprehensive understanding of landscape evolution processes at all relevant time scales in the N central European lowlands.

B) To elucidate the impact and interaction of different landscape forming processes (*i.e.* climate and land use) from natural environmental archives (lake sediments, tree rings, soil chronosequences) at an unprecedented level of detail and temporal accuracy.

C) To establish a synchronised regional chronology for the time interval since the last glaciation (Holocene and Lateglacial) for combining the investigated natural archives (lakes, trees, soil) through multiple dating approaches.

D) To provide data on natural background variability of climate and landscape evolution with quantified precision.

E) To set up a database with the best data available for assessing thresholds and tipping points, as well as establishing more realistic model scenarios for future landscape developments.

Work in ICLEA focuses on two regions in the N central European lowlands, NE Germany and N central Poland, which are both formed by late Quaternary glaciations and, thus, allow to trace landscape development since the retreat of glaciers at the end of the last ice age. Moreover, this area is characterized by a rather low annual precipitation, implying high susceptibility to hydrological changes in the landscape (Landesamt für Umwelt, 2000; Germer et al., 2011). The highly-resolved palaeoclimate reconstructions using annually laminated lake records focus on multiple sides in the ICLEA study region: (1) Lake Tiefer See and palaeolake Wukenfurche in NE Germany and (2) Lakes Czechowskie, Glebocek, Jelonek and palaeolake Trzechwoskie in N central Poland Figure 1.1. All of these lakes are located in the terminal moraine of the Pomeranian ice advance and are hence situated in an identical geomorphological location, but on a continental gradient (Kienel et al., 2013; Błaszkiewicz et al., 2015). The main ICLEA's input is the comparison of the profiles of Lake Tiefer See and Lake Czechowskie, as both lakes are also equipped with an onside monitoring concept. Improved regional comparison of both varved lake sediment archives is achieved by following identical analytical protocols, establishing robust and independent chronologies and searching for common cryptotephras. These prerequisites allow to understand the records and the sensitivity of proxy data of each record and, in a second step, to integrate both archives in a regional comparison.

This doctoral project deals with the analysis of sediment records from the NE German sides Lake Tiefer See and palaeolake Wukenfurche.

Figure 1.1: Geographic overview map of the northern central European low lands with the location of the lakes, which are main subject of the ICLEA project, with main focus on Lake Tiefer See and Lake Czechowskie.

1.3 Study sites

Lake Tiefer See (N 53° 35.5', E 12° 31.8') is located in the Mecklenburg lake district, NE Germany, ~20 km northwest of the town Waren Müritz (Mecklenburg Vorpommern) at an elevation of 62 m asl. The lake was formed during the last glaciation and is part of the Klocksin Lake Chain, which is a subglacial channel system that crosses the Pomeranian terminal moraine. The surface area of the north-south oriented and oval shaped lake amounts to 0.75 km^2. The maximum depth corresponds to 62 m. Monitoring at the lake showed that the lake is mesotroph and, depending on the existence of a winter ice cover either mono- or dimictic (Kienel et al., 2013). The catchment area of approximately 5.5 km^2 is dominated by glacial till of the Pomeranian terminal moraine (Kienel et al., 2013; Landesamt für Umwelt, 2000).

Palaeolake Wukenfurche (N 52° 46.6', E 13° 5.8') is located ~20 km northeast of Berlin and south of the Pomeranian terminal moraine of the Weichselian glaciation at an elevation of 61 m asl. The palaeolake is part of the Eberswalde ice-marginal valley system. While the northern part of the 1.1 km long SW-NE oriented and narrow valley (~100 m wide) is still water filled (lake Kleiner Wuken-see; 5 m maximum water depth), the southern part was filled up by sediments during the Holocene and is a swampy area today (Schlaak, 1993).

1.4 Scientific objectives of the doctoral project

This doctorate thesis aims to assess climate and environmental variability in NE Germany from annually laminated lake sediments. In order to achieve this goal, three main objectives were pursued in this doctorate project :

I.) Conducting high resolution sediment microfacies and geochemical analyses of Tiefer See and Wukenfurche sediment cores.

II.) Performing a reliable chronology for the Tiefer See sediment record using different independent methods: varve counting, tephrochronology and radiocarbon dating.

III.) Establishing microfacies and geochemical proxies as indicators for climate and environmental changes at Tiefer See.

IV.) Tracing the effects of climate variability and human activity on sediment deposition at Tiefer See.

1.5 Material and Methods

Sediment cores

Between 2011 and 2013 seven parallel long sediment cores and two surface sediment cores were retrieved from the deepest of Lake Tiefer See at a maximum distance of 10 m. Additionally, several surface cores were recovered from shallower water depths. All cores were split, photographed and described in the lab. A composite profile was constructed from the cores at the deepest location by correlating distinct and macroscopically visible 'marker' layers. However, correlation between the overlapping sediment cores indicated two sediment gaps at 7.7 m and 9.57 m depth, which were caused by sediment loss due to the expansion of the sediments during core recovery. Due to these coring gaps, detailed sediment analyses in this thesis focused on the uppermost 7.7 m continuous interval of the Lake Tiefer See sediment record covering the past ~6000 years.

Two parallel sediment cores were recovered in July 2014 from the presently swampy area of Palaeolake Wukenfurche within a distance of 0.5 m. As the sediment cores from Lake Tiefer See, the cores from palaeolake Wukenfurche were split, imaged and described in the lab. The correlation of distinct macroscopically visible 'marker layers' in both sediment cores allowed to compile a continuous composite profile. Detailed analysis focused on the ~3 m thick finely laminated interval located in the basal part of the sediment profile (14.3–11.35 m sediment depth). The investigation of palaeolake Wukenfurche samples turned out to be difficult, as the sediment self-combusted after freeze-drying releasing heat of more than 350°C.

Lake Tiefer See monitoring

The modern lake deposition is trapped since 2012 at three water depths; at bi-weekly resolution at 45 m water depth and at monthly resolution at 12 m and 5 m water depth. The weather (air temperature, precipitation, wind speed and direction, relative humidity) and lake conditions (water temperature, pH, electrical conductivity, dissolved oxygen, chlorophyll, turbidity, redox potential) are monitored on a floating platform in 10 min and 12 h intervals, respectively. The chemical properties of the lake catchment was determined at the beginning of the monitoring study by sampling the top soil, reed and plant litter.

Chronology

The chronology in the upper 7.7 m continuous sediment interval of the Lake Tiefer See sediment core was established by integrating age information from varve counting, tephrochronology and radiocarbon dating. Varve counting was conducted in petrographic thin sections in well- and poorly-varved intervals at seasonal resolution. In non-varved sections the chronology is based on sedimentation rate estimates. For the establishment of the tephrostratigraphy the entire profile of Lake Tiefer See was scanned for glass shard remains. Identified glass shards were analysed for major element composition to relate the tephras to the corresponding volcanic eruptions. Furthermore, 13 radiocarbon dates from terrestrial plant remains were used to establishment an independent radiocarbon chronology of the sediment profile.

Microfacies analysis

High resolution microfacies analysis was conducted on the sediment records of Lake Tiefer See and palaeolake Wukenfurche by microscopy of petrographic thin section. Given the varved nature of the sediment, this approach in combination with high-resolution μ-XRF core scanning facilitates the geochemical fingerprinting of sub-laminae and interpreting them in terms of seasonal sedimentation processes. The preparation of thin sections followed the standard procedure described in Brauer and Casanova (2001) including shock-freezing of the sediment blocks with liquid nitrogen, freeze-drying and impregnation with epoxy resin.

Geochemical analysis

Geochemical analyses of Lake Tiefer See and Palaeolake Wukenfurche sediments comprised different methodologies. μ-XRF element scanning was conducted directly on the split core surfaces continuously at 100 μm resolution with an ITRAX spectrometer. Geochemical analyses of bulk samples included total inorganic carbon, total organic carbon and total nitrogen contents. At Lake Tiefer See also the stable carbon isotopes of organic matter and stable nitrogen isotopes were measured of the bulk samples. At palaeolake Wukenfurche selected samples were analysed for the total sulphur content and for mineralogical composition. Furthermore, individual sediment components, such as diatoms, calcite, Ca-rhodochrosite and siderite, were additionally prepared and analysed with an electron microprobe and a scanning electron microscope.

Further methods applied for the Lake Tiefer See record, which were not conducted by the doctorate student, but which contributed to the interpretation of results in this

project included the analyses of pollen assemblage and reconstruction of vegetation openness (conducted by Dr. Martin Theuerkauf, University of Greifswald) and Cladocera analyses (conducted by Prof. Dr. Krystyna Szerosyńska, PAN Warsaw).

1.6 Thesis structure

This thesis is organized as a cumulative thesis consisting of six chapters and an appendix. This introduction part (Chapter 1) is followed by four chapters, which are based on four manuscripts (Chapters 2 to 5). The doctoral candidate is the leading author of three of the four manuscripts. Two manuscripts (Chapter 3 and Chapter 5) have been published and the other two are under review (Chapter 2 and Chapter 4). In the last chapter (Chapter 6 Synthesis) the results are summarized and discussed with respect to the aims of this doctorate project as well as to the overall objectives within the ICLEA project. The following section provides a summary of the four central manuscripts and the contribution of the doctoral candidate to these publications.

Manuscript # 1 (Chapter 2)

Title: Varve micro-facies and varve preservation record of climate change and human impact for the last 6000 years at Lake Tiefer See (NE Germany)

Authors: Nadine Dräger, Martin Theuerkauf, Krystyna Szeroczyńcka, Sabine Wulf, Rik Tjallingii, Birgit Plessen, Ulrike Kienel, Achim Brauer

Submitted to *The Holocene*, currently under review

This manuscript presents the chronology of the Lake Tiefer See sediment archive during the past ~6000 years and discusses the origin of sediment variability. The sediment record exhibits striking variations of varve preservation, which is related to changes in lake circulation. This study showed that changes of lake circulation at Lake Tiefer See are the result of a complex interaction of long-term and short-term climate changes and deforestation phases during human settlement periods.

The doctoral candidate was the leading author of this manuscript and contributed ~80% to this paper. She was attending the coring campaign, opened the sediment cores, compiled the composite profile, described the lithology, compiled the age model (varve counting, radiocarbon modelling and partly tephrochronology), conducted microfacies and geochemical analysis, evaluated all data and wrote the manuscript. M. Theuerkauf conducted pollen analysis and reconstructions, K. Szeroczyńcka performed Cladocera analysis, S. Wulf run tephrochronological analysis, R. Tjallingii was in charge of μ-XRF measurements. B. Plessen was in charge for bulk geochemical

analysis. All other co-authors act as principle investigator of the Lake Tiefer See sediment record and as such contributed through proof-reading and discussion to this manuscript, especially A. Brauer and M. Theuerkauf.

Manuscript # 2 (Chapter 3)

Title: Holocene tephrostratigraphy of varved sediment records from Lakes Tiefer See (NE Germany) and Czechowskie (N Poland)

Authors: Sabine Wulf, Nadine Dräger, Florian Ott, Johanna Serb, Oona Appelt, Esther Guðmundsdóttir, Christel van den Bogaard, Michał Słowiński, Mirosław Błaszkiewicz, Achim Brauer

Published in *Quaternary Science Reviews* 132: 1-14, 2016

This paper presents tephrochronologial results of the sediment records from Lakes Tiefer See Czechowskie covering the Holocene. In total thirteen tephras and cryptotephras were detected and chemically fingerprinted. These findings form the basis for absolute and independent dating of these sediments and for synchronization with other high-resolution archives in central and northern Europe. Three cryptotephras were identified in both records and thus give potential for high-resolution comparison of the proxy records.

The overall contribution of the doctorate student to this manuscript was ~50%. As fundamental contribution the doctoral candidate provided the varve and radiocarbon chronology, without which the study would not have been possible. Furthermore, she was involved in sediment sampling, separation of glass shards and sample preparation as well as identified the Saksunarvatn and Askja AD1875 tephra. The doctoral candidate further contributed to the writing of sections '2. Study area' and '3.1. Sediments and developing chronology', constructed Figure 2 and contributed through proof-reading and discussion to this manuscript.

Manuscript # 3 (Chapter 4)

Title: Varying control on $\delta^{13}C$ of sedimentary organic matter in the partially varved sediment record of Lake Tiefer See (NE Germany) over the last 6000 years

Authors: Nadine Dräger, Birgit Plessen, Miriam Groß-Schmölders, Ulrike Kienel, Arne Ramisch, Achim Brauer

Submitted to *Quaternary Science Reviews*

This manuscript examines the controlling factors of the stable carbon isotopes of sedimentary organic matter ($\delta^{13}C_{OM}$) in Lake Tiefer See sediments. The results indicate that the controlling factors of the $\delta^{13}C_{OM}$ ratio vary in time in response to the prevailing

oxygen regime in the lake. In periods of more anoxic lake conditions microbial carbon cycling appears to be the controlling factor of $\delta^{13}C_{OM}$. In contrast, during more oxygenated bottom water conditions the selective organic matter degradation becomes the most important for the $\delta^{13}C_{OM}$ ratios.

The doctoral candidate was the leading author and contributed ~80% to this paper. She described the lithology, compiled the age model, conducted microfacies, prepared samples for geochemical measurements and evaluated all data and wrote the manuscript. B. Plessen was in charge for geochemical measurements, U. Kienel was in charge instrumental monitoring at Lake Tiefer See, M. Groß-Schmölders analysed the surface sediment cores, A. Ramisch performed statistical calculations. All co-authors contributed through proof-reading and discussion to this manuscript, especially A. Brauer.

Manuscript # 4 (Chapter 5)

Title: Spontaneous self-combustion of organic-rich lateglacial lake sediments after freeze-drying

Authors: Nadine Dräger, Achim Brauer, Brian Brademann, Rik Tjallingii, Michał Słowiński, Mirosław Błaszkiewicz, Norbert Schlaak

Published in *Journal of Paleolimnology* 55: 185-194, 2016

This paper reports and investigates for the first time spontaneous self-combustion of freeze-dried lacustrine sediment samples immediately after ventilation of the vacuum freeze drier chamber. These sediment samples originate from the palaeolake Wukenfurche. The smouldering combustion exceeded temperatures of 350°C. Our findings suggest that the heating was induced by oxidation reactions in the sediment.

The doctoral student was the leading author of this manuscript and contributed ~80% to this paper. She was organizing the coring campaign, opened the sediment cores, compiled the composite profile, described the lithology, evaluated all data and wrote the manuscript. B. Brademann conducted the movie of self-combustion and heat images. R. Tjallingii was in charge of continuous μ-XRF measurements. All other co-authors act as principle investigator of the palaeolake Wukenfurche sediment record and as such contributed through proof-reading and discussion to this manuscript, especially A. Brauer.

2 Varve preservation and varve microfacies record of climate change and human impact for the last 6000 years at Lake Tiefer See (NE Germany)

Nadine Dräger[a,*], Martin Theuerkauf[b], Krystyna Szeroczyńska[c], Sabine Wulf[a,d], Rik Tjallingii[a], Birgit Plessen[a], Ulrike Kienel[a,b] Achim Brauer[a]

[a] GFZ German Research Centre for Geosciences, Section 5.2 Climate Dynamics and Landscape Evolution, Telegrafenberg C, D-14473 Potsdam, Germany

[b] Institute for Geography and Geology, Ernst-Moritz-Arndt University Greifswald, Friedrich-Ludwig-Jahn-Str. 16, D-17487 Greifswald, Germany

[c] Polish Academy of Sciences, Institute of Geological Sciences, Research Centre Warsaw, Twarda 51/55, Warszawa 00-818, Poland

[d] Senckenberg Research Institute and Natural History Museum, BIK-F, TSP6 Evolution and Climate, Senckenberganlage 25, D-60325 Frankfurt a.M., Germany

[*] Corresponding author

Abstract

The Holocene sediment record of Lake Tiefer See exhibits striking alternations between well-varved and non-varved intervals. Here we present a high resolution multi-proxy record for the past ~6000 years and discuss possible causes for the observed sediment variability. This approach comprises of microfacies, geochemical and microfossil ana-lyses as well as of a multiple dating concept including varve counting, tephrochrono-logy and radiocarbon dating. Four periods of predominantly well-varved sediment were identified at 6000–3950 cal. a BP, 3100–2850 cal. a BP, 2100–750 cal. a BP and AD 1924–present. Except of sub-recent varve formation, these periods are considered to reflect reduced lake circulation and consequently, stronger anoxic bottom water conditions. In contrast, intercalated intervals of poor varve preservation or even extensively mixed non-varved sediments indicate strengthened lake circulation. Sub-recent varve formation since AD 1924 is, in addition to natural forcing, influenced by enhanced lake productivity due to modern anthropogenic eutrophication. The general increase in periods of intensified lake circulation in Lake Tiefer See since ~4000 cal. a BP presumably is caused by gradual changes in Northern Hemisphere orbital forcing, leading to cooler and windier conditions in Central Europe. Superimposed decadal to centennial scale variability of the lake circulation regime likely is the

result of additional human-induced changes of the catchment vegetation. The coincidence of major non-varved periods at Lake Tiefer See and intervals of bioturbated sediments in the Baltic Sea implies a broader regional significance of our findings.

Keywords

Varve chronology – Microfacies – Lake circulation – Human impact – Climate change

2.1 Introduction

Annually laminated (varved) lake sediments represent unique archives, providing precise chronologies and seasonally resolved proxy data (*e.g.* Bonk et al., 2015; Brauer et al., 1999; Czymzik et al., 2016; Martin-Puertas et al., 2012b; Neugebauer et al., 2012; Zahrer et al., 2013; Zolitschka et al., 2015). Low-energy hypoxic to anoxic bottom water conditions favour deposition and preservation of varved sediments, as bottom water anoxia prevents life of burrowing organisms and minimizes post-depositional disturbances (Brauer, 2004; Tylmann et al., 2012; Zolitschka et al., 2015). Such conditions are mainly a function of lake stratification, mixing and productivity.

In northern Germany, the preservation of varves in lakes has primary been reported for the last century and ascribed to human-induced lake eutrophication (Kienel et al., 2013; Lüder et al., 2006; Neumann et al., 2002; Zahrer et al., 2013). This can be explained by nutrient enrichment, causing increased organic matter flux to the bottom waters and the formation of anoxic conditions (Carpenter, 2005; Jenny et al., 2016). Long varved lake sediment records in northern Germany, like lakes Woseriner See (Czymzik et al., 2016; Feeser et al., 2016) and Belauer See (Dörfler et al., 2012; Dreibrodt and Wiethold, 2015), are rare and none of these are continuously varved for the entire Holocene. As human eutrophication can be excluded for preservation of pre-industrial varved intervals, other factors must have triggered varve preservation before the 20^{th} century.

Surface sediments from Lake Tiefer See in the Mecklenburg lake district of NE Germany, show that varve formation initiated ~100 years ago, which likewise has been related to human eutrophication (Czymzik et al., 2015; Kienel et al., 2013; Theuerkauf et al., 2015). Here we study the sedimentary record of Lake Tiefer See for periods of natural varve preservation from mid to late Holocene, in order to evaluate possible trigger mechanisms. Furthermore, this study tests whether shifts between well-varved and non-varved intervals can be used as indicators of environmental and climate vari-

ations, as previously applied in marine sediment records (Behl and Kennett, 1995; Zillén et al., 2008). For this purpose, a multi-proxy study was combined with a multiple da-ting approach for the Lake Tiefer See sediment profile spanning the past ~6000 years. In particular, we aim to (1) establish a robust chronology based on varve counting, tephrochronology and radiocarbon dating, (2) characterize intervals of different varve formation and preservation, and (3) discuss the application of varve preservation at Lake Tiefer See as a proxy for lake circulation.

2.2 Study site

Lake Tiefer See (Figure 2.1; 53° 35.5' N, 12° 31.8' E; 62 m a.s.l) is located ~20 km NW of the town Waren (Müritz lake district, Mecklenburg Vorpommern) and is part of the Klocksin Lake Chain, a subglacial channel system that crosses the Pomeranian terminal moraine, formed during the last glacial period. The lake has a surface area of ~0.75 km^2 and a maximum depth of 62 m. The catchment area (~5.5 km^2) is dominated by glacial till of the Pomeranian terminal moraine (Kienel et al., 2013; Landesamt für Umwelt, 2000) and is mainly used for agriculture. Lake Tiefer See is mesotrophic and the circulation mode is either mono- or dimictic, depending on formation of a winter ice cover (Kienel et al., 2013; Nixdorf et al., 2004). The study site is characterized by a warm-temperate climate at the transition from oceanic to continental conditions. Mean monthly temperatures range from 0°C in January to 18°C in July. Mean monthly precipitation varies between 40 mm during winter to 60 mm in summer with a mean annual precipitation of 560 mm. The highest wind speed is between November and December, with an average of 6 m/s and maximum speeds of 23.1 m/s. The predominant wind direction is WSW (Meteorological data from DWD Station Schwerin AD 1890–2016; 80 km to the west of Lake Tiefer See). Generally, increased windiness in the southern Baltic region is related to cyclones from westerly directions during autumn and winter (Bierstedt et al., 2015a).

2.3 Material and Methods

2.3.1 Coring and sampling

Seven parallel sediment cores (Figure 2.1) were obtained in September 2011 (A, B, C) and March 2013 (D, E, F, G) from the deepest part of Lake Tiefer See, using a 90-mm UWITEC piston corer. Cores were split, photographed and described in the lab. A composite profile was constructed by correlating distinct and macroscopically visible

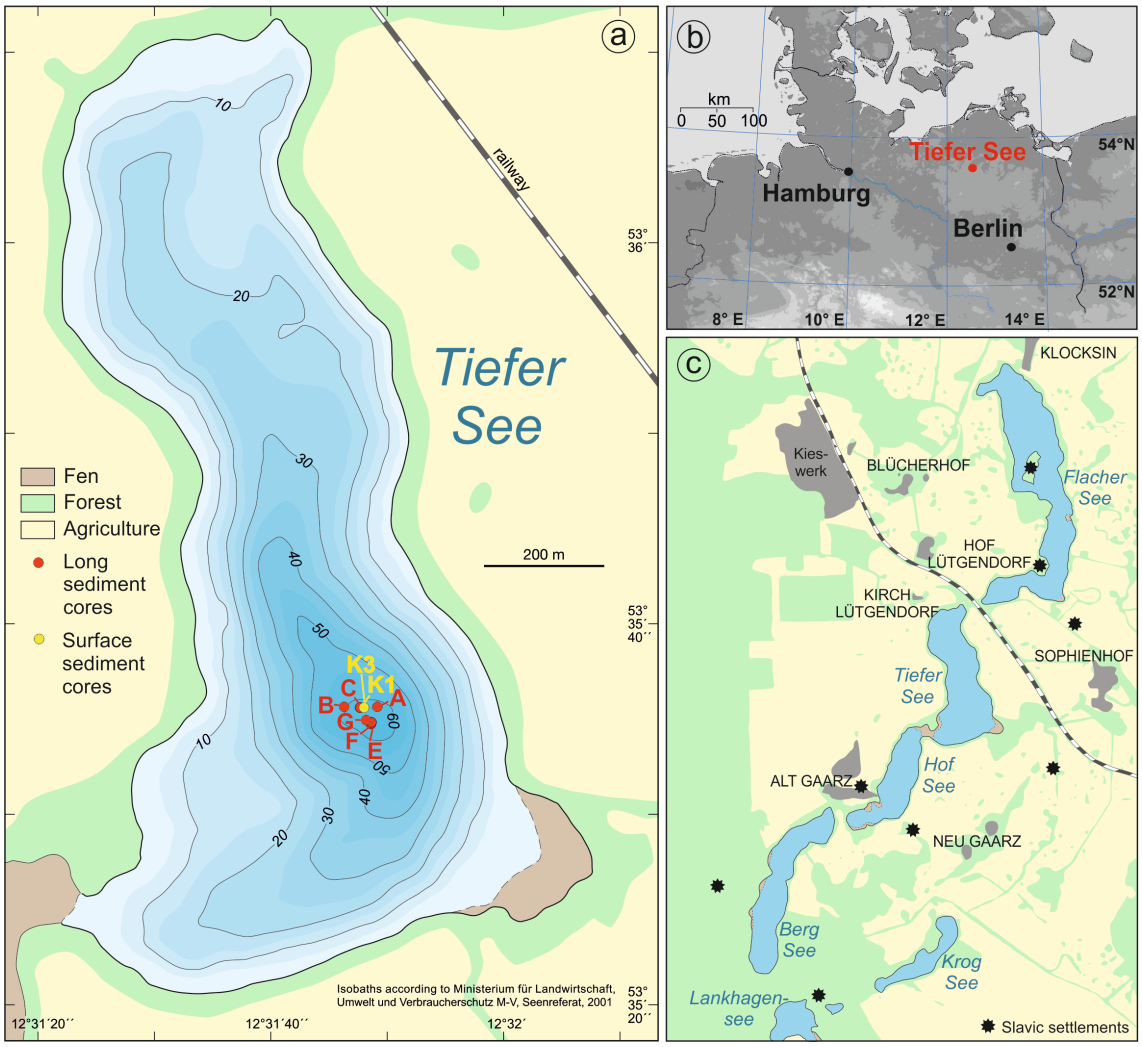

Figure 2.1: Bathymetric map (a) and location (b) of Lake Tiefer See in the Klocksin Lake Chain and land cover in the catchment area (c). Black stars show former Slavic settlements.

'marker' layers in all seven sediment cores. One half of the composite profile was used for non-destructive core scanning. The second half was subsampled for sedimentological, geochemical and microfossil analysis, and picked for plant macroremains for radiocarbon dating.

To prepare macroscopic thin sections, sediment bars with a size of 10 x 2 x 1 cm were cut out of the fresh sediment with 2 cm overlaps to enable continuous microfacies analysis. Thin sections were prepared according to a standard procedure including freeze-drying and impregnation with epoxy resin (Brauer and Casanova, 2001). Samples for geochemical, pollen and Cladocera analyses were obtained in continuous 1 cm increments, comprising 7 years per sample on average (2–6 years above 3.95 m; 4–24 years below 3.95 m depth).

2.3.2 Microfacies analysis

Detailed microfacies analysis was performed on the overlapping series of large-scale petrographic thin sections. Microscopic analysis included the investigation of sediment using a petrographic microscope with non-polarized and polarized light, at 50x to 400x magnifications (Carl Zeiss Axioplan). Microfacies analyses further involved the measurement and description of sub-layers in well- and poorly-varved sections and the identification of general sediment characteristics in non-varved intervals. Based on the microscopic inspection, for each varve a varve quality index (VQI) was assigned ranging from 4 (well-varved) to 0 (non-varved). This measure is an analogue to the Bioturbation Index (Behl and Kennett, 1995; Von Rad et al., 1999) and the Lamination Index (Deplazes et al., 2013) applied for marine sediment records. A VQI>1 represents undisturbed sediment with well identifiable varve sub-layers. A VQI between 0 and 1 indicates varves with indistinct sub-layer boundaries and no clear seasonal sub-layer succession. A VQI of 0 represents non-varved sediment.

Examples of specific microfacies were additionally analysed with a scanning electron microscope (SEM, Carl Zeiss SMT Ultra 55) and an electron microprobe (JEOL JXA-8230). For the latter, a slide of 100–150 μm thickness was prepared from a sediment bar (TSK11-A 3.37–3.47 m) parallel to the respective thin section, carbon coated and analysed for the elements Ca, Mn and Fe. Operating conditions used 15 kV voltage, a 10 nA beam current, 5 μm beam size and exposure times of 10 s for Ca and 20 s for Mn and Fe.

Table 2.1: AMS ^{14}C dates of macroscopic terrestrial plant remains from the composite profile of Lake Tiefer See. Conventional ^{14}C ages were calibrated with OxCal 4.2 (Bronk Ramsey, 2008, 2009) using the INTCAL13 calibration curve (Reimer et al., 2013).

Sample/lab code	Composite depth (m)	Dated material	AMS ^{14}C age (a BP $\pm 2\sigma$)	Calibrated age (cal. a BP $\pm 2\sigma$)
Poz-55878	1.24	leaf fragment	410 ± 25	424 ± 91
Poz-47656	1.89	leaf fragment	840 ± 30	789 ± 103
Poz-55879	2.14	bud scale	1045 ± 30	986 ± 65
Poz-47657	2.41	bud scale	1160 ± 30	1080 ± 115
Poz-47658	2.58	cereal hull	1270 ± 60	1180 ± 115
Poz-55880	2.77	branch	1370 ± 30	1302 ± 182
Poz-55881	3.24	leaf fragment	1795 ± 30	1721 ± 98
Poz-55883	3.59	leaf fragment	1995 ± 30	1940 ± 61
Poz-47661	4.0	seed hull	2230 ± 35	2243 ± 91
Poz-47660	4.17	leaf fragment	2325 ± 35	2320 ± 136
Poz-55884	4.22	leaf fragment	2340 ± 30	2386 ± 71
Poz-55885	5.95	branch	3800 ± 35	4196 ± 182
Poz-59082	7.26	leaf fragment	4930 ± 30	5662 ± 65
Poz-59080	10.4	leaf fragment	9970 ± 70	11,492 ± 253

2.3.3 Chronology

The age model for the TSK sediment profile was established by a multiple dating approach. Varve counting was carried out for the composite profile (0–7.7 m). In well- and poorly-varved intervals, the chronology was built at seasonal resolution by varve counting of two investigators, in parallel cores. In non-varved sections, a varve-based sedimentation rate chronology was established by inferring sedimentation rates from neighbouring varves and from singular preserved sub-layers within the non-varved interval. Independent age control is provided by a radiocarbon age model based on 13 accelerator mass spectrometer (AMS) ^{14}C dates of terrestrial plant remains (Table 2.1) and the identification of several cryptotephras (Wulf et al., 2016). Radiocarbon dates were calibrated with OxCal 4.2 (Bronk Ramsey, 2008, 2009) using the INTCAL13 calibration curve (Reimer et al., 2013). The age-depth model of radiocarbon dates was conducted with a poisson-mediated deposition model (p-sequence; Bronk Ramsey, 2008) incorporated in the software OxCal 4.2 by applying a variable κ-parameter (Bronk Ramsey and Lee, 2013). All ages are given as calibrated years before present AD 1950 (cal. a BP).

In addition to previously detected cryptotephras in Lake Tiefer See (Wulf et al., 2016), another tephra horizon found in core TSK13-F6 at 150–153 cm depth was sampled and prepared for geochemical analyses. The sample preparation followed the protocol illustrated in Wulf et al. (2016). The major element composition of single glass shards was obtained on the carbon-coated stubs at a JEOL JXA-8230 microprobe at the German Research Centre for Geosciences (GFZ) with 15 kV voltage, 10 nA beam current and 5 μm beam size. Beam exposure times were 20 s for the elements Fe, Cl, Mn, Ti, Mg and P, as well as 10 s for Si, Al, K, Ca and Na. Instrumental calibration used natural minerals and the Lipari obsidian glass standards (Hunt and Hillt, 1996; Kuehn et al., 2011)

2.3.4 Geochemical analysis

Relative changes of the sediment composition were obtained with an ITRAX μ-X-ray fluorescence (μ-XRF) core scanner at 200 μm step size from the split sediment cores. Prior to measuring, the core surface was cleaned and foil covered to prevent core desiccation. The sediment surface was irradiated for 10 s with a chromium X-ray tube ope-rated at 30 kV and 30 mA to acquire relative changes of 4 elements (calcium (Ca), iron (Fe), titanium (Ti) and manganese (Mn)). The results are expressed as element intensities in counts per seconds. The raw data is not only related to the element concen-

tration, but also to physical properties, sample geometry (*i.e.* water content, grain size), matrix enhancement and absorption effects (Tjallingii et al., 2007; Weltje and Tjallingii, 2008). Therefore, we present the data as log-ratios of element intensities (ln(Ca/Mn) and ln(Ti/Si)), which are linearly related to log-ratios of element concentrations (Weltje and Tjallingii, 2008).

Total organic carbon (TOC), total inorganic carbon (TIC) and total nitrogen (TN) contents were determined continuously at 1 cm increments from bulk samples with an elemental analyser (EA3000-CHNS Eurovector). Two cm^3 of fresh sediment were freeze-dried, ground and homogenized using an agate mortar. Total carbon (TC) and TN contents were measured from 5 mg of sediment in tin capsules. TOC was examined by decalcifying 3 mg of sediment in Ag-capsules by treating with 3% HCl, 20% HCl and drying at 75°C. Carbon and nitrogen contents were calibrated with BBOT, Sulfanilamide and with a soil reference sample (HEKATECH, Boden3). We are aware that the in situ decalcification might cause minor inaccuracies in the TOC contents due to the lower dissolution properties of Ca-rhodochrosite. TIC was calculated by subtracting TOC from TC. TOC and TN contents were used to calculate the atomic C:N ratio. TOC, TIC and TN contents are expressed as percent of dry weight (wt.%). According to replicate measurements of reference samples, the uncertainty of the elemental analyses is <0.2 wt.%.

2.3.5 Pollen analysis

Pollen samples (1 cm^3) were analysed continuously between 0 m and 0.38 m depth and at 1–10 cm intervals (at a temporal resolution of 10 to 50 years) below 0.38 m depth. Sample preparation followed Fægri and Iversen (1989), including the addition of one or two Lycopodium tablets (Lund University, batch-Nr. 1031 with ~20848 Lycopodium spores or batch-Nr. 3862 with ~9666 Lycopodium spores), treatment with HCL, 20% KOH, sieving (120 μm) and acetolysis (7 min). Samples were mounted in glycerine. Counting was carried out with 400x and 1000x magnification until a minimum sum of 600 pollen grains from terrestrial herbs and trees. Identification of pollen grains followed Beug (2004) and Moore et al. (1991).

We reconstructed past vegetation openness from pollen percentage data using the REVEALS model (Sugita, 2007). The model was applied with the REVEALSinR function from the DISQOVER package with the Lagrangian stochastic model for pollen dispersal and the PPE.MV2015 data set (Theuerkauf et al., 2016).

2.3.6 Cladocera analysis

Cladocera samples (1 cm^3 sediment) were analysed at 5 to 40 years resolution from 0–2.8 m depth and at 30–250 year resolution below 2.8 m depth. Sample preparation included treatment with 10% KOH, heating (20 min), sieving (33 μm), dissolution with 10 cm^3 distilled water and staining with safranine dye (Szeroczyńska and Sarmaja-Korjonen, 2007). Cladocera remains in the >33 μm grain size fraction were counted in 0.2 ml to 0.5 ml subsamples using a light microscope (100x to 200x magnification). Identification followed Flößner (2000) and Szeroczyńska and Sarmaja-Korjonen (2007). Species abundances are reflected by the most abundant body part (*i.e.* headshields, shells, ephippium or postabdomen).

2.4 Results

2.4.1 Sediment profile

A 10.8 m long sediment profile was recovered from the deepest part of Lake Tiefer See, mainly comprising of autochthonous lacustrine sediments. Correlation between the overlapping sediment cores indicated two gaps, located at 7.7 m and 9.57 m depth (Figure 2.2), which were caused by sediment loss due to expansion of the organic-rich sediments during heaving of the cores from the deep lake bottom. Therefore, we focus our detailed analyses on the uppermost 7.7 m of the Lake Tiefer See sediment record and provide only basic information for the lower 3 m.

The basal part (10.7–10.8 m) of the sediment profile consisted of sand mixed with plant remains and mussels. This sediment interval contained the macroscopically non-visible tephra TSK13_F6_150–153_T (>1000 glass shards cm^{-3}). Glass shards of this tephra were colourless, vesicular and showed a heterogeneous phonolitic composition (Figure 2.2; Chapter 6.3 Appendix). This composition is typical for the late Allerød Laacher See Tephra (LST) from the Eifel Volcanic Field, in particular for its middle-C (MLST-C) and upper (ULST) units. The LST is widespread in central and NE Germany (Dräger et al., 2016; Lane et al., 2012; Neugebauer et al., 2012) and has been detected as far as S Sweden, central N Poland, E France and NW Italy(*e.g.* Riede et al., 2011; van den Bogaard and Schmincke, 1985; Wulf et al., 2013). It has been varve dated at 12,880 ± 40 varve a BP (Brauer et al., 1999) and at 12,937 ± 23 cal. a BP according to Bayesian age modelling (Bronk Ramsey et al., 2015). Hence, the finding of the LST at the basal part of the sediment record suggests an onset of lake sedimentation around 13,000 cal. a BP, during the late Allerød (Brauer et al., 1999).

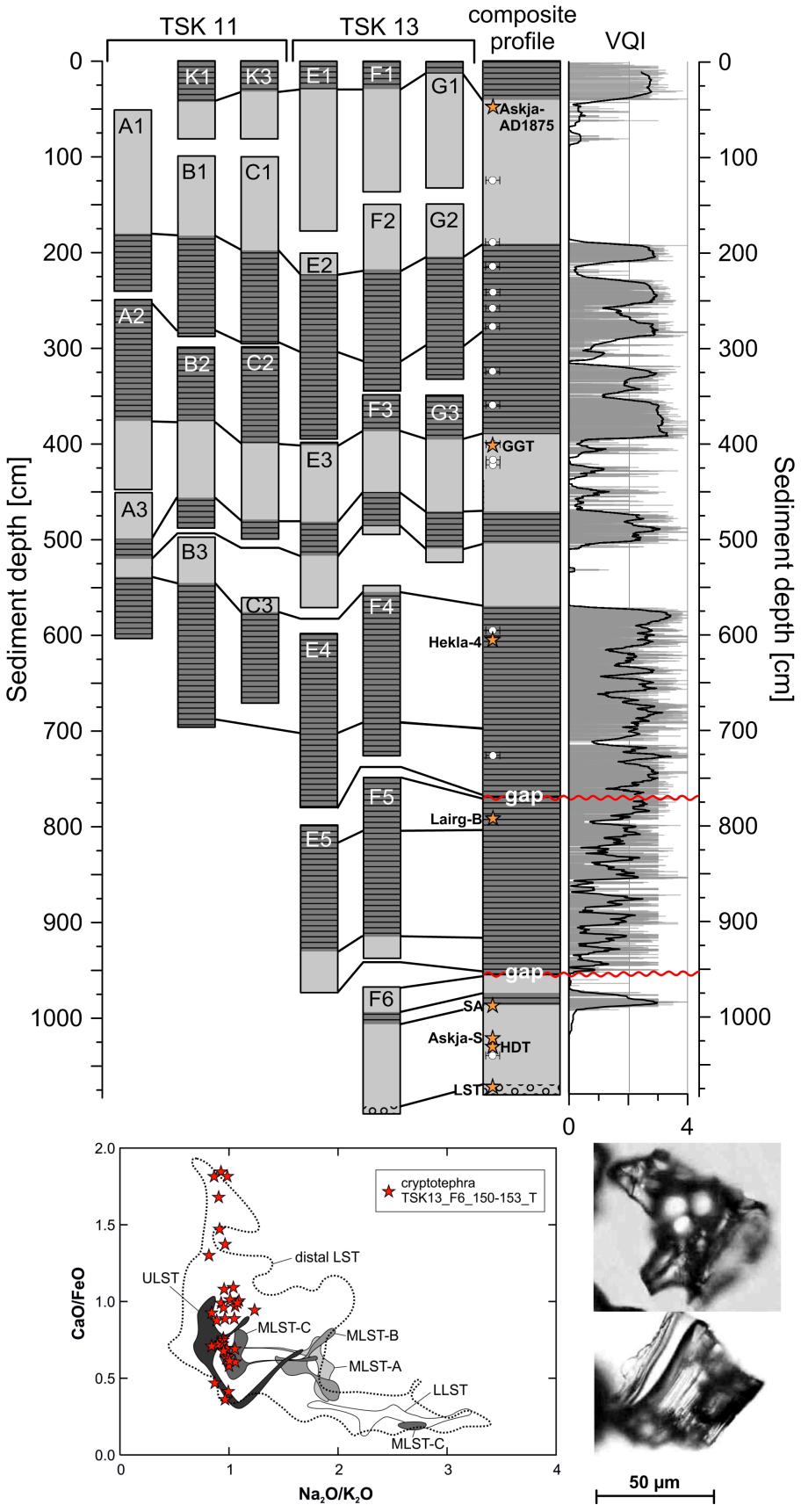
TSK 11
TSK 13
composite profile
VQI
Sediment depth [cm]
Askja-AD1875
GGT
Hekla-4
gap
Lairg-B
gap
SA
Askja-S
HDT
LST
cryptotephra TSK13_F6_150-153_T
distal LST
ULST
MLST-C
MLST-B
MLST-A
LLST
MLST-C
CaO/FeO
Na2O/K2O
50 µm

Figure 2.2: Top left: schematic profiles of Lake Tiefer See sediment cores and the respective composite profile with well-varved (dark grey) and non-varved (light grey) sections; white dots indicate AMS ^{14}C dates and orange stars show positions of cryptotephras (data from Wulf et al. (2016)). Top right: varve quality index (VQI; grey curve) with 51-year running mean (black line). Bottom left: Bivariate plot Na_2O/K_2O versus CaO/FeO of cryptotephra TSK13_F6_150–153_T for correlation with proximal (shaded fields) and distal (dotted line) units of the Laacher See Tephra (LST). Matrix glass data of proximal units LLST (Lower Laacher See Tephra), MLST-A to -C (Middle Laacher See Tephra A to C) and ULST (Upper Laacher Tephra) are obtained from Harms (1998) and Harms and Schmincke (2000). Distal LST glass data is obtained from Juvigné et al. (1995, 1996), Riede et al. (2011), Lane et al. (2011, 2012), Neugebauer et al. (2012) and Wulf et al. (2013). Bottom right: images of glass shard of cryptotephra TSK13_F6_150–153_T.

Autochthonous lacustrine sedimentation started at 10.7 m depth with massive deposits rich in calcite, plant remains and sand-sized detritus. A rapid transition to organic rich sediments occurred at 10.4 m sediment depth. The radiocarbon age of 11,492 ± 253 cal. a BP at this depth indicates that this change in sedimentation happened around the Younger Dryas/Holocene transition. This assumption is further supported by finding of glass shards of the Hässeldalen tephra (11,380 ± 216 cal. a BP; Davies et al., 2003; Ott et al., 2016; Wohlfarth et al., 2006) 8 cm above this transition (10.32 m depth; Wulf et al., 2016). A faint cm-scale dark brown and light grey lamination commenced at 10.16 m depth followed by distinct mm- to sub-mm scale alternations of light and dark layers between 9.88 and 9.75 m depth. The fine lamination consisted of sub-layers of organic matter and carbonate and are interpreted as varves. The presence of the Saksunarvatn ash at 9.89 m depth indicates that the varve formation commenced at ~10,200 cal. a BP (Lohne et al., 2014; Wulf et al., 2016). Above the varved interval, faint cm-scale dark brown and light grey lamination occurred from 9.75 m depth until the supposed core gap at 9.57 m depth. Between this gap and the second gap (located at 7.7 m depth) carbonate varves were preserved. This sediment facies pursued into the basal part of the continuous uppermost 7.7 m of the Lake Tiefer See sediment record, which was investigated in detail. Seven sediment units were distinguished based on the degree of varve preservation (Table 2.2, Figure 2.3): Varves were well-preserved in unit I (7.7–5.71 m), unit III (5.04–4.71 m), unit V (3.94–1.89 m) and unit VII (0.4–0 m), but non-preserved in unit II (5.71–5.04 m), unit IV (4.71–3.94 m) and unit VI (1.89–0.4 m).

2.4.2 Chronology

The varve chronology for the studied continuous interval consists of a floating lower part and a non-floating upper part linked to the present day varves. Both sections are separated by the non-varved unit II (Figure 2.3). From 7.7–5.71 m depth (unit I) a

floating varve chronology was established and anchored at the Hekla-4 cryptotephra (Wulf et al., 2016). The chronology for the uppermost 5.04 m (units III to VII) was built on downcore varve counting starting from the top (AD 2010) and calculated sedimentation rates for intercalated non-varved intervals. The age model of the non-varved unit II (5.71–5.04 m depth) was determined from linear interpolation between the ages of the top of the lower chronology and the bottom of the upper chronology. Based on the varve quality index (VQI) three levels of uncertainty were established: For VQI>1 (well-varved) the error is <1% comparable to other varve chronologies (*e.g.* Neugebauer et al., 2012; Swierczynski et al., 2013). For 0<VQI<1 (poorly-varved) an uncertainty of 5% is assumed, while for VQI=0 (non-varved) uncertainties of up to 10% can be reached.

Table 2.2: Description of sedimentary units I to VII in terms of the microfacies types with depths, time intervals, distribution of the varve quality index (VQI; >1=well-varved, 0-1=poorly-varved) and 0=non-varved), the mean sedimentation rates as well as distribution of the varve types (C=calcite varves; R=Ca-rhodochrosite varves; O=organic varves).

Sed. Units	Sed. depth [m]	Time interval [cal. a BP]	VQI [%] >1	0-1	0	Sed. rate [mm/a]	Varve type [%] C	R	O	Remarks
5	**0.40–0.00**	**37±1 to -60**	**95**	**5**	**0**	**4.1**	**99**	**0**	**1**	**well-varved; modern varves**
6	1.90–0.40	750±65 to 37±1	2	3	95	2.1	35	0	65	non-varved; calcite type; 3 poorly-varved periods of ~20 a duration (230–210, 145–120, 95–75)
5 c	**2.27–1.90**	**990±75 to 750±65**	**60**	**10**	**30**	**1.5**	**62**	**3**	**35**	**well-varved; 4 poorly-varved periods of 30–180 a duration (1825–1795, 1620–1440, 1240–1195, 990–895)**
5 b	**2.54–2.27**	**1840±100 to 990±75**	**98**	**2**	**0**	**1.2**	**2**	**3**	**95**	
5 a	**3.94–2.54**	**2100±105 to 1840±100**	**75**	**10**	**15**	**1.4**	**2**	**43**	**55**	
4	4.71–3.94	2850±135 to 2100±100	20	10	70	0.9	0	65	35	non-varved; organic type; 3 poorly-varved periods of ~50 a duration (2660–2610, 2430–2390, 2230–2185)
3	**5.04–4.71**	**3100±130 to 2850±135**	**80**	**15**	**5**	**1.2**	**35**	**5**	**60**	**well-varved**
2	5.71–5.04	3950±45 to 3100±130	0	2	98	0.8	0	0	0	non-varved; calcite type
1 b	**6.13–5.71**	**5350±70 to 3950±45**	**85**	**10**	**5**	**0.9**	**50**	**0**	**50**	**well-varved; 5 poorly-varved periods of 50–80 a duration (5930–5885, 5405-5360, 4985–4900, 4735–4680, 4435–4370)**
1 a	**7.70–7.30**	**6030±85 to 5350±70**	**80**	**10**	**10**	**0.8**	**10**	**10**	**80**	

Bold font indicates well-varved intervals

(i) The floating varve chronology of unit I (7.7–5.71 m depth) was anchored with the Hekla-4 cryptotephra identified at 6.06 m depth. The age of the Hekla-4 tephra is constrained by radiocarbon dating at 4218 ± 65 cal. a BP (Dugmore et al., 1995a) and 4260 ± 20 cal. a BP (Pilcher et al., 1996), and by varve counting in German and Swedish sites at 4342 ± 75 cal. a BP (Dörfler et al., 2012) and 4390 ± 107 cal. a BP (Zillén et al., 2002), respectively. We used the weighted mean age of 4293 ± 43 cal. a BP (calculated from the published ages after Froggatt and Lowe (1990)) for anchoring the chronology. The resulting absolute ages for the floating chronology are supported by the radiocarbon age model. A date 12 cm above the Hekla-4 tephra (POZ-55885; 4196 ± 182 cal. a BP) fit the varve-based age of 4176 ± 45 cal. a BP. Furthermore, a date 1.2 m below (POZ-59082; 5662 ± 65 cal. a BP) is only slightly older than the respective varve-based age of 5508 ± 75 cal. a BP. The resulting chronology for unit I yielded ages of 6030 ± 85 cal. a BP for the base at 7.7 m depth and of 3950 ± 45 cal. a BP for the top at 5.71 m depth (Figure 2.3).

(ii) The lower boundary of the varve-based chronology of the uppermost 5.04 m of the profile marked the top of the non-laminated sediment uni II and was dated at 3100 ± 130 cal. a BP. The independently established radiocarbon chronology based on eleven AMS ^{14}C dates (calibrated with Oxcal 4.2; Table 2.1), confirms the varve-based chronology within the uncertainties (Figure 2.3). In addition, the Glen Garry Tephra (2088 ± 122 cal. a BP; Barber et al., 2008) at 4.01 m depth (unit V; Wulf et al., 2016) further supports the age of the varve-based chronology of this horizon (2170 ± 110 cal. a BP). Another independent tephrochronological time marker for the varve-based chronology is the Askja AD 1875 tephra (Wulf et al., 2016).

2.4.3 Microfacies analysis

2.4.3.1 Well-varved sediment units and varve types

The well-varved sediment units I (6030–3950 cal. a BP), III (3100–2845 cal. a BP) and V (2095–750 cal. a BP; BC 145–AD 1200) included ~80% varves with a VQI>1. Units I and V were additionally intercalated by five and four, respectively, short periods of less well-preserved varves (Table 2.2). Unit VII (AD 1924–2010) contained the modern well-preserved varves (Kienel et al., 2013). In well-varved sediment we identified three different varve types: organic, calcite and Ca-rhodochrosite varves (Figure 2.4a, b, c). The occurrence of varve types was highly variable, with rarely more than 20 successive varves of the same type. Organic varves appeared in all well-varved sediment units except for unit VII. Calcite and Ca-rhodochrosite varves clustered in different inter-

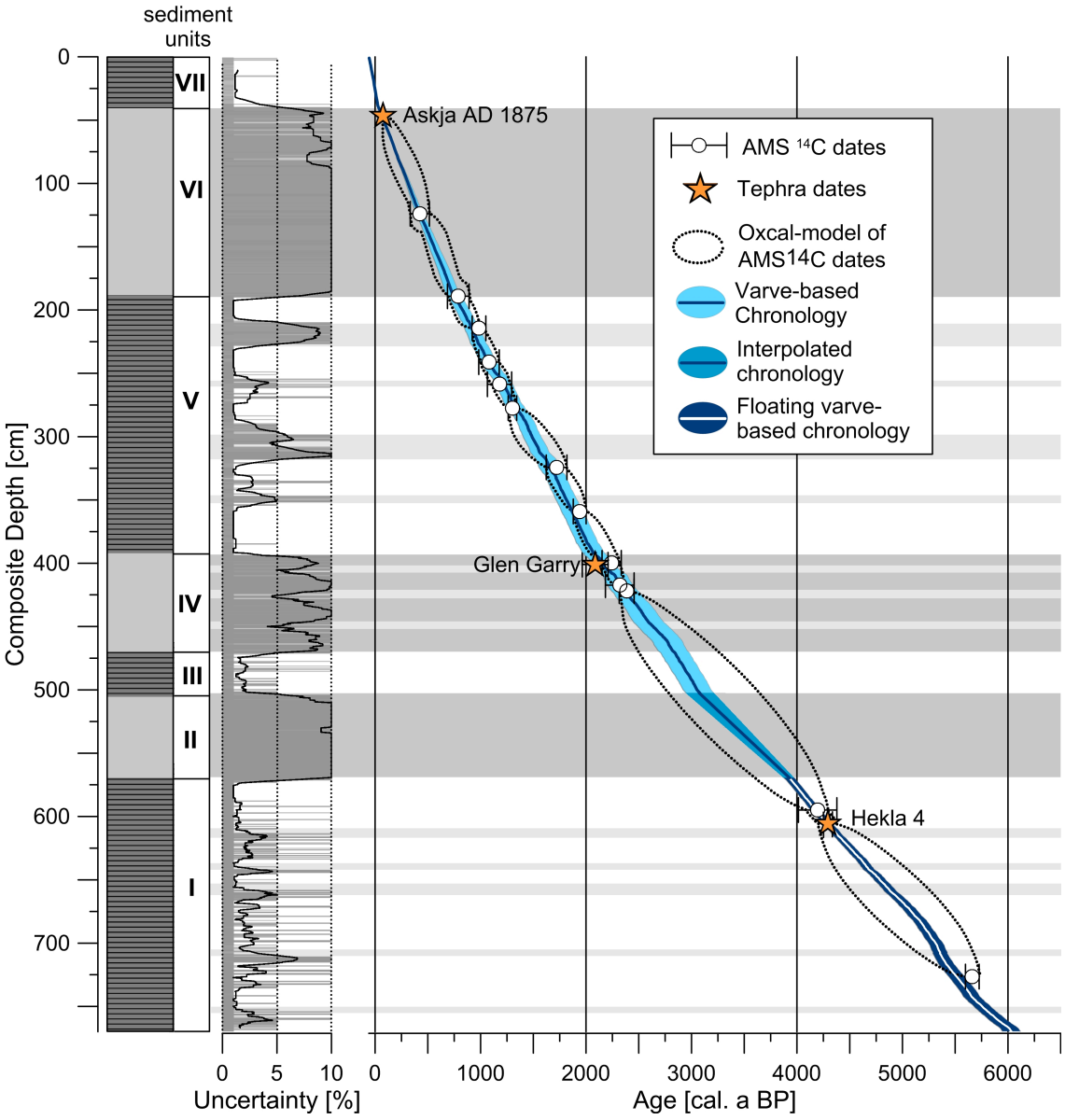

Figure 2.3: Age-depth model of the Lake Tiefer See composite profile: Solid blue line shows varve counts and varve-based interpolation; light blue shading illustrates the accumulated counting error of the different chronologies; white dots show AMS ^{14}C dates and orange stars indicate positions of cryptotephras; the black dotted line highlights upper and lower range of the AMS ^{14}C P_Sequence depositional model (variable κ-parameter) conducted with oxcal 4.2 (Bronk Ramsey, 2008, 2009). Dark and light grey shaded areas reflect non- and poorly-varved intervals, respectively.

vals. While Ca-rhodochrosite varves were detected in the lower part of unit I (6030–5360 cal. a BP) and in the lower part of unit V (2095–990 cal. a BP), calcite varves occurred in the upper part of unit I (5360–3940 cal. a BP), in unit III, in the upper part of unit V (990–750 cal. a BP) and in unit VII (AD 1924–2010). Typical varve compositions are described in the following.

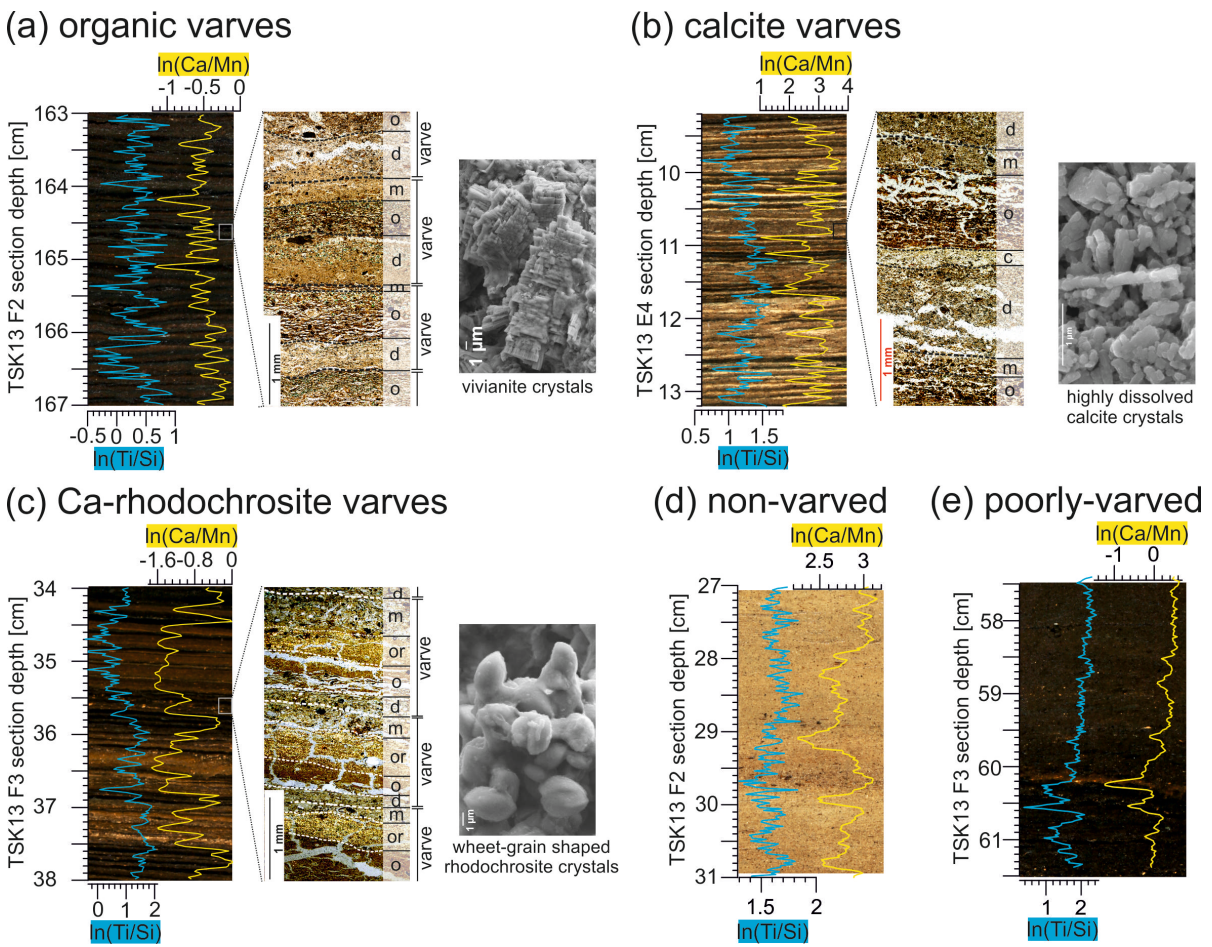

Figure 2.4: Structure and character of organic (a), calcite (b) and Ca-rhodochrosite varves (c) as well as of non-varved intervals (d) and poorly-varved intervals (e). From left to right: core photo and microscopic image from the thin section (half polarized light) with plotted boundaries of varves (thick white/black dashed lines) and sublayers (thin white/black dashed lines), corresponding varve cycle with sub-layer types (d: diatom, o: organic, or: organic and Ca-rhodochrosite, m: mixed, c: calcite) and REM images of characteristic components. The blue and yellow lines in core photos show the respective ln(Ti/Si) and ln(Ca/Mn) ratios.

(I) Organic varves (Figure 2.4a) mainly comprised four sublayers. The varve cycle either started with (i) a planktonic diatom sub-layer reflecting diatom blooms during spring to early summer, or with (ii) a mixed layer comprising quartz and plant fragments, in addition to planktonic and benthic diatom species and bivalves, likely reflecting sediment reworking from the littoral zone. The following (iii) organic sub-layer comprised of fine-grained, orange-brown, amorphous organic matter and usually included micritic- to mm-scale vivianite crystals. The presence of vivianite indicates anoxic conditions in a non-sulfidic environment during sediment deposition (Nriagu and Dell, 1974; Nriagu, 1972; Roden and Edmonds, 1997; Rothe et al., 2014). Sublayer (iv) was also a mixed layer, deposited during lake circulation in autumn. The varve cycle ended with (v) a thin organic sub-layer. Organic varves accounted for 55% of well-varved intervals (*i.e.* VQI>1), but are not represented by a modern analogue.

(II) Calcite varves (Figure 2.4b) mainly consisted of five sub-layers and resemble biochemical calcite varves described in Kelts and Hsü (1978) and Lotter and Lemcke (2008). The varve cycle of calcite varves in unit VII (sub-recent varves) started with the deposition of (i) a planktonic diatom layer. Most calcite varves in units I, III and V began with (ii) a mixed sub-layer. The following (iii) calcite sub-layer was constituted by fine-grained idiomorphic calcite crystals, which form by endogenic calcite precipi-tation in the epilimnion, *i.e.* when CO_2 consumption by algal blooms increases pH and reduces solubility of $CaCO_3$ (Kelts and Hsü, 1978; Koschel, 1990; Koschel et al., 1983, 1987). In sub-recent varves, calcite layers were normally graded from grain sizes of about 13 μm to micritic crystals (<1 μm) at the top of the sub-layer (Kienel2013). Calcite layers in units I, III and V only comprised micritic calcite crystals. The following (iv) organic sub-layer commonly contained calcite flocculates and vivianite. The varve cycle ended with (v) an autumn mixed sub-layer and (vi) a thin organic sub-layer.

(III) Ca-rhodochrosite varves (Figure 2.4c) mainly contained four sub-layers. Similar to organic varves, Ca-rhodochrosite varves either started with (i) a planktonic diatom layer or (ii) a mixed sub-layer. The following (iii) organic sub-layer included Ca-rhodochrosite crystals. The crystals were commonly aligned in the upper part of the sub-layer in a way that smaller spherical crystals (<1 μm) were grading to larger wheat grain shaped crystals of up to 10 μm diameter. Electron probe microanalyses of 23 measured Ca-rhodochrosite crystals indicated an average composition of 48 ± 10 wt.% MnO, 5 ± 2 wt.% CaO and 8 ± 7 wt.% FeO. The formation of Ca-rhodochrosite crystals in the sediment requires a sufficiently high concentration of reduced Mn and free HCO_3^- ions as well as low redox potentials (Robbins and Callender, 1975; Stevens et al., 2000). Ca-rhodochrosite crystals have been observed in both lacustrine and marine environ-

ments (Burke et al., 2002; Calvert and Price, 1970; Dean, 1993; Jouve et al., 2013; Stevens et al., 2000; Zen, 1959), but the present finding is the first in NE German lake records. The varve cycle ended with (iv) a mixed layer deposited during autumn and (v) a thin organic layer. Ca-rhodochrosite varves commonly did not contain calcite and vivianite.

2.4.3.2 Poorly- and non-varved sediment units

Poorly- and non-varved sediment sections showed increased proportions of minerogenic and plant detritus as well as benthic diatoms and occasionally bivalves. Bioturbation structures were not observed. The non-varved units II (3950–3100 cal. a BP) and unit VI (750–37 cal. a BP (AD 1200–1913)) consisted of extensively mixed sediment, which appeared homogenous by naked eye (Figure 2.4d). In unit VI, planktonic diatom layers (dominantly Aulacoseira sp. and Stephanodiscus sp.) with up to 2 mm thickness irregularly occurred in the mixed sediment. The distance between diatom layers ranged between 2 and 110 mm. These layers presumably reflect seasonal diatom blooms and were therefore included in sedimentation rate calculations.

In poorly-varved sections (unit IV 2845–2095 cal. a BP and nine short periods in units I and V; Table 2.2) the mixed sediment was frequently intercalated by preserved varves. Phases of non-varved sediment were on average 15 mm thick; the maximum thickness of 80 mm was observed in unit IV. These short non-varved phases were cha-racterized by planktonic diatom layers, frequently occurring in a distance of 1 to 30 mm. Maximum diatom layer thicknesses of up to 2 mm (dominantly Stephanodiscus sp.) were observed in poorly-varved periods after ~1500 cal. a BP (*i.e.* 1240–1195 cal. a BP and 990–895 cal. a BP). In contrast to non-varved sediments, poorly-varved sections contained slightly higher proportions of amorphous organic matter and irregularly dispersed sub-mm sized concretions of micritic vivianite or Ca-rhodochrosite (Figure 2.4e).

The contacts between poorly-/non-varved and well-varved sediment sections indicated a progressive decrease or increase of varve quality commonly within about a decade. Slightly longer transition phases of ~25 years and ~50 years were observed between units I and II and between units II and III. Transitional intervals showed obscure sublayer boundaries. Furthermore, sub-layering was reduced to a lower diatom layer and an upper mixed layer (VQI between 0 and 1). These rapid changes between varved and non-varved sediments indicate the presence of thresholds for varve preservation.

2.4.4 Bulk geochemistry

2.4.4.1 Carbon chemistry

The TIC contents (Figure 2.5) represents the proportion of calcite and Ca-rhodochrosite in the sediment. TIC contents reached highest values in the non-varved units II and VI (mean 5 wt.%) and lowest values in the basal part of unit I (6030–5360 cal. a BP) and in unit V (mean 1.5 wt.%). A correspondence between TIC content and varve preservation was not observed. Instead, a relationship of TOC contents and varve preservation was found. In non-varved sediments, values were typically lower (on average 5 wt.%), whereas well-varved sediment units showed higher TOC contents (on average 15 wt.%). An exception is the non-varved unit IV which was characterized by intermediate and highly fluctuating TOC contents.

The C:N ratios were not displaying strong variations and remained between 5 and 15 (mean 10.7), indicating that the organic matter is predominantly composed of autochthonous material. The curve showed no correspondence to changes in varve preservation.

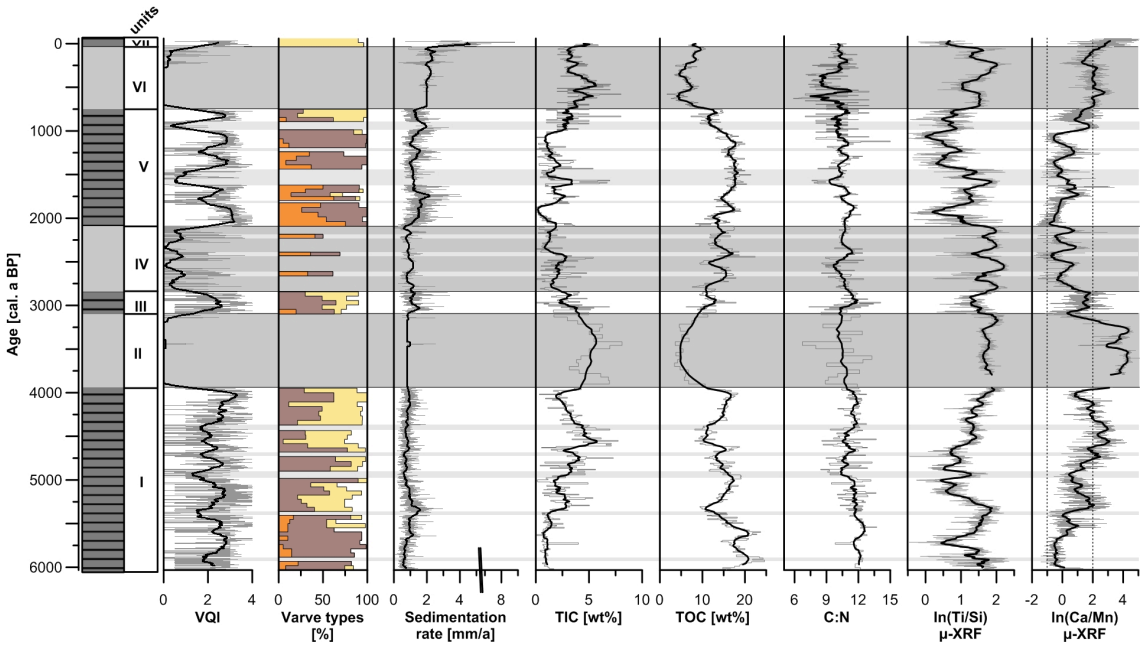

Figure 2.5: Composite profile with main sedimentological parameters. Sediment column with well-varved (striped dark grey) and non-varved (light grey) sections. Results of sedimentological analysis: varve quality index (VQI), occurrence of varve types (yellow=calcite varves; orange=Ca-rhodochrosite varves; brown=organic varves) and the sedimentation rate. Results of geochemical analysis: TIC content, TOC content, TOC and TN ratio (C:N), log-ratios of Ti and Si (ln(Ti/Si)) and Ca and Mn (ln(Ca/Mn) obtained from μ-XRF element scanning. Black lines indicate the 51 year running mean of the data plots. Dark and light grey shaded areas reflect non- and poorly-varved intervals, respectively.

2.4.4.2 μ-XRF element scanning

The main elements detected in the Lake Tiefer See sediments included Ca, Fe, K, Mn, Si and Ti. In poorly- and non-varved sediment units (units II, IV and VI) a high positive correlation was observed for Si-Ti and Si-K (r=0.81 and 0.89, respectively), whereas the correlation of these elements in dominantly well-varved units (units I, III, V and VII) was low (r=0.25 for Si-Ti and 0.31 for Si-K). The correlation of Si with the elements Ti and K indicates detrital input (Demory et al., 2005; Jouve et al., 2013) and a dominance of detrital Si incorporated in quartz and clay minerals in poorly- and non-varved intervals. The weak correlations in varved sediments, in contrast, point to the presence of Si bound in diatom frustules in these units. We interpret the ln(Ti/Si) ratio as a proxy of the relative variations of detrital sediment input and generally find low ln(Ti/Si) ratios in well-varved sediments and high ratios in poorly- and non-varved intervals.

The ln(Ca/Mn) ratio reflects variations of calcite, organic and Ca-rhodochrosite varves. Higher values occurred in the upper part of unit I (5360–3940 cal. a BP), in unit III, in the upper part of unit V (750–990 cal. a BP) and in unit VII. These periods all comprised calcite varves. Lower ln(Ca/Mn) values were found in organic varve dominated intervals, as in the lower parts of unit I (6030–5360 cal. a BP) and of unit V (2100–990 cal. a BP)), but also in sections with dominant Ca-rhodochrosite varves as in the lower part of unit V (2100–1840 cal. a BP). Consequently, the ln(Ca/Mn) ratio showed a similar pattern to the TIC curve.

2.4.5 Vegetation openness

The pollen based reconstruction displayed repeated changes in vegetation openness within the pollen source area of Lake Tiefer See over the past 6000 years (Figure 2.6 and Figure 2.7). The lowest values (<20%) were observed at around 6000 cal. a BP and during short phases between 1500 and 750 cal. a BP. Lowest openness was thus observed before the onset of Neolithic farming and during the 'Migration Period' (Büntgen et al., 2011). The highest openness (>60%) was reconstructed for the periods 3940–3100 cal. a BP, 2700–2200 cal. a BP, 990–895 cal. a BP (AD 960–1055) and since 750 cal. a BP (AD 1200). These intervals presumably represent settlement phases in this region. After 4000 cal. a BP, openness was negatively related to the VQI, *i.e.* increased openness was mostly observed during poorly- and non-varved periods. An exception is the recent well-varved sediment unit VII, which showed both, well-preserved varves and high vegetation openness.

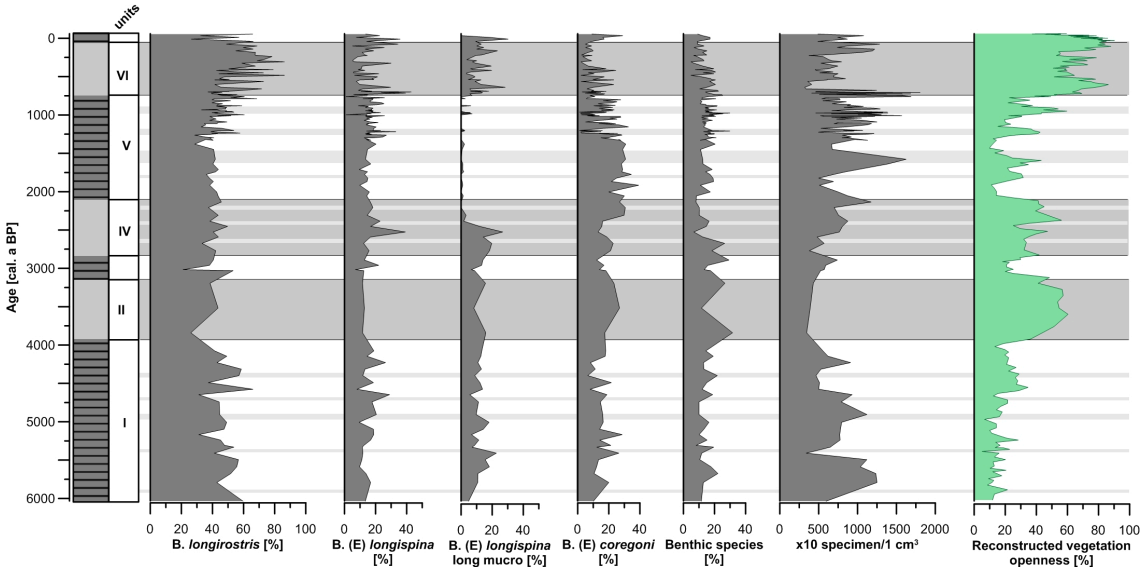

Figure 2.6: Selected results of Cladocera analysis. Sediment column with well-varved (striped dark grey) and non-varved (light grey) sections. Selected results of Cladocera analysis: *Bosmina longirostris*, *Bosmina (Eubosmina) longispina*, *Bosmina (Eubosmina) longispina* with long mucro, *Bosmina (Eubosmina) coregoni*, benthic Cladocera species, Cladocera specimen number per 1 cm^3 sample. The last column shows the reconstructed vegetation openness from pollen data.

2.4.6 Cladocera analysis

We identified 36 Cladocera species from 6 families in the Lake Tiefer See sediments during the past 6000 years. The assemblages were dominated by planktonic taxa of the Bosminidae family. *Bosmina longirostris* was the most abundant species. Cladocera assemblages mainly indicate relative changes in lake productivity (Polcyn, 1996; Szeroczyńska, 1998)

Benthic Cladocera species showed a higher abundance in poorly- and non-varved sediment intervals. The relation between the planktonic Cladocera assemblages and varve preservation changed through time (Figure 2.6). In units I to V (6030–1500 cal. a BP) changes of planktonic species did not correspond to varve preservation variability. In units V and VI (1500 cal. a BP–AD 1924), a relation between varve preservation and Cladocera assemblages was observed. In particular, the eutrophic species *Bosmina longirostris* and the specimen number were higher during poorly- and non-varved intervals, suggesting increased productivity during periods of low varve preservation after ~1500 cal. a BP. In contrast, well-varved phases were characterized by a dominance of the oligotrophic species *Bosmina (Eubosmina) coregoni*. In the sub-recent well-varved unit VII, a rise of planktonic species mainly recorded by *Bosmina longirostris* indicates higher productivity.

2.5 Discussion

2.5.1 Varve preservation and varve microfacies

The sediment record of Lake Tiefer See displays repeated changes between varved and poorly-/non-varved intervals. The preservation of varves indicates anoxic bottom water conditions strong enough to prevent microbenthic life in the pelagic zone (Brauer, 2004; Kelts and Hsü, 1978). The prevalence of anoxic conditions during well-varved intervals of Lake Tiefer See sediments is supported by the presence of vivianite and Ca-rhodochrosite crystals, which preferentially form during oxygen deficiency (Nriagu and Dell, 1974; Nriagu, 1972; Roden and Edmonds, 1997; Rothe et al., 2014).

TOC contents in lake sediments are either interpreted as proxy for productivity (*e.g.* Lüder et al., 2006; Schelske and Hodell, 1991) and/or for organic matter preservation (*e.g.* Hartnett et al., 1998; Meyers and Ishiwatari, 1993). Since higher TOC contents in the Lake Tiefer See sediments occur in intervals of well-preserved varves, we consider TOC values in our record mainly as a preservation signal. This is supported by the observation that periods of increased productivity are not characterized by higher TOC contents. In the non-varved unit VI with low TOC contents (~5 wt.%), for example, we noticed higher abundances of mesotrophic and eutrophic diatoms (*i.e. Stephanodiscus sp.* and *Aulacoseira sp.*) as well as of the eutrophic Cladocera species *Bosmina longirostris* (Szeroczyńska, 1998; Polcyn, 1996).

The oxygen budget in the hypolimnion is primary controlled by lake circulation and productivity (Demaison and Moore, 1980; Niessen et al., 1992). Since no indications for enhanced lake productivity in well-varved intervals have been found, except for the sub-recent varve formation (Kienel et al., 2013), we suggest that changes of varve preservation before the 20^{th} century was mainly caused by variations in lake circulation. This interpretation is supported by enhanced reworking of littoral sediments during poorly- and non-varved phases, which is inferred from higher portions of epiphytic/benthic Cladocera remnants. Higher portions of these Cladocera species are a result of increased wave activity as well as longer and more intense lake circulation. In addition, higher ln(Ti/Si) ratios suggest a higher influx of detrital matter during poorly- and non-varved periods. The higher detrital input might reflect both enhanced sediment flux from the catchment due to higher rainfall and erosion, as well as intensified littoral sediment reworking. Consequently, the varve quality index (VQI) is considered as an indicator for lake circulation except for the recent period of varve formation, which is related to lake eutrophication.

A further differentiation of anoxic conditions in well-varved sediments can be inferred from variations in varve-microfacies types (Figure 2.5). While organic varves occur in all well-varved units and are thus not indicative, Ca-rhodochrosite and calcite varves cluster in specific intervals. The dominance of either Ca-rhodochrosite or calcite varves suggests different redox-potential levels at the sediment-water interface (Stevens et al., 2000). Generally, low potentials are required for the formation of Ca-rhodochrosite crystals to reduce Mn-ions to the mobile phase and enable anaerobic microbial activity in order to produce high concentrations of HCO_3^- ions (Robbins and Callender, 1975; Stevens et al., 2000). As these conditions are less favourable for the preservation of calcite crystals (Dean, 1999), we assume that intervals dominated by calcite varves indicate higher redox potentials. However, since the redox potential at the lake bottom is the result of a complex interaction of different influences (including the bottom water oxygen content, pH and temperature) this interpretation should be considered with caution.

2.5.2 Drivers of lake circulation – present and past

Lake circulation is dominantly affected by wind stress and lake stratification (Magee et al., 2016). Today, Lake Tiefer See is mono- to dimictic. Lake monitoring since 2012 indicates that circulation commonly lasts from September/October to April/May (unpublished data). The circulation period is interrupted during cold winters when the lake is frozen. Interestingly, oxygen concentrations in the hypolimnion do not start to rise before December, reaching maximum values in April/May (up to 12 mg/l oxygen), towards the end of the circulation phase and at the onset of summer stratification. The slow increase in oxygen concentration in the hypolimnion reflects the inertia of the large water body, suggesting that oxygenation would be significantly hampered by a shortening of the circulation period.

The strength and duration of lake stratification is an important factor for lake circulation intensity and is mainly controlled by temperature and seasonality (Boehrer and Schultze, 2008). Warm and long summers and/or cold winters with ice cover promote enhanced stability of lake stratification, reduced lake circulation and development of anoxia. On the other hand, cool summers and/or warm winters cause reduced stability of lake stratification, enhancing the susceptibility of the lake to wind-driven lake circulation and result in more oxygenated bottom water conditions.

Other possible influences on lake circulation include wind shelter and lake level changes. A reduced wind shelter, for example induced by anthropogenic deforestation, might lead to increased sensitivity of lake circulation to wind stress (Bierstedt et al.,

2015b; Boehrer and Schultze, 2008; Stevens et al., 2000). In addition, lake circulation in Lake Tiefer See might be affected by lake level changes, as a level rise over a certain threshold would connect Lake Tiefer See with the neighbouring lakes of the Klocksin lake chain (Figure 2.1). In result, the lake-surface size would be more than doubled, thereby enhancing the susceptibility of lake circulation to wind stress.

2.5.3 Imprint of climate change and human impact on lake circulation

Longer and more frequently occurring non- and poorly-varved intervals during the past ~4000 years suggest a trend of intensified lake circulation in Lake Tiefer See, which likely is related to weaker and shortened lake-stratification periods and/or increased windiness. Similar trends towards less stable lake stratification and stronger lake circulation after ~5000 cal. a BP have been previously reported from other Central European lakes as well (*e.g.* Pędziszewska et al., 2015; Finsinger et al., 2014; Eusterhues et al., 2005). A possible explanation for weaker lake stratification during the late Holocene are changes in orbital forcing (Laskar, 1990; Laskar et al., 2004), causing lower summer and warmer winter temperatures in Central Europe (Wanner et al., 2008). The insolation changes further enhanced the temperature gradient in the northern hemisphere, resulting in higher cyclone activity (Gill, 1982; Lamy et al., 2010; Raible et al., 2007) and increased windiness in Central Europe during the Late Holocene (*e.g.* Orme et al., 2016; Figure 2.7). However, elevated windiness occurred ~1000 years after the onset of the first major non-varved interval in Lake Tiefer See (~4000 cal. a BP; Figure 2.7), suggesting that additional factors affected lake circulation at that time. A likely candidate is anthropogenic deforestation, because the increase of reconstructed vegetation openness is recorded exactly at the same time as the onset of the non-varved interval (Figure 2.7). We infer from the general coincidence of enhanced land openness and non-varved sediments that anthropogenic deforestation became an important factor for lake circulation in Lake Tiefer See since ~4000 cal. a BP.

Before this time, from ~6000 to ~4000 cal. a BP, the sediments are predominantly varved, indicating generally stable stratification and minor lake mixing. Only five intercalated decadal periods of poorly-varved sediments indicate short phases of slightly increased lake circulation. As aforementioned, the interval of stable stratification ended rather abruptly at ~4000 cal. a BP and was followed by non-varved sediments (unit II) lasting for ~840 years. After this phase of intensified lake circulation, the recurrence of well-varved sediments suggests again stable stratification, but only for the duration of ~250 years (unit III). This period ended, again abruptly, at ~2850 cal. a BP and was followed by unit IV with poorly-varved sediments (2850–2100 cal. a BP). This transition

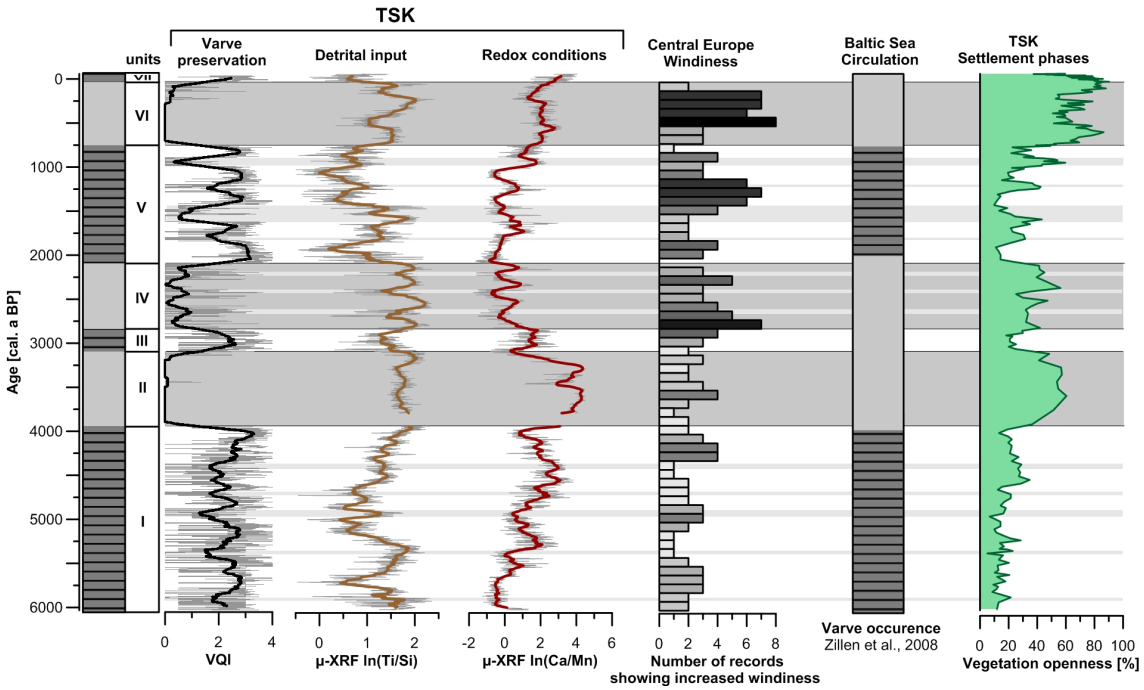

Figure 2.7: Overview of main results in comparison to Central European windiness and to varved (striped dark grey) and bioturbated (light grey) sections in Baltic Sea basins (Zillén et al., 2008). Dark and light grey shaded areas reflect non- and poorly-varved intervals, respectively. Central European windiness reflects the state of research in 100-year-windows from wind reconstructions from different archives: dune records (Bateman and Godby, 2004; Clemmensen et al., 2009; Gilbertson et al., 1999; a.a. Sommerville et al., 2003; Wilson et al., 2004), peat sequences (Björck and Clemmensen, 2004; de Jong et al., 2006; Orme et al., 2015), coastal deposits (Sorrel et al., 2012; Tisdall et al., 2013), and lake sediment records (Martin-Puertas et al., 2012a).

concurs with a well-known time interval of climate deterioration with colder, moister and windier conditions in Central Europe (*e.g.* Martin-Puertas et al., 2012b; Van Geel et al., 1996), but also with a parallel increase in vegetation openness, indicating decreased wind shelter of the lake during this time. The coincidence of climatic change and reduced wind shelter makes it difficult to evaluate the contribution of each factor for lake circulation. Most likely it was the combination of climate and human influences that resulted in the observed enhanced lake circulation. In contrast to the earlier period (unit II) of non-varved sediments, this poorly-varved interval (unit IV) is frequently intercalated by short well-varved phases of ~60 years duration, suggesting that the lake system was in a transitional state close to the threshold towards a more stable water column.

Concurrent with the Roman climate optimum (~2100 cal. a BP; Holzhauser et al., 2005) well-varved sediments dominated again (unit V) and continued until the 12^{th} century AD (Figure 2.7), but with several decadal-scale interruptions by poorly-varved

sediment. These poorly-varved episodes partly concur with peaks of vegetation openness, indicating that deforestation contributed to declining varve preservation in these intervals. The longest of these poorly-varved intercalations (~1620–1440 cal. a BP (AD 330–510)) coincides with the 'Migration Period' (also 'Dark Ages'; Büntgen et al., 2011), for which colder, moister and windier conditions are reported from Central Europe. Since deforestation was less intense during this time (Figure 2.7), we suggest a dominant climate influence in this period.

The following extended interval of non-varved sediments (unit VI) corresponds to the 'Little Ice Age' (13^{th}–19^{th} century). Characteristic for this period were cooler temperatures, stronger westerlies (*e.g.* Lamb, 1979; Mayewski et al., 2004; Pfister et al., 1998; Wanner et al., 2011) and a particularly marked increase in summer storminess (Wheeler and Suarez-Dominguez, 2006; Wheeler et al., 2010) in Central Europe. The combination of colder and windier summers during the 'Little Ice Age' should have sufficiently weakened and shortened the summer stratification period to outpace the probably stronger winter stratification due to colder conditions and formation of lake ice cover. The parallel increase of vegetation openness further favoured strengthened lake circulation.

The striking alternation of well-varved and poorly-/non-varved sediments is primary a result of variations in the intensity of the lake-circulation regime. However, it is challenging to disentangle the ultimate driving mechanisms for these variations, as several different factors can influence lake circulation. One difficulty is that only vegetation openness data are directly obtained from the Lake Tiefer See sediment record, while the assessment of the role of climate effects is limited to comparisons with published palaeoclimate data from other records. Nevertheless, the influence of regional climate change is strongly supported by the striking correspondence of the main phases of increased lake circulation at Lake Tiefer See and bioturbated sediments in the Baltic Sea basins (Figure 2.7), which are interpreted as signal of enhanced river inflow and windier conditions (Andrén et al., 2000; Jilbert et al., 2015; Ning et al., 2016; Zillén et al., 2008). Therefore, we hypothesise that the driving mechanism for the variability of lake circulation at Lake Tiefer See during the last ~6000 years is a complex coupling of long-term insolation-driven climatic changes and deforestation phases during human settlement periods. Climate likely affected lake circulation by decreasing summer and increasing winter temperatures; both causing weakened seasonal lake stratification. In addition, lake circulation presumably was intensified by centennial-scale intervals of colder, moister and windier conditions, like at ~2850 cal. a BP and during the 'Dark Ages' and the 'Little Ice Age'. Deforestation in the catchment during

human settlement phases led to a reduced wind shelter and thus increased the susceptibility of the lake to wind stress. In result, the strengthened lake circulation prevented preservation of varves. Since such distinct alternations in varve preservation as observed in Lake Tiefer See are rarely reported, we consider Lake Tiefer See as exceptionally sensitive to the above discussed combination of different factors controlling lake circulation and deep-water anoxia.

2.6 Conclusion

Varve formation and preservation in Lake Tiefer See during the last ~6000 years is particularly sensitive to changes in lake circulation, causing distinct alternations of varved and poorly-/non-varved intervals. Except for the most recent period since AD 1924, during which human induced eutrophication was the most important factor for varve preservation, variations in lake-circulation strength mainly controlled varve preservation in Lake Tiefer See. Most probably, the driver for the variability in lake circulation is a combination of long-term and centennial- to decadal-scale climatic changes as well as anthropogenic deforestation during settlement periods, enhancing the sensitivity of the lake to wind stress. However, it remains difficult to disentangle in detail between these factors, partly due to the lack of independent wind proxies at Lake Tiefer See. An intriguing observation is the coincidence of non-varved intervals in Lake Tiefer See with phases of bioturbated sediments in the Baltic Sea. This similarity suggests a common driver for sediment variability in both sediment archives, which, however, needs to be verified and explained by further and more detailed investigations.

Acknowledgements

We would like to thank all technicians and the coring team of GFZ-section 5.2 that assisted in the field and lab (G. Arnold, D. Berger and, B. Brademann, S. Lauterbach, P. Meier, F. Ott, S. Pinkerneil, M. Słowiński, R. Schedel, R. Weißbach). We further acknowledge P. Dulski for μ-XRF scanning of the sediment cores, M. Köhler (MKfactory) for assistance during coring, O. Appelt for electron probe microanalyses, E. Dietze for fruitful discussions and valuable comments on the original manuscript and M. Pauly for improving the language of the manuscript. We are grateful to two anonymous reviewers for their constructive comments on this manuscript. This study is a contribution to the Virtual Institute of Integrated Climate and Landscape Evolution Analysis –ICLEA- of the Helmholtz Association (grant number VH-VI-415). It is further a contribution to

the climate initiative REKLIM Topic 8 "Abrupt climate change derived from proxy data" and uses infrastructure of the Terrestrial Environmental Observatory (TERENO), both of the Helmholtz Association. Varve microfacies, geochemistry, Cladocera and pollen data files for the investigated Lake Tiefer See sediment interval are stored at the PANGAEA data library.

3 Holocene tephrostratigraphy of varved sediment records from Lakes Tiefer See (NE Germany) and Czechowksie (N Poland)

Sabine Wulf[a,b,*] Nadine Dräger[a] , Florian Ott[a], Johanna Serb[a], Oona Appelt[c], Esther Guðmundsdóttir[d], Christel van Bogaard[e], Michał Słowińsski[f], Mirosław Błaszkiewicz[f], Achim Brauer[a]

[a] GFZ German Research Centre for Geosciences, Section 5.2 Climate Dynamics and Landscape Evolution, Telegrafenberg C, D-14473 Potsdam, Germany

[b] Senckenberg Research Institute and Natural History Museum, BIK-F, TSP6 Evolution and Climate, Senckenberganlage 25, D-60325 Frankfurt a.M., Germany

[c] GFZ German Research Centre for Geosciences, Section 3.3 e Chemistry and Physics of Earth Materials, Telegrafenberg, D-14473 Potsdam, Germany

[d] Faculty of Earth Sciences, Institute of Earth Sciences, University of Iceland, Strulugata 7, 101 Reykjavík, Iceland

[e] Helmholtz Centre for Ocean Research Kiel, GEOMAR, Wischhofstrasse 1-3, D-24148 Kiel, Germany

[f] Department of Environmental Resources and Geohazards, Institute of Geography and Spatial Organization, Polish Academy of Sciences, Kopernika 19, 87-100 Toruń, Poland

[*] Corresponding author

Abstract

A detailed Holocene tephrostratigraphic framework has been developed for two predominately varved lake sediment sequences from NE Germany (Lake Tiefer See) and central N Poland (Lake Czechowskie). A total of thirteen tephras and cryptotephras of Icelandic provenance were detected and chemically fingerprinted in order to define correlatives and to integrate known tephra ages into the sediment chronologies. Out of these, three cryptotephras (Askja-AD 1875, Askja-S and Hässeldalen) were identified in both records, thus allowing a detailed synchronization of developing high-resolution palaeoenvironmental proxy data. The early Holocene Saksunarvatn Ash layer and the middle Holocene Lairg-B and Hekla-4 cryptotephras in Lake Tiefer See are further important anchor points for the comparison with other high-resolution palaeoclimate records in Central and Northern Europe. Tentative correlations of cryptotephras have

been made with a historical basaltic Grimsvötn eruption (~AD 890–856) and three late Holocene rhyolitic eruptions, including the 2.1 ka Glen Garry and two unknown high-silicic cryptotephras of probably Icelandic provenance (~1.9 cal. ka BP).

Keywords

Cryptotephra – Icelandic volcanism – Tiefer See – Lake Czechowskie – Lateglacial – Holocene – ICLEA

3.1 Introduction

In the light of global warming and possibly related socioenvironmental responses it is essential to understand the mechanism and timing of abrupt climate changes. Past climate variability can be best reconstructed by studying high-resolution geological records, *e.g.* annually laminated (varved) lake sediments. However, such records are rare in northern central Europe and are restricted to either the Lateglacial (*e.g.* Brauer et al., 1999; Goslar et al., 1999, 1993; Merkt and Müller, 1999; Neugebauer et al., 2012) or the Holocene epoch (*e.g.* Dörfler et al., 2012; Enters et al., 2010; Zolitschka, 1990).

The Virtual Institute for Integrated Climate and Landscape Evolution Analyses ICLEA (www.iclea.de) aims at the continuous and high-resolution reconstruction of past climate variability and environmental changes in the northern central European Lowlands since the end of the last Ice Age. A current focus is set on two predominately varved sediment sequences from NE Germany (Lake Tiefer See; Dräger et al., 2014) and central N Poland (Lake Czechowskie; Ott et al., 2014). A high-resolution palaeoenvironmental reconstruction and the establishment of independent chronologies of both records is in progress and will enable the determination of effects of spatial and temporal climatic changes due to the existing gradient of increasing climatic continentality from the western (Tiefer See) towards the eastern archive (Czechowskie). Independent chronologies will be achieved by varve counting, radiometric dating and tephrochronology. The latter method involves the use of tephra layers (volcanic fallout material) in sedimentary repositories as a dating and synchronization tool (*e.g.* Lowe, 2011). Several distinct tephras of Icelandic and Eifel provenance have been reported from sites in NE Germany and western Poland, *i.e.* the Saksunarvatn Ash (Bramham-Law et al., 2013), the Askja-S, Hässeldalen and Laacher See tephras (*e.g.* Housley et al., 2013b; Juvigné et al., 1995; Lane et al., 2012; Riede et al., 2011; Wulf et al., 2013). Those tephras, however, are restricted to the Lateglacial and early Holocene epoch. The iden-

tification of younger tephras is so far limited to a single finding of the late Holocene Glen Garry cryptotephra (non-visible tephra) in an archaeological site in NW Poland (Housley et al., 2013a).

In this study, we present a comprehensive tephrostratigraphy for the northern central European Lowlands for the last ca. 11,500 years, constrained from the ICLEA sites Lake Tiefer See and Lake Czechowskie. The tephra results are used to construct robust tephrochronologies for both records in order to support their varve chronologies. They furthermore provide important anchor points for the synchronization of palaeoproxy data of these records with each other and with other high-resolution terrestrial records in northern central Europe.

3.2 Study area

Lake Tiefer See (TSK=Tiefer See Klocksin) and Lake Czechowskie (JC=Jezioro Czechowskie) are both located in the northern central European Lowlands in the foreland of the terminal moraine of the Pomeranian ice advance of the last glaciation, which is dated at 15.6 ± 0.6 ^{10}Be ka (Rinterknecht et al., 2014) (Figure 3.1). Both lakes have a melt genesis, namely lake basins formed by the melting of buried ice blocks (Błaszkiewicz, 2011; Błaszkiewicz et al., 2015; Kaiser et al., 2012; Van Loon et al., 2012; Słowiński, 2010; Słowiński et al., 2015). Lake Tiefer See is a 1.6 km N-S elongated lake located in the natural park of Nossentiner-Schwinzer Heide, NE Germany (53° 35.50' N, 12° 31.80' E, 62 m a.s.l.). It is part of the Klocksin Lake Chain that formed in a subglacial gully system during the last deglaciation. The lake has a surface area of 0.75 km^2 and a maximum water depth of 62.5 m (Dräger et al., 2014; Kienel et al., 2013).

Lake Czechowskie is situated in the eastern part of the Pomeranian Lakeland in the Tuchola Pinewoods, central N Poland (53° 52.20' N, 18° 14.10' E, 108 m a.s.l.). The current lake together with the adjacent Trzechowskie palaeolake (TRZ) basin (53° 52.40' N, 18° 12.90' E, 111 m a.s.l.) developed in a subglacial channel in the outwash plain of the Wda river, which was accumulated during the retreat of the Late Weichselian ice sheet recession between 17 and 16 cal. ka BP (Błaszkiewicz et al., 2015; Marks, 2012). Lake Czechowskie has an oval-shaped basin with a surface area of 0.73 km^2 and a maximum water depth of 32 m (Błaszkiewicz et al., 2015; Ott et al., 2014).

Lake Tiefer See and Lake Czechowskie are both located in a distal position to Icelandic volcanoes (2150–2400 km SE) and the W German Eifel Volcanic Field (500–840 km NE).

Figure 3.1: Overview map of NE Germany and NW Poland showing the location of Lake Tiefer See (TSK) and Lake Czechowskie (JC). The red dotted line indicates the position of the southerly ice advance of the Pomeranian phase at the end of the Weichselian glaciation. Inlet map is showing the position of European volcanoes mentioned in the text (black triangles) in relation to studied sites (black stars).

3.3 Methods

3.3.1 Sediments and developing chronology

3.3.1.1 Lake Tiefer See

In the years 2011 and 2013, a total of seven parallel sediment sequences and several surface cores were recovered from the deepest part of Lake Tiefer See using an UWITEC piston corer (Figure 3.1b). These sequences were used to construct a composite profile of 1083 cm length that reaches the basal glacio-fluvial sand deposits (Figure 3.2a). Two sediment gaps probably of several decimetres each occur at 769.5 cm and 956.5 cm depth as a result of technical problems during coring. The chronology of the composite profile is under construction and will incorporate several dating methods, *i.e.* varve counting, estimation of sedimentation rates in poorly- and non-varved sections, AMS ^{14}C dating (Dräger et al., 2014) and tephrochronology (this paper). Lacustrine sediments are characterized by alternating finely laminated and homogenous diatomaceous gyttia with various amounts of calcareous and detrital matter (Dräger et al., 2014; Kienel et al., 2013).

3.3.1.2 Lake Czechowskie

Four parallel and overlapping sediment sequences as well as numerous short cores were retrieved between 2009 and 2012 from the deepest parts of Lake Czechowskie (Figure 3.1b) using an UWITEC piston corer and a Ghilardi Gravity Corer (KGH 94), respectively. A continuous composite profile of 1346 cm length has been constructed (Figure 3.2b) by defining unambiguous correlation layers. Holocene sediments are dominated by finely laminated calcareous gyttia with various amounts of organic and detrital matter. The base of Lateglacial sedimentary deposits is characterised by coarse glacio-fluvial sand deposits (Ott et al., 2014). Dating of sediments is in progress and will include varve counting, AMS 14C dating, radionuclide distribution (^{137}Cs) (Ott et al., 2014) and tephrochronology (this paper).

3.3.2 Tephrochronological methods

A systematic scanning for cryptotephras in TSK and JC sediments was carried out using preliminary chronostratigraphical information, high-resolution sampling and processing of sediments for each archive. Continuous sediment samples of 1 cm^3 were taken in 0.5 cm–5 cm intervals for the entire Holocene TSK sequence as well as for the early Holocene part of JC sediments. A selective search in the middle to late Holocene section of the JC sequence was carried out depending on tephra findings in this time interval in the TSK sequence. In order to remove organic matter, samples were individually treated with a 15% hydrogen peroxide (H_2O_2) solution (overnight) and subsequently wet-sieved over a 100-μm and 20-μm mesh sieve. In the following, a 10% hydrochloric acid (HCl) solution was added to the 20-100 μm fractions in order to dissolve calcium carbonates (maximum 1 h). The residual samples were then repeatedly rinsed with deionized water and dried with Ethanol at 60°C. Samples with high diatom abundances were additionally heated in a 2 M sodium carbonate (Na_2CO_3) solution in a water bath for 5 h, neutralized with a 10% hydrochloric acid solution and rinsed with deionized water before drying. Dried samples were inspected for volcanic glass shards on plastic lids using a transmitted light microscope (Zeiss Jenapol). Identified shards were handpicked into a single-hole-stub, embedded in Araldite 2020 resin, sectioned and polished by hand on wet silicon carbide paper.

The major element composition of single glass shards was obtained on the carbon-coated stubs at a JEOL JXA-8230 microprobe at the German Research Centre for Geosciences (GFZ). Operating conditions used a 15 kV voltage, a 10 nA beam current and beam sizes of 5 μm, 8 μm or 10 μm. Exposure times for each analysis were 20 s

for the elements Fe, Cl, Mn, Ti, Mg and P, as well as 10 s for F, Si, Al, K, Ca and Na. Instrumental calibration used natural mineral and the Lipari obsidian glass standards (Hunt and Hillt, 1996; Kuehn et al., 2011). Raw values of glass data are provided in Table 3.1 and Table 3.2. For comparison, several Holocene Icelandic tephras were analysed with the same instrument, *i.e.* Askja-AD 1875 (sample provided by C. van den Bogaard), Landnám-AD 870, Eldgjá-AD ~934, Hekla-3 and Hekla-4 (see Chapter 6.3 Appendix). Geochemical biplots used normalized (water-free) data of the TSK, JC and proximal tephra samples for the comparison with other published EPMA glass data (Figure 3.4).

3.4 Results and discussion

3.4.1 Lake Tiefer See Holocene tephrostratigraphy

Sample TSK13_F6_99–100_T (Hässeldalen)

The lowermost cryptotephra TSK13_F6_99–100_T in Lake Tiefer See occurs in 1031.7 cm composite depth in a non-varved interval and reveals only 2 shards cm^{-3}. No further glass shards have been detected in the overlying and underlying sediments, suggesting an undisturbed and primary deposition of this cryptotephra. Both colourless, highly vesicular glass shards (Figure 3.3) show rhyolitic compositions that are best comparable with those of the early Holocene Hässeldalen tephra (HDT) from the Snæfellsjökull volcano (?) in W Iceland (Davies et al., 2003) (Figure 3.4f). The HDT was first reported at the distal Hässeldala port palaeolake site in southern Sweden and dated by Bayesian ^{14}C modelling at 11,380 ± 216 cal. a BP (Davies et al., 2003; Wohlfarth et al., 2006). Further findings include sites in SW Sweden (Lilja et al., 2013), Denmark (Larsen and Noe-Nygaard, 2014) and on the Faroe Islands (Lind and Wastegård, 2011). The occurrence of the HDT in TSK is in agreement with recent findings at Endinger Bruch in NE Germany (Lane et al., 2012) and at the Węgliny site in SW Poland (Housley et al., 2013b)(Figure 3.5).

Sample TSK13_F6_91-92_T (Askja–S)

Sample TSK13_F6_91–92_T in 1023.2 cm composite depth exhibited 3 shards cm^{-3} (Figure 3.3) that occurs within a non-laminated section 7 cm above the Hässeldalen Tephra. Glass shards are colourless, highly vesicular and display a homogenous Icelandic rhyolitic composition with relatively low potassium values of ca. 2.5 wt.% and high CaO concentrations (ca. 1.6–1.7 wt.%) (Figure 3.4f). Both the glass chemistry and the position of cryptotephra TSK13_F6_91–92_T above the biostratigraphically defined

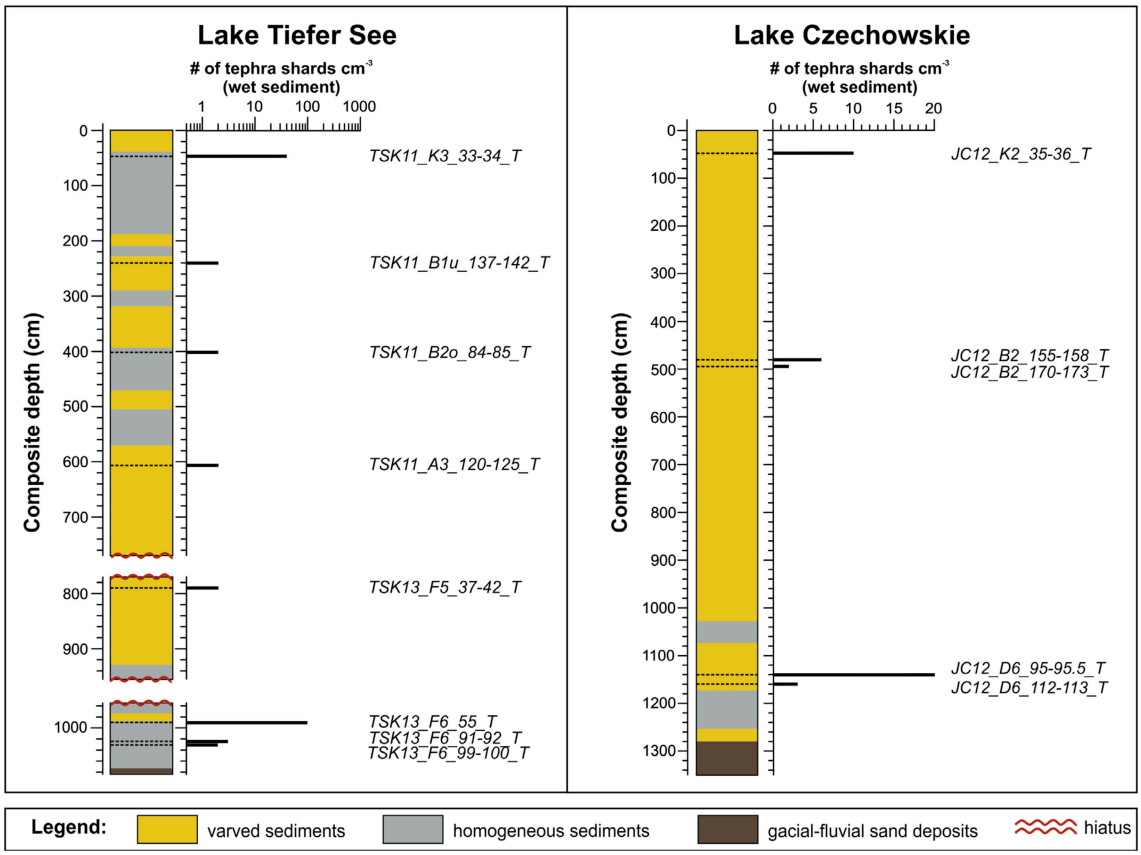

Figure 3.2: Lithology of the composite profile of Lake Tiefer See (left) and Lake Czechowskie (right) with positions of cryptotephras.

Younger Dryas/Holocene transition confirm an origin from the Askja-S caldera forming eruption of the Dyngjufjöll volcanic centre in north-eastern Iceland (Sigvaldason, 2002). The Askja-S tephra has been so far identified in lake and peat sequences on the Faroe Islands (Lind and Wastegård, 2011) in N Ireland (Turney et al., 2006), S Sweden (Davies et al., 2003; Lilja et al., 2013), NE Germany (Lane et al., 2012) and Switzerland (Lane et al., 2011) (Figure 3.5). Its age is constrained by Bayesian ^{14}C modelling at the Hässeldala port palaeolake site in SE Sweden at 10,810 ± 240 cal. a BP (Wohlfarth et al., 2006) and in Lake Soppensee at 10,846 ± 145 cal. a BP (Lane et al., 2011). An age estimate from Faroe Island provided a much younger time constraint at 10,350–10,500 cal. a BP (Lind and Wastegård, 2011). Ages from Hässeldala port and Soppensee were incorporated into a new age model by Bronk Ramsey et al. (2015) providing the most recent age estimate of the Askja-S tephra at 10,830 ± 57 cal. a BP.

Sample TSK13_F6_55_T (Saksunarvatn)

In 989.2 cm composite depth a 0.3 mm thick, macroscopic visible tephra layer occurs directly below a varved interval, here labelled as sample TSK13_F6_55_T. Volcanic glass

Table 3.1: Individual, non-normalized major element glass data of cryptotephras found in Lake Tiefer See

Sample	SiO_2	TiO_2	Al_2O_3	FeO_{tot}	MnO	MgO	CaO	Na2O	K2O	P_2O_5	Total	Cl	F
TSK11_K3_	74.14	0.77	12.19	3.23	0.11	0.69	2.26	3.38	2.48	0.12	99.37	0.05	0.00
33-34_T	74.45	0.78	12.09	3.15	0.12	0.71	2.22	3.49	2.42	0.13	99.57	0.04	0.00
46.7 cm	74.83	0.83	12.29	3.36	0.10	0.70	2.54	3.52	2.31	0.15	100.64	0.03	0.00
Askja-	75.72	0.91	12.36	3.11	0.08	0.66	2.31	3.12	2.44	0.12	100.83	0.03	0.00
AD1875	75.41	0.74	12.23	3.19	0.08	0.65	2.33	3.18	2.46	0.13	100.40	0.04	0.00
	75.38	0.78	12.31	3.16	0.07	0.65	2.41	3.36	2.39	0.12	100.63	0.03	0.00
	75.17	0.82	12.21	3.35	0.11	0.74	2.48	3.63	2.31	0.12	100.94	0.03	0.00
	75.19	0.78	12.54	3.42	0.12	0.71	2.55	3.60	2.30	0.14	101.34	0.04	0.00
	73.39	0.91	12.59	3.73	0.13	0.86	2.72	3.21	2.26	0.17	99.96	0.04	0.00
	73.73	0.86	12.79	3.90	0.11	0.83	2.75	3.28	2.24	0.18	100.67	0.04	0.00
	71.81	1.08	13.01	4.57	0.12	1.06	3.28	3.72	2.13	0.24	101.01	0.03	0.00
	72.45	0.99	12.45	4.77	0.12	1.02	3.36	3.43	2.07	0.25	100.91	0.03	0.00
	71.67	1.17	12.54	4.78	0.13	0.96	3.33	3.55	2.25	0.24	100.62	0.03	0.00
TSK11_B1u_	50.55	2.73	12.87	13.10	0.24	5.79	9.44	2.89	0.51	0.33	98.46	0.01	0.00
137-142_T	50.54	2.77	12.89	12.65	0.21	5.66	9.53	2.81	0.51	0.32	97.89	0.02	0.00
240.6 cm													
unknown													
Grimsvötn													
TSK11_A3_	73.68	0.10	13.03	1.93	0.07	0.01	1.31	3.97	2.74	0.01	96.85	0.08	0.03
120–125_T	72.56	0.12	12.80	1.94	0.12	0.04	1.32	3.71	2.70	0.01	95.32	0.07	0.00
607.9 cm													
Hekla-4													
TSK13_F5_	69.18	0.17	13.78	2.05	0.09	0.12	0.57	5.10	4.37	0.00	95.43	0.20	0.00
37–43_T	69.44	0.20	13.94	2.28	0.10	0.15	0.63	5.31	4.22	0.00	96.27	0.21	0.00
791.5 cm													
Lairg-B													
TSK13_F6_	50.42	3.05	12.73	13.90	0.24	5.56	9.46	2.83	0.43	0.33	98.95	0.01	0.00
55_T	50.14	2.99	12.71	14.19	0.21	5.63	9.69	2.65	0.40	0.32	98.94	0.02	0.00
989.2 cm	50.85	3.14	12.86	14.08	0.20	5.26	9.40	2.66	0.48	0.33	99.25	0.00	0.00
Saksunar-	51.03	3.10	12.65	14.15	0.22	5.21	9.52	2.45	0.49	0.28	99.09	0.02	0.00
vatn	51.80	2.92	13.24	14.26	0.23	5.02	9.66	2.49	0.47	0.31	100.40	0.02	0.00
	50.58	2.83	12.97	13.35	0.27	5.71	9.90	2.64	0.42	0.37	99.03	0.02	0.00
	50.90	3.13	12.83	14.53	0.23	5.88	9.88	2.16	0.55	0.30	100.39	0.01	0.00
	50.61	2.81	12.88	13.73	0.25	5.78	9.72	2.51	0.43	0.33	99.04	0.02	0.00
	50.71	2.90	12.68	13.88	0.21	5.73	9.69	2.79	0.41	0.34	99.35	0.03	0.00
	50.77	2.89	12.97	13.73	0.22	5.62	9.87	2.51	0.40	0.32	99.30	0.00	0.00
	50.40	1.37	13.58	11.06	0.21	7.95	12.36	2.15	0.13	0.06	99.27	0.02	0.00
	50.80	2.75	12.98	13.61	0.23	5.61	9.68	2.53	0.46	0.31	98.97	0.02	0.00
	50.04	1.43	13.44	11.21	0.19	8.17	12.32	2.12	0.16	0.12	99.20	0.00	0.00
	50.15	3.08	12.42	14.01	0.21	5.69	9.56	2.77	0.49	0.31	98.69	0.02	0.00
	50.48	3.10	12.56	13.73	0.22	5.31	9.48	2.80	0.44	0.34	98.46	0.02	0.00
	50.90	3.15	12.88	14.04	0.25	5.24	9.41	2.60	0.49	0.32	99.28	0.01	0.00
	49.92	2.96	12.72	13.70	0.26	5.58	9.56	2.71	0.45	0.37	98.24	0.01	0.00
	50.10	1.55	13.69	10.90	0.18	7.82	12.56	2.08	0.13	0.13	99.14	0.01	0.00
	51.01	3.16	12.97	13.85	0.29	5.29	9.51	2.60	0.52	0.37	99.56	0.02	0.00
	50.77	3.07	12.88	13.84	0.24	5.48	9.47	2.67	0.48	0.37	99.26	0.02	0.00
	50.52	3.02	12.79	13.98	0.23	5.31	9.40	2.66	0.42	0.33	98.66	0.01	0.00

Sample	SiO_2	TiO_2	Al_2O_3	FeO_{tot}	MnO	MgO	CaO	Na2O	K2O	P_2O_5	Total	Cl	F
	49.92	2.89	12.79	13.82	0.24	5.87	9.74	2.76	0.45	0.29	98.77	0.02	0.00
	50.22	1.63	13.86	11.32	0.24	7.60	12.01	1.96	0.17	0.14	99.14	0.00	0.00
	50.07	2.97	13.08	14.46	0.25	5.56	9.39	2.74	0.47	0.37	99.36	0.02	0.00
	50.49	2.85	12.96	13.75	0.21	5.60	9.77	2.71	0.45	0.33	99.12	0.01	0.00
	49.89	2.83	13.01	13.84	0.19	5.92	9.89	2.73	0.43	0.30	99.03	0.01	0.00
	50.38	3.01	12.49	14.04	0.23	5.55	9.60	2.70	0.49	0.35	98.84	0.01	0.00
	49.85	3.13	12.85	13.84	0.23	5.46	9.38	2.81	0.46	0.34	98.35	0.02	0.00
	49.62	2.91	12.89	13.76	0.24	5.48	9.57	2.73	0.41	0.34	97.95	0.02	0.00
	50.07	2.81	12.96	13.43	0.27	5.97	9.82	2.57	0.42	0.34	98.66	0.01	0.00
TSK13_F6	74.50	0.29	11.83	2.51	0.11	0.22	1.60	3.16	2.31	0.02	96.55	0.06	0.00
_91–92_T	675.80	0.32	12.12	2.48	0.10	0.25	1.62	3.40	2.44	0.00	98.53	0.05	0.00
1023.2 cm	673.37	60.28	611.80	2.41	0.09	0.25	1.53	3.21	2.44	0.00	95.38	0.05	0.00
Askja-S													
TSK13_F6	76.87	0.07	11.60	1.08	0.05	0.04	0.44	3.19	4.04	0.01	97.40	0.13	0.00
_99–100_T	76.46	0.08	11.52	1.11	0.07	0.02	0.46	3.15	3.82	0.01	96.71	0.14	0.00
1031.7 cm													
Hässel dalen?													

shards (>100 shards cm^{-3}) of this tephra are brownish, show a low vesicularity (Figure 3.3), and display a basaltic composition. The stratigraphic position in faintly laminated TSK sediments indicates a deposition during the Early Holocene (Figure 3.2). Both the geochemical and chronostratigraphical data confirm a correlation with the Saksunarvatn Ash (SA) from the Grimsötn volcanic system (Figure 3.4e). The Saksunarvatn Ash is an important isochron in environmental records in northern Europe (*e.g.* Aarnes et al., 2012; Birks et al., 1996; Bramham-Law et al., 2013; Jóhansen, 1985; Lind and Wastegård, 2011; Lind et al., 2013; Mangerud et al., 1986; Merkt et al., 1993), the North Atlantic region (*e.g.* Andrews et al., 2002; Haflidason et al., 1990; Jóhannesdóttir et al., 2005; Kylander et al., 2012; Jennings et al., 2014) and Greenland (*e.g.* Abbott and Davies, 2012; Grönvold et al., 1995; Mortensen et al., 2005; Zielinski et al., 1997). At least two distinct SA plumes/eruptions are proposed (*e.g.* Jóhannesdóttir et al., 2005; Davies et al., 2012; Bramham-Law et al., 2013): one is distributed towards the SE and radiocarbon dated in Lake Kråkenes, Norway, at 10,210 ± 35 cal. a BP (Lohne et al., 2013) and another one towards the NW revealing an slightly older age but overlapping within the 2σ error range at 10,297 ± 45 cal. a BP (10,347 ± 45 a b2k; Rasmussen et al., 2006) in the Greenland ice core record. The Saksunarvatn Ash in Lake Tiefer See is most likely related to the south-easterly dispersal fan (Figure 3.5) at 10,210 ± 35 cal. a BP. Since this tephra occurs right below a laminated section (Figure 3.2), it represents an important time and correlation marker in TSK sediments (Figure 3.6)

Table 3.2: Individual, non-normalized major element glass data of cryptotephras found in Lake Czechowskie.

Sample	SiO_2	TiO_2	Al_2O_3	FeO_{tot}	MnO	MgO	CaO	Na2O	K2O	P_2O_5	Total	Cl	F
JC12_K2_	74.44	0.78	12.43	3.39	0.10	0.74	2.38	3.87	2.22	0.12	100.47	0.04	0.00
35–36_T	75.08	0.77	12.27	3.33	0.10	0.71	2.36	3.67	2.34	0.14	100.77	0.05	0.00
48.5 cm													
Askja-AD1875													
JC09 _B2_	74.63	0.06	12.11	0.49	0.00	0.06	0.49	3.79	4.32	0.00	95.96	0.11	0.00
155–158_T	73.99	0.06	12.38	0.58	0.05	0.06	0.44	3.38	4.52	0.01	95.46	0.09	0.00
480.5 cm	73.89	0.07	12.02	0.53	0.04	0.03	0.55	3.35	4.28	0.00	94.77	0.11	0.00
unknown Icelandic?	74.22	0.09	12.18	0.49	0.09	0.06	0.51	3.81	4.20	0.00	95.64	0.11	0.00
JC09_B2_	74.04	0.04	11.88	0.54	0.08	0.05	0.53	3.44	4.09	0.00	94.70	0.11	0.00
170–173_T	73.71	0.08	11.96	0.52	0.06	0.06	0.51	3.48	4.18	0.01	94.58	0.10	0.00
495.5 cm													
unknown Icelandic?													
JC12_D6_	74.24	0.34	12.10	2.48	0.07	0.22	1.52	4.00	2.40	0.06	97.42	0.05	0.00
95–95.5_T	73.20	0.27	11.72	2.38	0.06	0.24	1.52	3.75	2.52	0.06	95.71	0.04	0.00
1141.25 cm	74.04	0.31	12.43	2.60	0.10	0.23	1.58	3.49	2.40	0.02	97.21	0.03	0.00
Askja-S	73.25	0.33	11.76	2.43	0.07	0.23	1.52	3.87	2.45	0.05	95.96	0.03	0.00
	75.52	0.32	12.01	2.45	0.06	0.23	1.53	3.83	2.55	0.04	98.54	0.04	0.00
	74.40	0.31	11.92	2.51	0.08	0.26	1.54	3.81	2.51	0.01	97.35	0.05	0.00
	75.75	0.31	12.24	2.53	0.09	0.23	1.58	3.79	2.39	0.01	98.91	0.05	0.00
	74.21	0.28	11.86	2.48	0.06	0.21	1.56	3.80	2.47	0.10	97.03	0.04	0.00
	74.02	0.29	11.90	2.57	0.09	0.25	1.57	3.77	2.49	0.05	97.01	0.06	0.00
	75.70	0.26	12.25	2.59	0.13	0.28	1.60	3.85	2.48	0.04	99.19	0.06	0.00
	76.11	0.28	12.13	2.49	0.10	0.26	1.54	3.53	2.49	0.00	98.93	0.06	0.00
	75.75	0.32	12.17	2.38	0.08	0.22	1.49	3.44	2.49	0.04	98.37	0.04	0.00
	74.38	0.29	11.94	2.43	0.09	0.22	1.54	3.07	2.52	0.01	96.49	0.04	0.00
JC12_D6_	74.67	0.09	11.69	0.88	0.00	0.00	0.40	3.22	4.27	0.00	95.21	0.13	0.00
112–113_T	74.49	0.13	12.05	1.15	0.07	0.03	0.47	2.97	3.75	0.01	95.12	0.13	0.00
1158.5 cm	73.24	0.10	11.83	1.13	0.06	0.04	0.47	2.96	4.02	0.04	93.89	0.13	0.02
Hässeldalen													

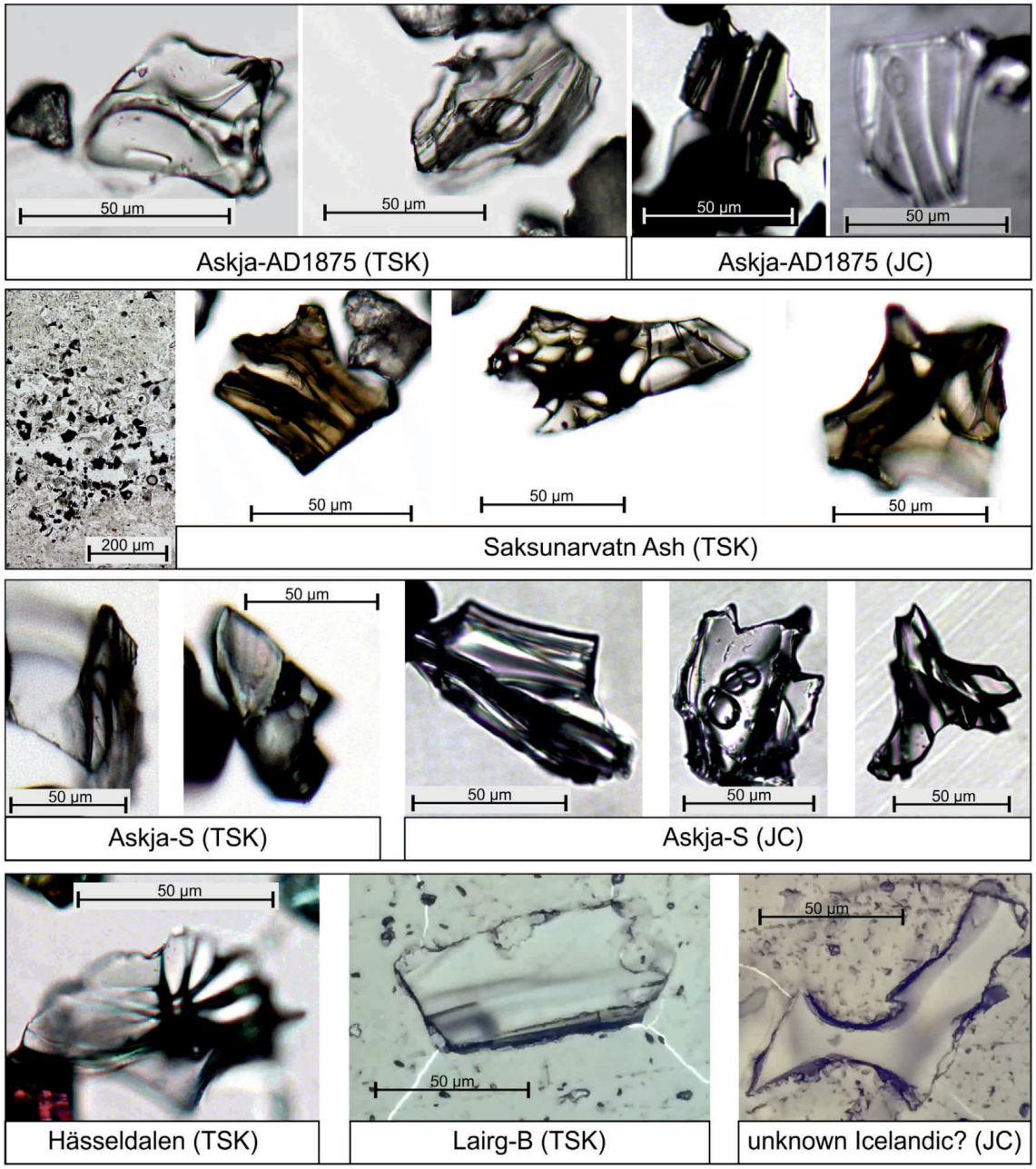

Figure 3.3: Transmitted light images of tephra glass shards from TSK and JC sediments correlated with Askja-AD 1875 (TSK11_K3_33–34_T, JC12_K2_35–36_T), Saksunarvatn (TSK13_F6_55_T), Askja-S (TSK13_F6_91–92_T, JC12_D6_95–95.5_T), Hässeldalen (TSK13_F6_99–100_T), Lairg-B (TSK13_F5_37–42_T, polished surface) and an unknown silicic Icelandic eruption (JC09_B2_170–173_T, polished surface).

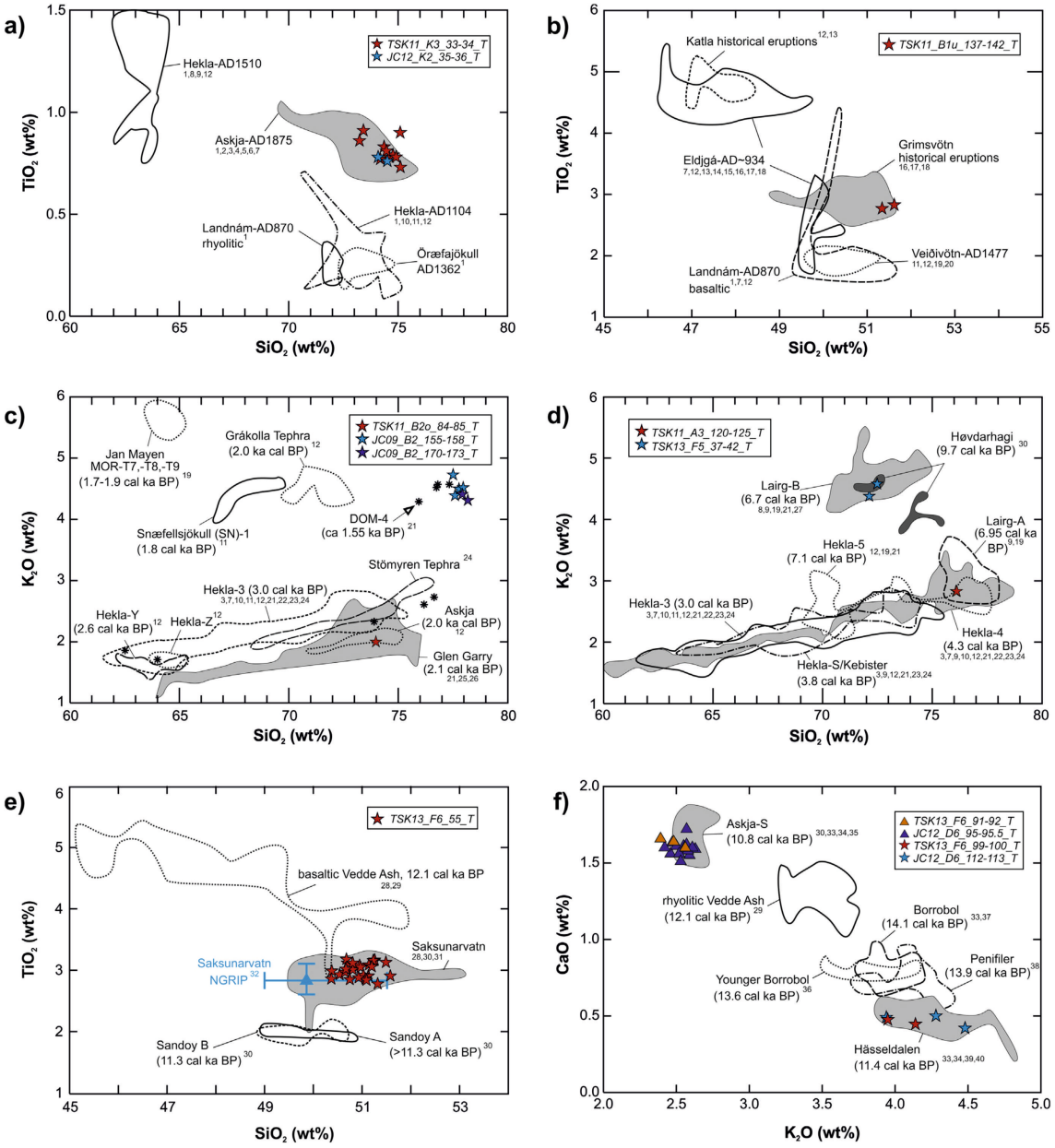
a)
TSK11_K3_33-34_T
JC12_K2_35-36_T
Hekla-AD1510
1,8,9,12
Askja-AD1875
1,2,3,4,5,6,7
Hekla-AD1104
1,10,11,12
Landnám-AD870
rhyolitic
1
Öræfajökull
AD1362
1
TiO2 (wt%)
SiO2 (wt%)
b)
TSK11_B1u_137-142_T
Katla historical eruptions
12,13
Eldgjá-AD~934
7,12,13,14,15,16,17,18
Grimsvötn
historical eruptions
16,17,18
Veiðivötn-AD1477
11,12,19,20
Landnám-AD870
basaltic
1,7,12
TiO2 (wt%)
SiO2 (wt%)
c)
TSK11_B2o_84-85_T
JC09_B2_155-158_T
JC09_B2_170-173_T
Jan Mayen
MOR-T7,-T8,-T9
(1.7-1.9 cal ka BP)
19
Grákolla Tephra
(2.0 ka cal BP)
12
Snæfellsjökull (SN)-1
(1.8 cal ka BP)
11
DOM-4
(ca 1.55 ka BP)
21
Stömyren Tephra
24
Hekla-3 (3.0 cal ka BP)
3,7,10,11,12,21,22,23,24
Hekla-Y
(2.6 cal ka BP)
12
Hekla-Z
12
Askja
(2.0 ka cal BP)
12
Glen Garry
(2.1 cal ka BP)
21,25,26
K2O (wt%)
SiO2 (wt%)
d)
TSK11_A3_120-125_T
TSK13_F5_37-42_T
Høvdarhagi
(9.7 cal ka BP)
30
Lairg-B
(6.7 cal ka BP)
8,9,19,21,27
Lairg-A
(6.95 cal ka BP)
9,19
Hekla-5
(7.1 cal ka BP)
12,19,21
Hekla-3 (3.0 cal ka BP)
3,7,10,11,12,21,22,23,24
Hekla-4
(4.3 cal ka BP)
3,7,9,10,12,21,22,23,24
Hekla-S/Kebister
(3.8 cal ka BP)
3,9,12,21,23,24
K2O (wt%)
SiO2 (wt%)
e)
TSK13_F6_55_T
basaltic Vedde Ash, 12.1 cal ka BP
28,29
Saksunarvatn
28,30,31
Saksunarvatn
NGRIP
32
Sandoy B
(11.3 cal ka BP)
30
Sandoy A
(>11.3 cal ka BP)
30
TiO2 (wt%)
SiO2 (wt%)
f)
TSK13_F6_91-92_T
JC12_D6_95-95.5_T
TSK13_F6_99-100_T
JC12_D6_112-113_T
Askja-S
(10.8 cal ka BP)
30,33,34,35
rhyolitic Vedde Ash
(12.1 cal ka BP)
29
Borrobol
(14.1 cal ka BP)
33,37
Penifiler
(13.9 cal ka BP)
38
Younger Borrobol
(13.6 cal ka BP)
36
Hässeldalen
(11.4 cal ka BP)
33,34,39,40
CaO (wt%)
K2O (wt%)

Figure 3.4: Geochemical bi-plots of normalized tephra glass data for tephra discrimination and correlation. (a) Askja-AD 1875 tephra (TSK, JC); (b) Unknown Grimsvötn Ash (TSK); (c) Glen Garry and unknown late Holocene Icelandic tephras (TSK, JC); (d) Hekla-4 and Lairg-B tephras (TSK); (e) Saksunarvatn Ash (TSK); (f) Askja-S and Hässeldalen tephras (TSK, JC). EPMA reference data are obtained from: [1]Larsen et al. (1999); [2]Andersson et al. (2010); [3]Bergman et al. (2004); [4]Boygle (1998); [5]Oldfield et al. (1997); [6]Pilcher et al. (2005); [7]this study; [8]Pilcher et al. (1996); [9]Dugmore et al. (1995a); [10]Eiríksson et al. (2000); [11]Larsen et al. (2002); [12]Óladóttir et al. (2011); [13]Óladóttir et al. (2008); [14]Thordarson et al. (2001); [15]Zielinski et al. (1995); [16]Grönvold and Jóhannesson (1984); [17]Larsen (1982); [18]Steinthórsson (1977); [19]Chambers et al. (2004); [20]Davies et al. (2007); [21]Van Bogaard and Schmincke (2002); [22]Gudmundsdóttir et al. (2011); [23]Meara (2012); [24]Wastegård (2005); [25]Barber et al. (2008); [26]Housley et al. (2013b); [27]Dörfler et al. (2012); [28]Birks et al. (1996); [29]Lane et al. (2012); [30]Lind and Wastegård (2011); [31]Bramham-Law et al. (2013); [32]Mortensen et al. (2005); [33]Davies et al. (2003); [34]Lane et al. (2011); [35]Lane et al. (2011); [36]Ranner et al. (2005); [37]Turney et al. (1997); [38]Pyne-O'Donnell et al. (2008); [39]Housley et al. (2013b); [40]Lilja et al. (2013). Note that there are some effects of slight sodium migration (slightly higher SiO_2 values, lower Al_2O_3 and Na_2O concentrations) due to the small grain sizes of glass shards and respective small beam sizes that have been applied for EPMA.

Sample TSK13_F5_37–43_T (Lairg B)

Cryptotephra TSK13_F5_37–43_T occurs in 791.5 cm composite depth and is represented by the finding of two glass shards in a 5 cm^3 sediment sample obtained from varved sediments ca. 22 cm below the upper sediment gap (Figure 3.2). Glass shards are colourless, highly vesicular and show a rhyolitic composition, which strongly resembles the glass composition of early Holocene tephras from the Torfajökull volcanic system in southern Iceland. The best chemical match is given for the Lairg-B and Høvdarhagi tephras (Figure 3.4d). Lairg-B has been identified in sites in Scotland (Dugmore et al., 1995a; Pilcher et al., 1996), Ireland (Chambers et al., 2004) and N Germany (Van Den Bogaard et al., 2002; Dörfler et al., 2012) and is radiocarbon dated at 6675 ± 49 cal. a BP (Pilcher et al., 1996) and 6723 ± 108 cal. a BP (Dörfler et al., 2012), respectively. The Hødarhagi tephra is only known from Faroe Islands lake sediment sequences, where it is dated at 9850–9600 cal. a BP (Lind and Wastegård, 2011) and thus only few hundred years younger than the Saksunarvatn Ash. Cryptotephra TSK13_F5_37–43_T, however, is positioned ca. 2 m above the Saksunarvatn Ash in TSK sediments and preliminary varve counts and sedimentation rate estimates indicate a few thousand years younger age in the range of the Lairg-B tephra. In addition to the finding of Lairg-B in the nearby Lake Belauer See (Dörfler et al., 2012), this is a major criterion for a preferred correlation of cryptotephra TSK13_F5_37–43_T with Lairg-B. Despite the low number of detected glass shards and the relatively broadly defined position within a 5 cm sediment interval (higher resolution sampling revealed no further

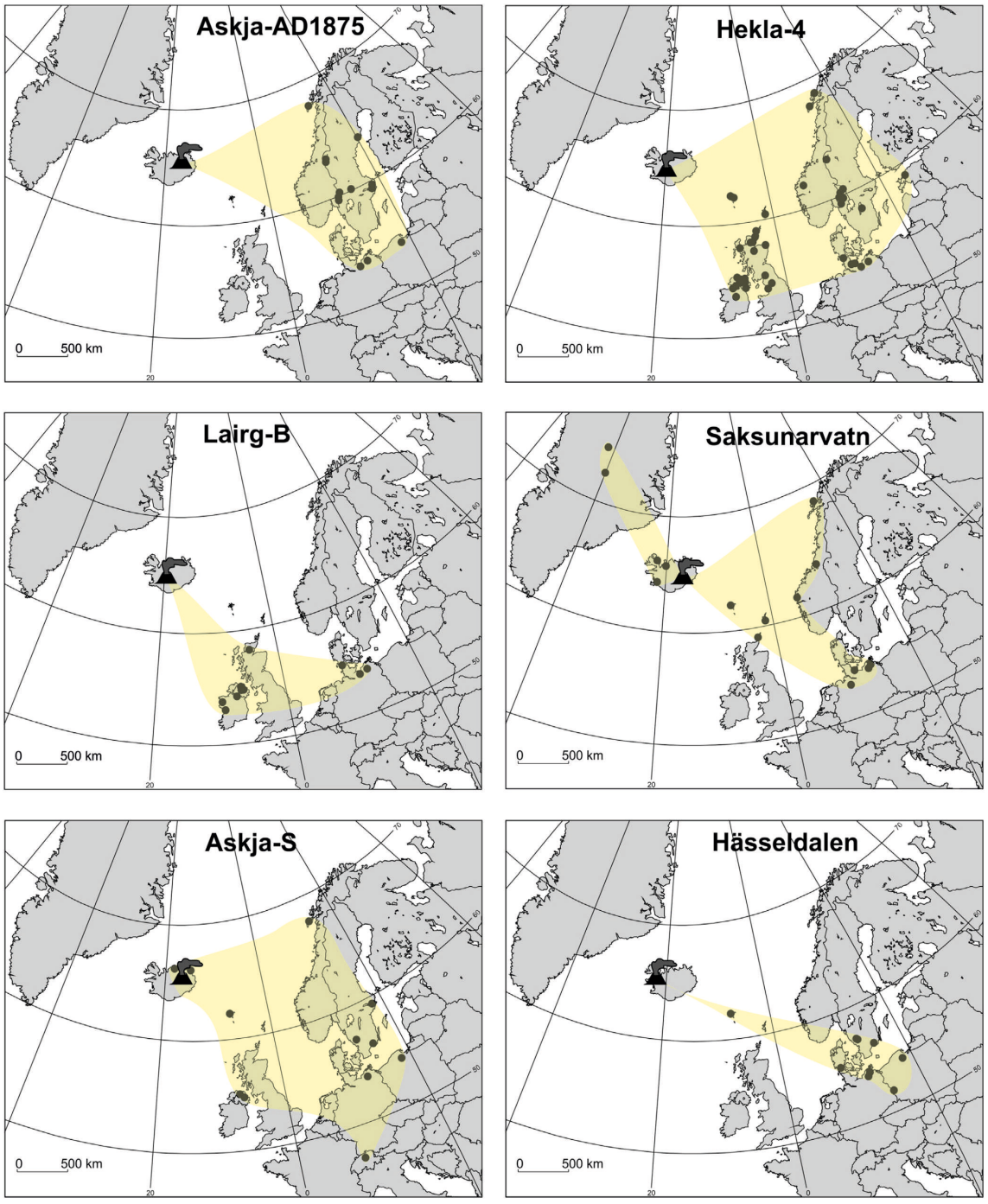

Figure 3.5: Dispersal maps of Holocene and Lateglacial tephras in northern-central Europe modified after Lawson et al. (2012) and Davies et al. (2012). Black filled dots represent terrestrial sites of tephra findings (references see text).

shard findings), the Lairg-B tephra is considered to provide an anchor point at a weighted mean age of 6683 ± 45 cal. a BP (calculated after Froggatt and Lowe, 1990) for the floating TSK varve chronology (Figure 3.2 and Figure 3.7).

Sample TSK11_A3_120–125_T (Hekla-4)

Cryptotephra TSK11_A3_120–125_T occurs at 607.9 cm composite depth and revealed two colourless, highly vesicular glass shards in a 5 cm^3 sample. The rhyolitic composition of both shards is almost identical and resembles the glass composition of distal middle to late Holocene tephras from Hekla volcano (*e.g.* Larsen and Thorarinsson, 1977; Sverrisdottir, 2007)(Figure 3.4d). At least five widespread and geochemically similar tephras occurred during this time from Hekla, *i.e.* Hekla-3 (3.0 cal. ka BP), Hekla-S/Kebister (3.8 cal. ka BP), Hekla-4 (4.3 cal. ka BP), Lairg-A (6.95 cal. ka BP) and Hekla-5 (7.1 cal. ka BP) (*e.g.* Dugmore et al., 1995b; Óladóttir et al., 2011; Gudmundsdóttir et al., 2011). All these tephras are confirmed in sites in N central Germany (Van Den Bogaard et al., 2002; Van Bogaard and Schmincke, 2002; Dörfler et al., 2012) (Figure 3.5). The best geochemical and chronostratigraphical match of the TSK tephra is achieved with the Hekla-4 tephra (Figure 3.4c). The age of the Hekla-4 tephra is constrained by radiocarbon dating at 4218 ± 65 cal. a BP (Dugmore et al., 1995b) and 4260 ± 20 cal. a BP (Pilcher et al., 1996), and by varve counting in Lake Belauer See and Swedish sites at 4342 ± 75 cal. a BP (Dörfler et al., 2012) and 4390 ± 107 cal. a BP (Zillén et al., 2002), respectively. Independent age control for the Hekla-4 cryptotephra in TSK is provided by an accelerator mass spectrometer (AMS) ^{14}C date (Poznan radiocarbon laboratory, sample POZ-55885) of a small twig located just 12 cm above the glass shard findings at 595 cm depth. The calibrated age of 4196 ± 182 cal. a BP (3800 ± 35 ^{14}C a BP) of the macrofossil remain corresponds well with the published age estimates for the Hekla-4 eruption and thus supports the correlation to this event.

Sample TSK11_B2o_84–85_T (Glen Garry?)

Two shards cm^{-3} were found in sample TSK11_B2o_84—85_T in non-laminated sediments at 401.4 cm composite depth. The major element data of one of these colourless, highly vesicular shards indicate a high silica rhyolitic composition with relatively high silica (ca. 77 wt.%) and low K_2O (ca. 2.0 wt.%) concentrations that resembles that of the late Holocene Glen Garry Tephra (GGT) (Figure 3.4c). The GGT was first detected in peat deposits in central Scotland (Dugmore et al., 1995b) and radiocarbon dated at 2088 ± 122 cal. a BP (Barber et al., 2008). The source of the GGT has not been identified yet, but geochemical similarities with the 2 ka Askja tephra point to the Dyngjufjöll vol-

canic system (Barber et al., 2008)(Figure 3.4c). The GGT was recently also identified and OSL dated at 2.1 ± 0.1 ka in the Mirkovice 33 archaeological site in NW Poland (Housley et al., 2013a)(Figure 3.5). However, the correlation of the Glen Garry tephra in TSK sediments is based only on one single analytical point and thus needs further proof. Therefore, we only tentatively attribute this glass shard to this event mainly based on its dating in TSK sediments at ca. 2100 cal. a BP (Figure 3.6).

Sample TSK13_B1u_137–142_T (unknown Grimsvötn)

Two brown, low vesicular glass shards occur in sample TSK11_B1u_137–142_T between 237.7 and 243.5 cm composite depth (240.6 cm mid-point composite depth). This basaltic cryptotephra is located in the uppermost, non-laminated sediments of the TSK record and dates between ca. 1060 ± 75 and 1094 ± 75 cal. a BP (~AD 890–856) according to varve supported sedimentation rate estimates. During historical times, at least three basaltic eruptions occurred from Icelandic volcanoes with widespread tephra dispersal, *i.e.* the AD 870 Landnám eruption from the Vatnaöldur crater, the AD ~934 Eldgjá fissure eruption in the Eastern Volcanic Zone and the AD 1477 Veiðivötn eruption (Larsen et al., 1999, 2002; Óladóttir et al., 2011). The major element chemistry of the TSK tephra, however, does not match the composition of either of those tephra, but shows a strong affinity to the Grimsvötn system due to the typical high TiO_2 concentrations of ca. 2.8 wt.% (Figure 3.4b). (Larsen, 1984) noted Grimsvötn activity between the Landnám and Eldgjá eruptions; furthermore, still emerging medial-distal tephra data indicate that the Grimsvötn system produced at least six individual tephra layers with almost identical glass composition during this time interval (Óladóttir et al., 2011)(Figure 3.4b). Therefore, and because of the low number of detected glass shards in TSK sediments prevents from an attribution to a specific event.

Sample TSK11_K3_33–34_T (Askja-AD 1875)

The uppermost cryptotephra in the TSK sequence, TSK11_K3_33–34_T, occurs in 46.7 cm composite depth and encompasses at least 40 colourless to light brownish glass shards (Figure 3.3). The cryptotephra is positioned in non-laminated sediments ca. 9 cm below the topmost well-varved interval which dates between AD 2010 and AD 1924 (Kienel et al., 2013). The major element composition of glass shards is heterogeneous rhyolitic with two populations that mainly differ in CaO (2.3–2.8 wt.% vs. 3.2–3.4 wt.%) and FeO(3.1–3.9 wt.% vs. 4.5–4.8 wt.%) concentrations (Table 3.1). The glass chemistry shows some affinity to the Glen Garry Tephra with slightly higher TiO_2 (ca. 0.7–1.2 wt.%) and MgO (ca. 0.7–1.0 wt.%) contents. Several historical, silicic and

widespread eruptions before AD 1924 are reported from Iceland, *i.e.* Askja-AD 1875, Hekla-AD 1510, Öræfajökull-AD 1362 and Hekla-AD 1104 (*e.g.* Larsen et al., 1999, 2002; Óladóttir et al., 2011). The best geochemical match of tephra TSK11_K3_33–34_T is given for the Askja-AD 1875 tephra (Figure 3.4a). The Plinian Askja-AD 1875 eruption occurred at the Dyngjufjöll volcanic centre in NE Iceland and resulted in the formation of the Öskjuvatn caldera, which is nested within the larger and older (10 ka) Askja caldera (*e.g.* Sigurdsson and Sparks, 1978, 1981). Askja-AD 1875 was one of the largest historical eruption on Iceland with a magnitude of VEI 5 (http://www.volcano.si.edu; Carey et al., 2009). The main eruption started on March 28th 1875 and produced a series of subplinian fallout (Unit B), phreatoplinian fall (Unit C1) and flow (Unit C2) and Plinian fallout deposits (Unit D) (Carey et al., 2009; Self and Sparks, 1978). Tephra from units C and subunits D1, D3 and D5 were widely dispersed towards the East and Southeast over Scandinavia (Carey et al., 2009; Mohn, 1878) and have been found in numerous lake and peat records in Norway (*e.g.* Pilcher et al., 2005), Sweden (*e.g.* Bergman et al., 2004; Boygle, 1998; Davies et al., 2007; Oldfield et al., 1997; Wastegård, 2005; Wastegård and Davies, 2009), and possibly N central Germany (Van Bogaard and Schmincke, 2002)(Figure 3.5). The composition of the Askja-AD 1875 tephra in TSK sediments is similar to that of other distal tephras and that of proximal Unit D fallout deposits (Figure 3.4a). The Askja-AD 1875 tephra is an excellent time marker in TSK sediments that allows the precise synchronization with palaeoenvironmental records from Scandinavia and across the western and central Baltic region

3.4.2 Lake Czechowskie Holocene tephrostratigrapgy

Sample JC12_D6_112–113_T (Hässeldalen)

The lowermost cryptotephra JC12_D6_112–113_T in Lake Czechowskie is embedded in laminated sediments in 1158.5 cm composite depth, 18 cm above the biostratigraphically defined Younger Dryas/Holocene transition. The tephra exhibited 3 colourless, high-vesicular shards cm^{-3}, which all show a rhyolitic composition. The major element glass chemistry is characterized by relatively low FeO (ca. 1.2 wt.%) and CaO (ca. 0.5. wt.%) contents, as well as high SiO_2 (77.9–78.3 wt.%) and K_2O (3.9–4.5 wt.%) concentrations. The glass chemical composition in combination with the stratigraphic position of tephra JC12_D6_112–113_T above the Younger Dryas/Holocene boundary suggest a correlation with the early Holocene Hässeldalen tephra (HDT; 11,380 ± 216 cal. a BP; Wohlfarth et al., 2006)(Figure 3.4f) and is also comparable to tephra TSK13_F6_99–100_T from Lake Tiefer See. The HDT represents an isochron

for the synchronization of JC and TSK sediment records ca. 200 after the onset of the Holocene.

Sample JC12_D6_95–95.5_T (Askja-S)

Cryptotephra JC12_D6_95–95.5_T is positioned in laminated sediments in 1141.25 cm composite depth, ca. 17 cm above the Hässeldalen Tephra. It contained 22 colourless, high vesicular to cuspate glass shards cm^{-3} (Figure 3.3), of which 13 shards have been geochemically analysed. The major element chemistry revealed a homogeneous, high silica (76.2–77.1 wt.%) rhyolitic composition that matches best the glass compositions of the early Holocene Askja-S tephra (Figure 3.4d). Since it further resembles the Tiefer See tephra TSK13_F6_91–92_T both lake records can be unequivocally synchronized using this tephra.

Samples JC09_B2_170–173_T and JC09_B2_155–158_T (unknown Icelandic?)

Two cryptotephras of identical composition have been identified in varved late Holocene JC sediments in 495.5 cm and 480.5 cm composite depth. Samples JC09_ B2_170–173_T and JC09_B2_155–158_T exhibited 2 and 6 shards per 3 cm^3 sediment sample, respectively. All shards are colourless, highly vesicular and of high silica rhyolitic composition (Figure 3.4c). Preliminary varve counting suggests a deposition of cryptotephras at 1960 ± 20 varve a BP and 1890 ± 20 varve a BP, respectively. Comparison with major element glass data of proximal and distal tephras from Iceland and Jan Mayen from this time period suggests a tentative match with the high-silica glass population of the DOM-4 tephra (ca. 1550 interpolated ^{14}C a BP) from Dosenmoor in N Germany (Van Bogaard and Schmincke, 2002)(Figure 3.4c). DOM-4 has been assigned to unknown Icelandic silicic activities (Van den Bogaard and Schmincke, 2002). Therewith, tephras JC09_B2_170–173_T and JC09_B2_155–158_T cannot be used as isochrones for synchronization.

Sample JC12_K2_35–36_T (Askja-AD 1875)

The uppermost cryptotephra JC12_K2_35–36_T is located in varved sediments in 48.5 cm composite depth. It revealed ten colourless to light brownish, high-vesicular glass shards (Figure 3.3) of homogenous rhyolitic composition. The major element glass chemistry strongly resembles that of the less evolved glass population of tephra TSK_K3_33–34_T and the proximal Askja-AD 1875 tephra deposits (Figure 3.4a). The

Askja-AD 1875 tephra in Lake Czechowskie sediments is the first finding in Polish sites (Wulf et al., 2014). It provides an excellent correlation marker for the comparison of historical palaeoenvironmental data with Lake Tiefer See as well as other records.

3.4.3 Tephrochronologies

Lake Tiefer See

One visible tephra layer and seven cryptotephras have been identified in the sediment sequence of Lake Tiefer See. Six of these tephras were correlated with dated erupted events and thus represent well-suited time markers for the construction of a detailed tephrochronology of TSK sediments (Figure 3.6a). The possible Hässeldalen and Askja-S tephras likely represent anchor points for the non-laminated early Holocene interval. The Saksunarvatn Ash layer (10,210 ± 35 cal. a BP), Lairg-B (6683 ± 45 cal. a BP) and Hekla-4 (4293 ± 43 cal. a BP) cryptotephras represent isochrones for the floating varved early to mid-Holocene intervals. The historical Askja-AD 1875 tephra forms an essential time marker for the validation of sedimentation rate estimates in the partially non-laminated, late Holocene sediments. The tentatively assigned Glen Garry Tephra (2088 ± 122 cal. a BP) is not used in the TSK age model since tephrochronological correlation still needs further proof. Based on the tephrochronological results, a preliminary chronology is constructed for the TSK sediment sequence. This chronology will be compared in detail with the on-going independent dating based on varve counting, sedimentation rate estimates and radiocarbon dating. Presently, we can roughly infer mean sedimentation rates of ~0.7 mm/a for the mid-Holocene since the deposition of the Hekla-4 tephra and 1.0 mm/a up to 3.5 mm/a during the late Holocene and recent time periods, respectively.

Lake Czechowskie

Five cryptotephra horizons have been identified in Lake Czechowskie sediments, of which three tephras provide robust anchor points for the JC chronology (Figure 3.6b). The early Holocene Askja-S and the likely Hässeldalen tephras are especially important since they represent isochrones within the floating varved section between ca. 12 m and 11 m composite depth. The Askja-AD 1875 tephra is a time marker for the varved sediments of historical times and is applicable to validate varve counts in sub-recent sediments. Based only on the tephra occurrences we can calculate rough and average sedimentation rates for the Holocene (ca. 1 mm/a) and historical times after the Askja-

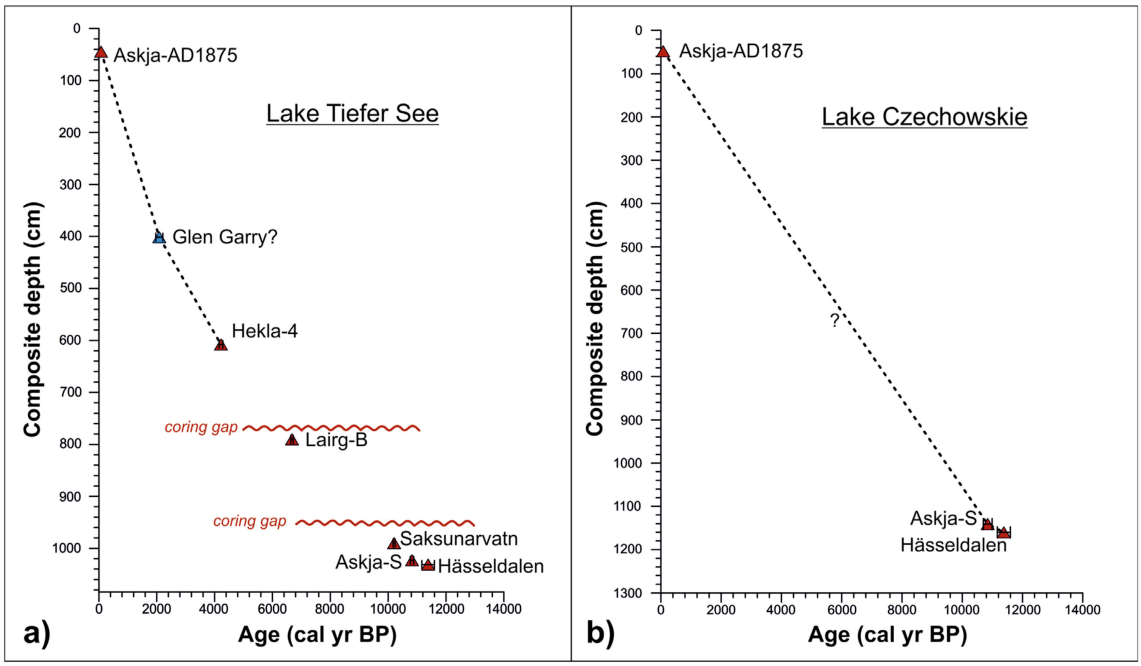

Figure 3.6: Tephrochronologies of sediment sequences from Lake Tiefer See (a) and Lake Czechowskie (b). Red triangles are imported tephra ages (references see text) with a 2σ error bar. The dotted lines result from linear interpolation between tephra ages, whereby the question mark at the JC tephrochronology indicates the difficulty of sedimentation rate estimations.

AD 1875 tephra (ca. 3.6 mm/a). However, the limited number of tephra anchor points obviously does not allow more detailed measurements of the variability.

3.4.4 Tephra dispersal in central and northern Europe

The tephra findings in the partially varved sediment records of Lake Tiefer See and Lake Czechowskie provide the potential to directly compare palaeoclimate information of these records with other high-resolution data from continental Central and Northern Europe. First examples from comparisons of varved Lateglacial records along E–W (Lake Meerfelder Maar, Rehwiese and Trzechowskie palaeolakes; Słowiński et al., 2015; Wulf et al., 2013) and N–S transects (Lakes Meerfelder Maar and Kråkenes; Lane et al., 2013; Rach et al., 2014) have demonstrated the capability of detangling temporal and spatial offsets of palaeoenvironmental and palaeoecological responses to past abrupt climate changes by using tephra isochrones. With the new results presented here, it is possible to extend these comparisons to the Holocene and historical time periods (Figure 3.7).

The Askja-S and likely the Hässeldalen tephras are unequivocal marker layers for the synchronization of early Holocene sediment records. The number of sites where they have been found, however, is restricted to a few records in northern and central

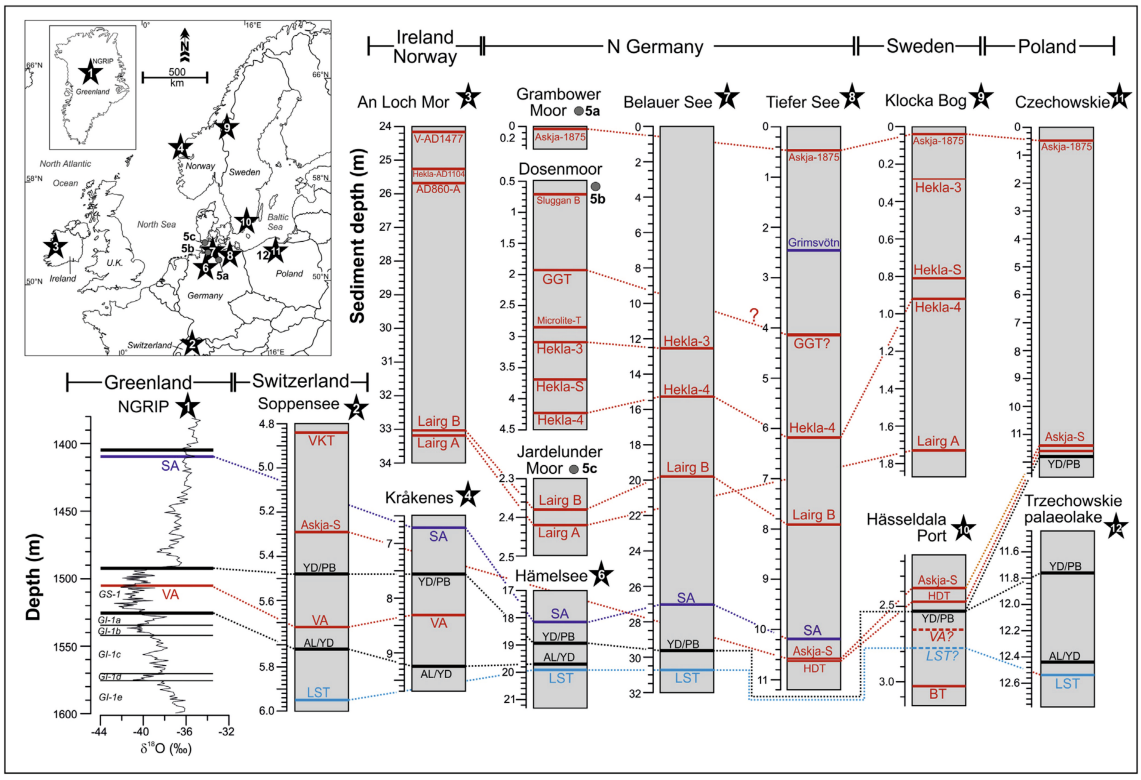

Figure 3.7: Tephrostratigraphical linking of Lake Tiefer See and Lake Czechowskie sediment sequences with other high-resolution records from northern and central Europe. Note that all records are plotted against sediment depth in meter. Acronyms for biostratigraphical boundaries (black lines): PB=Preboreal, YD=Younger Dryas, AL=Allerød. Tephra acronyms: GGT=Glen Garry Tephra, VKT=Vasset-Kilian Tephra (French Massif Central), SA=Saksunarvatn Ash, HDT=Hässeldalen Tephra, VA=Vedde Ash, LST=Laacher See Tephra, BT=Borrobol Tephra. Inlet map of central and northern Europe showing the location of sites used for tephrostratigraphical comparison. Data are obtained from: (1) NGRIP (Mortensen et al., 2005; Rasmussen et al., 2006, 2014; Vinther et al., 2006); (2) Lake Soppensee (Lane et al., 2011); (3) An Loch Mor (Chambers et al., 2004); (4) Kråkenes (Lohne et al., 2013), (5a) Grambower Moor; (5b) Dosenmoor; (5c) Jardelunder Moor (Van Bogaard and Schmincke, 2002); (6) Hämelsee (Merkt and Müller, 1999; Merkt et al., 1993); (7) Lake Belauer See (Dörfler et al., 2012; Merkt and Müller, 1999); (8) Lake Tiefer See (this study); (9) Klocka Bog (Bergman et al., 2004); (10) Hässeldala Port (Davies et al., 2003; Wohlfarth et al., 2006); (11) Lake Czechowskie (this study); (12) Trzechowskie palaeolake (Wulf et al., 2013).

Europe (Figure 3.5). Therefore, our new findings in the TSK and JC records are a further addition to the construction of a more detailed dispersal map (Figure 3.5). Their occurrences in the Polish site even are of particular interest, since this is, on the one hand, the furthest south-easterly dispersal so far (Figure 3.5). Furthermore, the Hässeldalen and Askja-S tephras in Lake Czechowskie are the first occurrences in annually laminated sediments, thus allowing to apply a differential dating for estimating the time span between these two eruptions.

The finding of the visible Saksunarvatn Ash in the TSK record, in turn, is in agreement with previous finds in NE Germany (Merkt et al., 1993; Bramham-Law et al., 2013) and thus confirms the proposed dispersal map by Davies et al. (2012) (Figure 3.5). The Lairg-B and Hekla-4 tephra occurrences in TSK are the furthest towards the southeast and, similar to the likely Glen Garry tephra, supplements the previous findings in northern central Germany. The distribution of the historical Askja-AD 1875 tephra has been eye-witnessed and described by an initial easterly dispersal axis that changed over Sweden into a southerly direction (Mohn, 1878; Carey et al., 2009). However, findings of this tephra in sedimentary repositories are mainly restricted to Norway and Sweden; a single occurrence in N Germany is still debated (Van Bogaard and Schmincke, 2002). With the unambiguous identification of the Askja-AD 1875 tephra in TSK and JC sediments we confirm the southerly dispersal direction and extend the distribution limit further to the east than previously supposed (Figure 3.5).

3.5 Conclusions

The recently developed methods for cryptotephra identification allowed detecting and geochemical fingerprinting of thirteen cryptotephras from at least ten distinct eruptions of Icelandic volcanoes in the Holocene sediments of Lake Tiefer See and Lake Czechowskie. Half of cryptotephras are characterized by very low glass shard concentrations (*e.g.* 1–3 shards per 1–5 cm^3 sediment samples) due to the extreme distal location of investigated sites. Those shards are interpreted as primary deposits based on (1) the lack of findings in over- and underlying samples and (2) the non- disturbed and varved character of Holocene sediments. We need to stress, however, that further shard findings and geochemical analyses are needed to enhance the reliability of some of our tephra correlations. Accordingly, we used mainly tephras with higher shard concentrations, *i.e.* the Askja-AD 1875, Saksunarvatn and Askja-S tephras, to construct reliable tephrochronologies that will, on the one hand, validate established varve chronologies and, on the other hand, provide valuable anchor points for chronologies of intercalated varved and non-varved sections. In addition, these tephrochronologies are a prerequisite for the synchronization of proxy data from sediment records in the southern Baltic region and beyond, which was recently stresses by the INTIMATE (INTegrating Ice core, Marine and TErrestrial records) group (Feurdean et al., 2014). The cryptotephra findings especially in Lake Czechowskie evidence a further eastward dispersal of Lateglacial and Holocene volcanic ash from Iceland than previously proposed. Moreover, our results demonstrate the great potential also for other recently reported

varved lake sediment records from northern Poland (Kinder et al., 2013; Tylmann et al., 2013a,b) and the key palaeoclimate records from Lake Gościąż and Perespilno (Goslar et al., 1999, 1993).

Acknowledgements

We are grateful to the German-Polish team, Brian Brademann, Robert Schedel, Michael Köhler (MKfactory), Stefan Lauterbach, Robert Weißbach, Mateusz Kramkowski, Sebastian Tyszkowski, and Jarosław Kordowski, for sediment coring in Lakes Tiefer See and Lake Czechowskie. Andreas Hendrich kindly helped with the improvement of the figure design. We especially thank our student helpers for tephra sample processing, namely Katharina Schorling, Alexander Adams, Nadine Schilling, Nathalie Dust, and Yevheniia Korniienko. We thank Jörg Gast and Ralf Koch from the Naturpark Nossentiner Schwinzer Heide and the mayor Reinhard Block of the village Neu Gaarz for support. We are furthermore very grateful to two anonymous journal reviewers for their constructive comments on our manuscript. This study has been financed by the Virtual Institute of Integrated Climate and Landscape Evolution Analysis -ICLEA-, grant number VH-VI-415, of the Helmholtz Association and the National Science Centre, Poland (grants no. NN306085037 and 2011/01/B/ST10/07367). It is further a contribution to the climate initiative REKLIM Topic 8 "Abrupt climate change derived from proxy data" and has used infrastructure of the Terrestrial Environmental Observatory (TERENO), both of the Helmholtz Association.

4 Varying controls on $\delta^{13}C_{OM}$ of sedimentary organic matter in the partially varved sediment record of Lake Tiefer See (NE Germany) over the last 6000 years

Nadine Dräger[a,*],Birgit Plessen[a], Ulrike Kienel[a,b], Miriam Groß-Schmölders[a], Arne Ramisch[a], Achim Brauer[a]

[a] GFZ German Research Centre for Geosciences, Section 5.2 Climate Dynamics and Landscape Evolution, Telegrafenberg C, D-14473 Potsdam, Germany

[b] 2 Institute for Geography and Geology, Ernst-Moritz-Arndt University Greifswald, Friedrich-Ludwig-Jahn-Str. 16, D-17487 Greifswald, Germany

[*] Corresponding author

Abstract

The stable carbon isotopic composition of sedimentary organic matter ($\delta^{13}C_{OM}$) is widely used for palaeoclimate and -environmental studies, but proxy interpretation is not straightforward as different factors influence $\delta^{13}C_{OM}$. In order to understand the controlling mechanisms of $\delta^{13}C_{OM}$ in the partly annually laminated (varved) sediment profile of Lake Tiefer See during the last ~6000 years, we complemented measurements from a long sediment profile with analyses of surface cores from different water depths and monitoring data. The $\delta^{13}C_{OM}$ record of the long sediment core exhibits abrupt variations corresponding to changes in varve preservation and total organic carbon (TOC) contents, with more negative $\delta^{13}C_{OM}$ ratios in the organic-rich and well-varved sediment intervals (on average -31‰) as compared organic-poor and non-varved intervals (on average -29‰). Our results indicate that the fluctuations of $\delta^{13}C_{OM}$ observed in the long sediment profile are caused by a combination of factors, whose relative influence changes over time. Depleted $\delta^{13}C_{OM}$ ratios in well-varved intervals are probably related to increased microbial carbon cycling in oxygen deficient bottom waters, as suggested by significant negative correlations of $\delta^{13}C_{OM}$ and $\delta^{15}N$. On the contrary, in non-varved intervals increased OM degradation in the oxygen rich bottom waters presumably induced positive shifts of $\delta^{13}C_{OM}$. This is indicated by a strong negative correlation of $\delta^{13}C_{OM}$ and TOC contents. Further evidence is provided by the surface cores, which exhibit a negative shift of $\delta^{13}C_{OM}$ at the most recent transition

from non-varved to well-varved sediments. Depending on the water depth the onset of varve preservation occurred at different times (*e.g.* AD 1924 in 62 m water depth; AD 1981 in 20 m water depth). Since sediment trap data indicate $\delta^{13}C_{OM}$ values (-30.5‰) in the entire water column similar to the uppermost well-varved parts of the surface cores, it is unlikely that the more enriched $\delta^{13}C_{OM}$ ratios are caused by processes in the water column, because this should be seen in all cores at the same time. The presented results imply that $\delta^{13}C_{OM}$ may not always represent a uniform proxy within a sediment profile. A combination of $\delta^{13}C_{OM}$ analysis with complementary microfacies analysis is a suitable approach to facilitate an improved interpretation of stable carbon isotope data.

Highlights

- Complementary analyses of a long multi-proxy sediment record, surface sediment cores from different water depths and monitoring data
- New $\delta^{13}C_{OM}$ and $\delta^{15}N$ records for the last 6000 years at decadal resolution
- $\delta^{13}C_{OM}$ is a complex proxy which controlling factors change in response to the redox regime
- knowledge of sediment facies is important for $\delta^{13}C_{OM}$ interpretation

4.1 Introduction

Stable carbon isotopes of sedimentary organic matter ($\delta^{13}C_{OM}$) are commonly used as proxy in palaeolimnological studies and provide a valuable indicator for reconstructing palaeoclimate and -environmental conditions (Lamb et al., 2004; Meyers and Ishiwatari, 1993; Meyers, 1994). However, proxy interpretation is not straightforward, as different factors influence $\delta^{13}C_{OM}$ including productivity, source of organic matter (OM), microbial carbon cycling and diagenetic processes.

Commonly, the $\delta^{13}C_{OM}$ ratio is applied as a proxy for the primary productivity in the phototrophic zone of the lake (*e.g.* Brenner et al., 1999; Lücke et al., 2003; Stuiver, 1975). As photosynthesis preferentially utilises ^{12}C, the dissolved inorganic carbon pool in the lake water becomes enriched in ^{13}C during phases of increased productivity (Talbot and Lærdal, 2000)). As a result, $\delta^{13}C_{OM}$ values of algal biomass are more enriched with higher lake productivity.

The source of OM is another determinant factor of sedimentary $\delta^{13}C_{OM}$ (Cheung et al., 2015; Müller and Voss, 1999) . Particulate OM in lake sediments is often a mixture

of *e.g.* terrestrial plants, aquatic macrophytes and phytoplankton, which are characterized by different $\delta^{13}C_{OM}$ signatures (lacustrine plankton -20‰ to -35‰ and aquatic and terrestrial plants -15‰ to -28‰) (Meyers, 1994). A change of the contribution of these sources may thus lead to shifts in $\delta^{13}C_{OM}$ (Emerson and Hedges, 1988).

Microbial carbon cycling is rarely considered to affect $\delta^{13}C_{OM}$ ratios. However, seasonally anoxic lakes may favour microbial processes (*e.g.* methanogenesis, sulphate reduction, chemoautrophy and methanotrophy), which have been shown to influence sedimentary $\delta^{13}C_{OM}$ ratios (Hollander and Smith, 2001). For example, biogenic methane and respired CO_2 produced by anaerobic decomposition of OM are characterized by strongly depleted $\delta^{13}C$ signatures (Hollander and Smith, 2001; Whiticar et al., 1986). Incorporation of the ^{13}C-depleted methane and CO_2 in methanotrophic organisms, chemoautrophs and planktonic algae results in the production of highly $\delta^{13}C$ depleted biomass (Heyng et al., 2012; Hollander and Smith, 2001; Lehmann et al., 2004), resulting in decreased sedimentary $\delta^{13}C_{OM}$.

Sediment diagenesis is further considered to weakly influence $\delta^{13}C_{OM}$ values (Hodell and Schelske, 1998; Meyers and Lallier-Vergés, 1999). Significant $\delta^{13}C_{OM}$ enrichment (+1.5‰) in lake sediments associated with OM deposition during a more oxygenated water column have been explained by the absence of microbial carbon cycling (Kohzu et al., 2011). Furthermore, more positive $\delta^{13}C_{OM}$ values during more oxic conditions have been related to increased OM degradation (Mollenhauer and Eglinton, 2007). OM degradation is not homogenous, as the labile fraction of OM produced by phytoplankton is re-mineralized more quickly relative to allochthonous terrigenous OM, due to the intrinsic chemical stability of the latter and their physical association with mineral matrices (Canuel and Martens, 1996; Hedges et al., 1999; Ingalls et al., 2004; Mollenhauer and Eglinton, 2007). Increased OM degradation leads to an enrichment in terrestrial OM, which is characterized by higher $\delta^{13}C_{OM}$ values and, consequently, results in a positive shift of sedimentary $\delta^{13}C_{OM}$ (Goossens et al., 1989).

This broad range of potential controls challenges the interpretation of the $\delta^{13}C_{OM}$ record in a palaeoenvironmental context. Some of the controlling factors, as microbial carbon cycling and diagenetic processes, are influenced by the prevailing redox conditions in the lake. The sediment record of lake Tiefer See, located in NE Germany, reveals striking fluctuation of bottom water oxygenation during the past 6000 years on decadal to multi-centennial time scales (Dräger et al., 2016). Here we analyse the impact of distinct anoxic-oxic oscillations on the $\delta^{13}C_{OM}$ record of Lake Tiefer See. In particular, we test the range of potential controls by comparing $\delta^{13}C_{OM}$ to indicators of productivity, OM source as well as microbial carbon cycling and diagenesis.

4.2 Study Site

Lake Tiefer See (Figure 4.1; 53°35.5'N, 12°31.8'E; 62 m a.s.l) is located in the Mecklenburg lake district, NE Germany, approximately 20 km NW of Waren Müritz (Mecklenburg Vorpommern). The lake was formed during the last glaciation. Lake Tiefer See is part of the Klocksin Lake Chain, which is a former subglacial channel system that crosses the Pomeranian terminal moraine. The surface area of the north-south oriented and oval shaped lake amounts to 0.75 km^2. The maximum depth corresponds to 62 m. An ongoing monitoring study at Lake Tiefer See showed that the lake is mesotrophic and either mono- or dimictic, depending on the formation of a winter ice cover (Kienel et al., 2013; Nixdorf et al., 2004). The catchment area of approximately 5.5 km^2 is dominated by glacial till of the Pomeranian terminal moraine (Kienel et al., 2013; Landesamt für Umwelt, 2000) and is presently used as arable land. Mean monthly temperatures range from 0°C in January to 18°C in July. Mean monthly precipitation values fluctuate between ~40 mm during winter to ~60 mm in summer with a mean annual precipitation of 560 mm.

4.3 Material and Methods

4.3.1 Long sediment core

Seven parallel long sediment cores were retrieved between 2011 and 2013 at the deepest part of Lake Tiefer See using a 90-mm UWITEC piston corer. The constructed composite profile extends down to 10.8 m sediment depth and reaches glacial sands on the base. Due to sediment loss during the coring process the sediment profile indicates to gaps and thus is non-continuous below 7.7 m depth (for further details see Dräger et al. (2016)). Therefore, we restricted the investigation to the uppermost 7.7 m long continuous composite profile. Sub-sampling for bulk geochemical analyses was carried out continuously at 1 cm resolution, comprising 7 years per sample on average (2–6 years above 3.95 m; 4–24 years below 3.95 m depth).

The sediments of the analysed 7.7 m long section of the composite profile alternate between well-varved and non-varved intervals. Well-varved sediments are mainly composed of carbonates (calcite and Ca-rhodochrosite), diatoms and organic matter. Poorly- and non-laminated sediment intervals are enriched in quartz grains, plant fragments, benthic diatoms and occasionally bivalves. Distinctness of lamination is expressed by the varve quality index (VQI; details see Dräger et al., 2016), which was obtained during microfacies analysis of the sediment and ranges between 4 (well-varved)

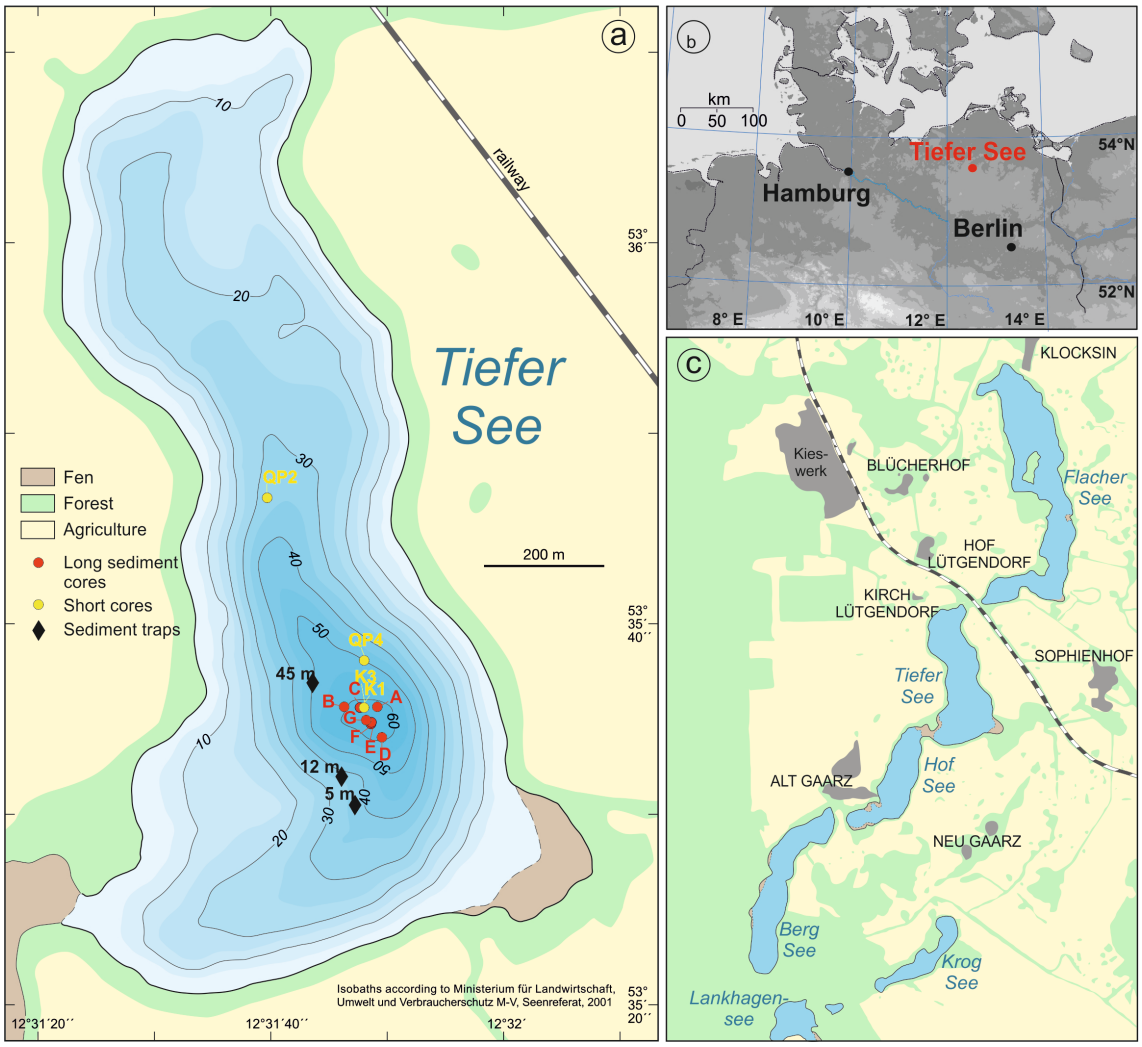

Figure 4.1: Bathymetric map (a) showing the locations of the long sediment cores (red dots), the surface cores (yellow dots) and the sediment traps (black diamonds). Location (b) of Lake Tiefer See in the Klocksin Lake Chain and land cover in the catchment area (c).

and 0 (non-varved) (Figure 4.2). According to the level of varve quality seven multi-centennial scale sediment units are distinguished (Dräger et al., 2016). The chronology of the long sediment profile (0–7.7 m) is based on varve counting in well- and poorly-varved intervals, varve-based sedimentation rate estimates in non-varved sections and tephrochronology (Dräger et al., 2016; Wulf et al., 2016). Chronology uncertainties are variable along the sediment record and amount to 6030 ± 85 cal. a BP at the base of the studies interval. All ages in this study are given as calibrated years before present AD 1950 (cal. yr BP) or in the historic period in years Anno Domini (AD).

4.3.2 Surface sediment cores

Four parallel surface cores were recovered in 2013 at different water depths (TSK13-QP2 at 35 m, TSK13-QP4 at 48 m)of Lake Tiefer See using a 90-mm UWITEC gravity corer.The surface cores were sampled for preparation of thin sections and parallel in 1 cm intervals for bulk geochemical analysis from 0–65 cm sediment depth. For preparation of thin sections, sediment bars (10 x 2 x 1 cm) were cut out of the fresh sediment with 2 cm overlaps to enable continuous analysis. The thin sections were prepared according to the standard procedure including freeze-drying and impregnation with epoxy resin (Brauer and Casanova, 2001). Microscopic analysis comprised of varve counting in well laminated sediment intervals using a petrographic microscope with parallel and polarized light and 50x to 400x magnifications (Carl Zeiss Axioplan).

4.3.3 Sediment trap material and catchment samples

The modern lake deposition was trapped at three water depths between 2012 and 2015. At 5 m and 12 m water depth material was collected with 4-cylinder traps with a sampling period of one month. An automated trap (Technicap PPS 3/3) equipped with 12 sample bottles was used at 45 m water depth with a bi-weekly sampling period. In addition, 33 catchment samples were collected in the surrounding of Lake Tiefer See, including 21 top soil samples, four reed samples and eight plant litter samples.

4.3.4 Geochemical and isotopic analysis of bulk samples

Total organic carbon (TOC) and total nitrogen (TN) contents were determined continuously at 1 cm increments in the long (731 samples) and the surface sediment cores (65 samples each core). The $\delta^{13}C_{OM}$ ratios were measured in the long sediment profile continuously from 0–0.4 m depth and at 2 cm resolution (~15 year resolution) from 0.4–7.7 m depth (in total 369 samples), and continuously in the surface sediment cores. $\delta^{15}N$ values were determined in the long sediment profile continuously from 0–2.5 m depth and at 2 cm intervals from 2.5–7.7 m depth (in total 529 samples).

For geochemical and isotopic analysis all samples were freeze-dried and homogenized with an agate mortar. For estimation of the total organic carbon (TOC) content and the stable carbon isotope ratio of organic matter ($\delta^{13}C_{OM}$), about 1 to 4 mg sediment were weighted in Ag capsules, treated with 20% HCl, dried at 75°C and subsequently processed in a Carlo Erba NC 2500 elemental analyser coupled to a Finnigan DELTAplusXL isotope ratio mass spectrometer (IRMS). The calibration was performed using elemental (Urea) and certified isotopic standards (USGS24, CH-7) and proved

with an internal soil reference sample (Boden3). The reproducibility for replicate analyses is 0.2 wt.% for TOC and 0.2‰ for $\delta^{13}C_{OM}$.

In order to test if the TOC and $\delta^{13}C_{OM}$ results are biased by incomplete dissolution of Ca-rhodochrosite during *in situ* decalcification, ten samples containing Ca-rhodochrosite were additionally decalcified in heated glass beakers for one day allowing the entirely dissolution of the different carbonate fractions. Deviations of both methods are in the order of $\pm$ 0.2‰ and are thus within the standard deviation of isotope measurement and prove the validity of using *in situ* decalcification.

Additionally to $\delta^{13}C_{OM}$, stable nitrogen isotopes ($\delta^{15}N$) were analysed in the long sediment profile at the same resolution. The measurements were carried out with the identical isotopic facility as used for $\delta^{13}C_{OM}$ measurements, but 3–15 mg sediment was weighted in Sn capsules without acid treatment. Total nitrogen (TN) contents were calibrated against Acetanilide and $\delta^{15}N$ using two ammonium sulphate standards (*e.g.* IAEA N-1 and N-2). Values for $\delta^{15}N$ of replicate digestions of reference samples show a standard deviation better than 0.2 wt.% for TN and 0.2‰ for $\delta^{15}N$.

TOC and TN contents were used to calculate the atomic C:N ratio. Results of $\delta^{13}C_{OM}$ and $\delta^{15}N$ are expresses in the conventional δ-notation relative to the Vienna PeeDee Belemnite (VPDB) and atmospheric nitrogen (AIR) standards, respectively.

4.4 Results

4.4.1 Long sediment record

4.4.1.1 $\delta^{13}C_{OM}$ and $\delta^{15}N$

The $\delta^{13}C_{OM}$ ratio varied by nearly 5‰, with values between -32.7‰ and -27.8‰ (Figure 4.3). In general, $\delta^{13}C_{OM}$ exhibited an opposite pattern to the VQI, meaning that intervals of enriched $\delta^{13}C_{OM}$ are coinciding with phases of poorly- and non-preserved varves and depleted $\delta^{13}C_{OM}$ ratios occur in well-varved intervals. $\delta^{13}C_{OM}$ reached highest values in the non-varved sediment units II (3940–3100 cal. a BP) and VI (AD 1200–1924) with an average of -29 ‰ and maximum values of up to -27.8‰. The poorly-varved unit IV (2850–2100 cal. a BP) and decadal scale poorly-varved intervals in unit I (5930–5885 cal. a BP, 5405–5360 cal. a BP, 4985–4900 cal. a BP, 4735–4680 cal. a BP and 4435–4370 cal. a BP) and in unit V (1825–1795 cal. a BP, 1620–1440 cal. a BP, 1240–1195 cal. a BP and 990–895 cal. a BP) showed intermediate values with an average of -30 ‰. Well-varved intervals in units I (6030–3950 cal. a BP), III (3100–2850 cal. a

BP), V (2100–750 cal. a BP) and VII (AD 1924–2010) were characterized by lower $\delta^{13}C_{OM}$ ratios with an average of 31‰ and lowest values of -32.7‰.

$\delta^{15}N$ ratios varied between 4 and 0.8‰ from 6000 cal. a BP to AD 1800 (Figure 4.3). Up to the onset of the poorly-varved unit IV (2850 cal. a BP) $\delta^{15}N$ fluctuated around a constant mean of ~3‰. After 2850 cal. a BP $\delta^{15}N$ abruptly decreased towards minimum values between ~2750 and ~2500 cal. a BP with on average 1.2‰ and minimum values of 0.8‰. After 2500 cal. yr BP $\delta^{15}N$ values rose again towards mean values of 2.1‰ at the transition to the well-varved unit V at 2100 cal. a BP. In units V and VI (2100 cal. a BP–AD 1800) the values varied around a mean of 3‰, whereas the fluctuation of values became higher in unit VI. Since AD 1800 $\delta^{15}N$ exceeded the preindustrial maximum values of 4‰ and reached highest ratios 7.9‰ at AD 1985.

The relationship between $\delta^{13}C_{OM}$ and $\delta^{15}N$ varies in the different sediment units. In the dominantly well-varved sediment units I, III and V $\delta^{13}C_{OM}$ and $\delta^{15}N$ ratios were negatively correlated (r=-0.47; Table 4.1). In contrast, in non- and poorly-varved sediment units II, IV and VI both isotopes exhibit a positive relationship (r=0.61; Table 4.1) with higher values of both in unit VI (AD 1200–1800) compared to units II (3950–3100 cal. a BP) and IV (2850–2100 cal. a BP). The sub-recent sediments since ~AD 1800 showed a different signature with much higher $\delta^{15}N$ values of up to 8.5‰ and intermediate $\delta^{13}C_{OM}$ ratios.

4.4.1.2 TN, TOC and C:N

The total nitrogen (TN) content and the total organic carbon (TOC) contents are positively correlated (r=0.94; Figure 4.4; Table 4.1) suggesting that both elements are present as organically bound compounds (Talbot and Johannessen, 1992). Furthermore, TOC and TN contents indicated a relation to changes of varve preservation. The values were typically lower (TN: ~0.6 wt.%; TOC: ~5 wt.%) in non-varved and increased (TN: ~1.5 wt.%; TOC: ~15 wt.%) in well-varved sediment units. An exception was the poorly-varved unit IV, which was characterized by intermediate and highly fluctuating TN and TOC contents (Figure 4.3).

TOC and $\delta^{13}C_{OM}$ are negatively correlated (r=-0.66). Depleted $\delta^{13}C_{OM}$ values coincide with higher TOC contents and originate from well-varved sediment intervals (Units I, II and V). In contrast, the non-varved units II and VI indicate more enriched $\delta^{13}C_{OM}$ ratios and lower TOC contents. The non-varved unit IV partly falls into the well-varved point cloud, but in the field with more positive $\delta^{13}C_{OM}$ values as compared to well-varved intervals.

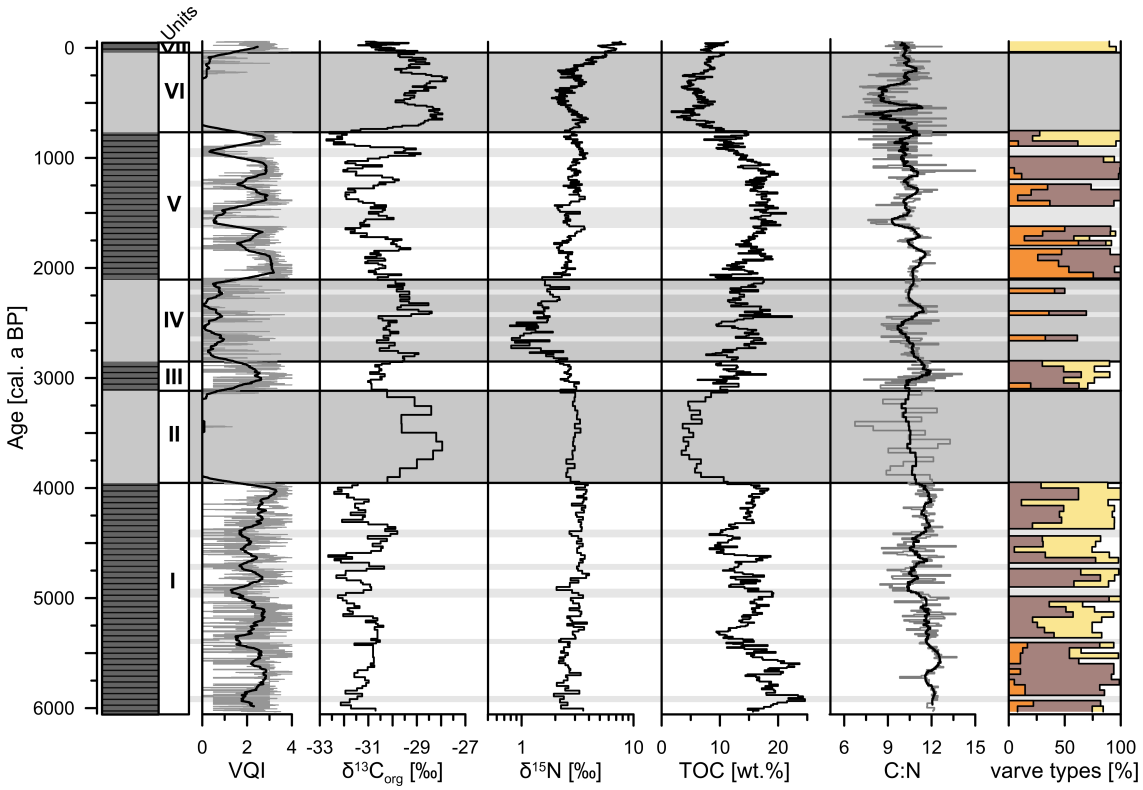

Figure 4.2: Results of sediment core analysis of the long sediment record. Lithology log indicates well-varved (striped dark grey) and non-varved (light grey) sections. Results of geochemical analysis conducted in this study: $\delta^{13}C_{OM}$, $\delta^{15}N$, TOC contents and C:N ratios. Results of sedimentological and geochemical analysis (Dräger et al., 2016): varve quality index (VQI; black line represents the 100 year running mean) and occurrence of varve types (yellow= calcite varves; orange=Ca-rhodochrosite varves; brown=organic varves).

The C:N ratio varies around a mean of 10.7 with values between 5 and 15, indicating a predominant autochthonous origin of the OM. The curve indicated no trend and shows only a weak relation to $\delta^{13}C_{OM}$ values (r=-0.27).

4.4.2 Surface sediment cores

4.4.2.1 Sediment profiles

In all surface sediment cores a lower non-varved sediment section was distinguished from an upper well-varved sediment interval. The transition between both facies types varied for each surface core in depths and time in dependence of water depth. While varves in unit VII of the long sediment core at 62 m water depth were developed since AD 1924, the onset of varve preservation began successively later at shallower water depths (AD 1940 at 48 m water depth and AD 1980 at 35 m water depth). As in the long sediment core (unit VII), varved sediments were composed of carbonate, diatoms and organic matter. The non-laminated sediment intervals were enriched in quartz grains,

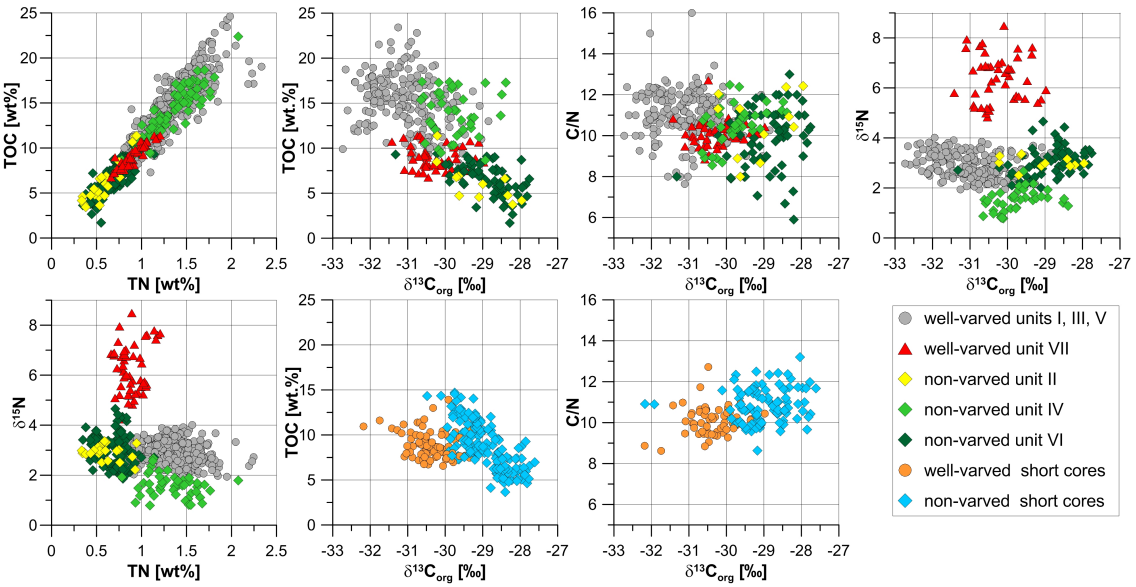

Figure 4.3: Scatter plots of geochemical results of the long sediment record and the surface cores.

plant fragments, benthic diatoms and occasionally bivalves comparable to unit VI in the long sediment core.

4.4.2.2 $\delta^{13}C_{OM}$

$\delta^{13}C_{OM}$ in surface cores varied between values of -32‰ and -27.5‰, which is similar to the range in the top of unit VI and in unti VII of the long sediment profile. As in the long core the non-varved intervals were characterized by more enriched $\delta^{13}C_{OM}$ ratios with on average -29‰, whereas more depleted $\delta^{13}C_{OM}$ values occurred in well-varved intervals with a mean of about -30.5‰.

Table 4.1: Calculated correlation coefficients (Pearsons r) of $\delta^{13}C_{OM}$ with TOC, C/N and $\delta^{15}N$ in the long sediment cores and of $\delta^{13}C_{OM}$ and TOC and C/N in surface sediment cores.

		C:N	TOC		$\delta^{15}N$	
			well-varved	non-varved	well-varved	non-varved
Long core						
7.7–0.65 m (units I-VI)	$\delta^{13}C_{OM}$	**-0.27**	**-0.45**	**-0.78**	**-0.53**	**+0.37**
Long core						
0.65–0 m (units VI-VII)	$\delta^{13}C_{OM}$	*+0.23*	*-0.14*	*-0.28*	*0.17*	*-0.12*
Surface core QP4	$\delta^{13}C_{OM}$	**+0.50**	**+0.40**	**-0.63**		
Surface core QP2	$\delta^{13}C_{OM}$	**+0.55**	*-0.28*	**-0.87**		

Bold and italic fonts indicate significant ($p<0.05$) and not significant ($p>0.05$) correlations, respectively.

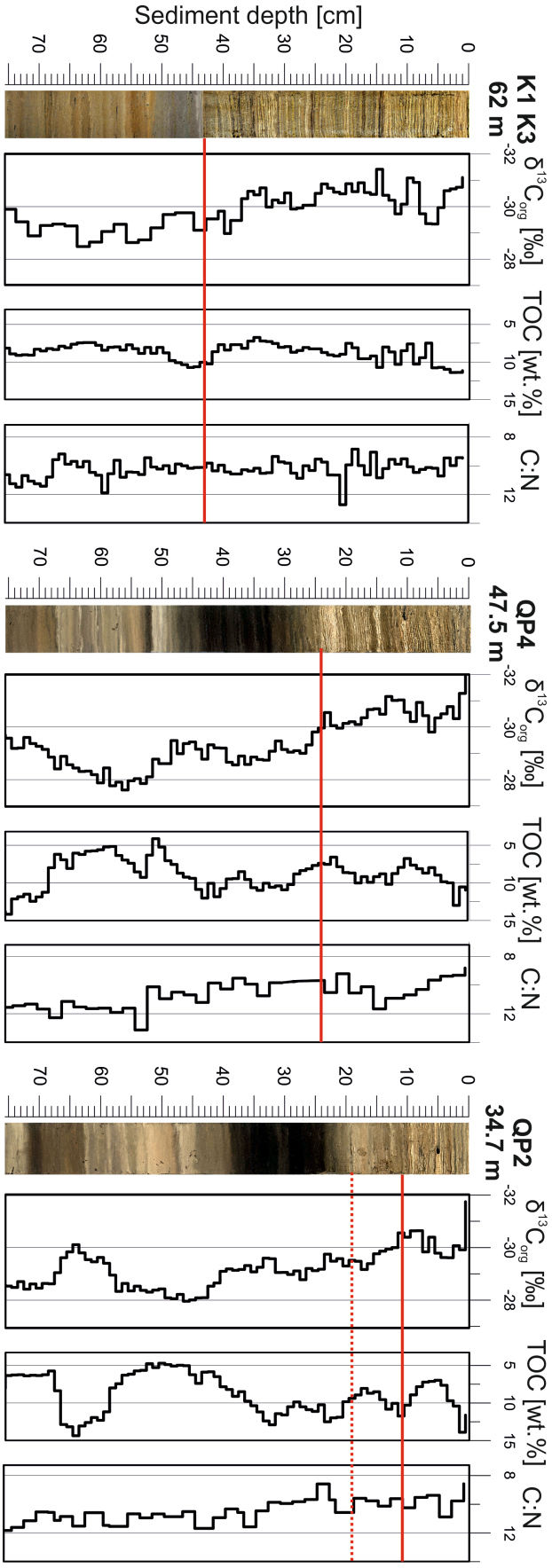

Figure 4.4: Results of surface core geochemistry. From left to right are displayed the core image, $\delta^{13}C_{OM}$, TOC contents and the TOC/TN ratio. Analysis has been conducted on core K1 (until 37 cm depth and K3 (from 37 cm depth on) both located at 62 m water depth and part of the long core, QP4 located at 47.5 m water depth and QP2 located at 34.7 m water depth. The red line indicates the onset of continuous varve preservation in all four cores. The dotted line in QP2 highlights the first occurrence of varves.

4.4.2.3 TN, TOC, C:N

Comparable to the long core, TOC and TN were strongly correlated in the surface cores (r=0.95). Fluctuations of TOC and TN contents were not corresponding to changes of varve quality as it had been observed in the long profile. In all surface cores TOC fluctuated around a mean of 8.7%. TOC and $\delta^{13}C_{OM}$ showed a negative correlation in non-varved intervals (r=-0.8) with intervals of higher TOC contents corresponding to depleted $\delta^{13}C_{OM}$ values. In well-varved intervals no correlation between both was observed.

The C:N ratio fluctuated around an average of 10.5 in the surface cores and showed a decreasing trend. Furthermore, C:N and $\delta^{13}C_{OM}$ show a positive correlation (r=0.5), which is different from the the long core from the deepest location where no correlation between C:N and $\delta^{13}C_{OM}$ was observed.

4.4.3 Sediment trap material and catchment samples

The annual means of $\delta^{13}C_{OM}$ of modern deposited organic matter in sediment traps scattered within a range of -31.7‰ to -30‰ and thus reflect $\delta^{13}C_{OM}$ ratios of the recent varved sediments in the surface cores (on average -30.5‰). Furthermore, the values show a trend towards slightly more depleted values from the epilimnion trap (5 m) towards the hypolimnion trap (45 m). $\delta^{13}C_{OM}$ in reed and soil samples ranged between -25.5‰ and -28‰, while $\delta^{13}C_{OM}$ in leaves was more widespread with values ranging between -27.5‰ and -32.5‰.

4.5 Discussion

4.5.1 $\delta^{13}C_{OM}$ in well-varved sediment intervals

The sediment record of Lake Tiefer See indicates distinct fluctuations of $\delta^{13}C_{OM}$ ratios during the past ~6000 years, corresponding to changes of varve preservation. More depleted $\delta^{13}C_{OM}$ values (on average -31‰) are associated with well-varved intervals, which have been shown to reflect phases of seasonally lake anoxia formation caused by reduced lake circulation before AD 1924 and by lake eutrophication during the last century (Dräger et al., 2016; Kienel et al., 2013).

More depleted $\delta^{13}C_{OM}$ values are commonly interpreted as indication for reduced lake productivity (*e.g.* Brenner et al., 1999) or a lower proportion of terrestrial OM (*e.g.* Müller and Voss, 1999). However, this interpretation is not supported by our data for well-varved intervals. Variation of lake productivity has been shown to differ from

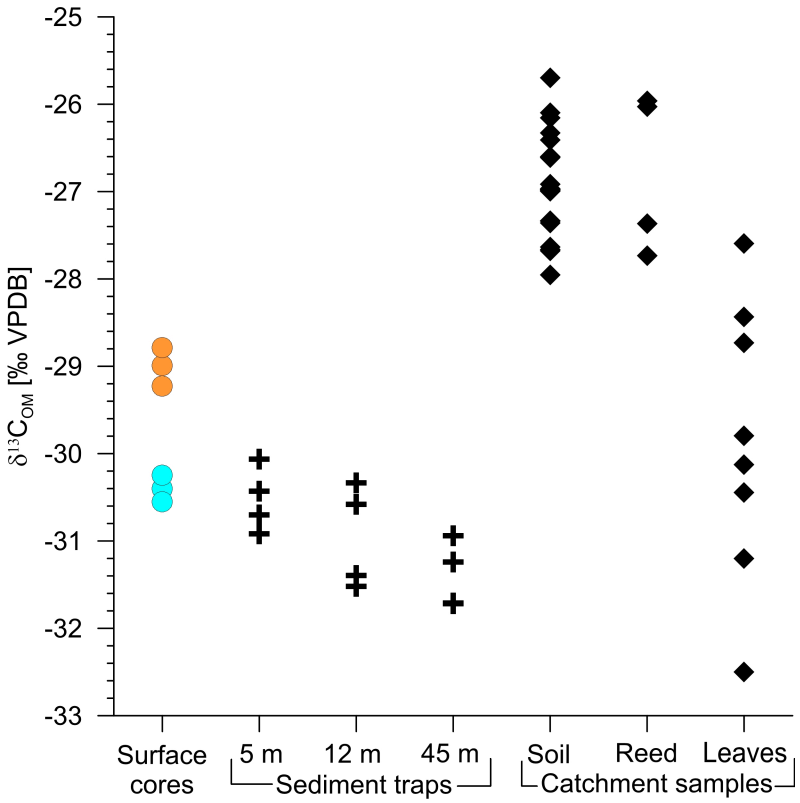

Figure 4.5: $\delta^{13}C_{OM}$ values of surface cores, sediment trap material and catchment samples. Means of well-varved intervals are marked with orange circles and those of non-varved intervals with blue circles. Crosses represent annual means of sediment traps. Diamonds represent individual measurements of catchment samples.

changes in varve preservation during the past ~6000 years. As $\delta^{13}C_{OM}$ values closely follow the varve quality, we consider that $\delta^{13}C_{OM}$ values are not associated to changes of productivity either. We further exclude changes of the organic matter source (terrestrial vs. autochthonous) as an controlling factor for $\delta^{13}C_{OM}$, because of the weak correlation between $\delta^{13}C_{OM}$ and the C:N ratios (r=-0.27; Table 4.1). Only in surface cores from shallower water depths $\delta^{13}C_{OM}$ and C:N are positively correlated (r=0.5; Table 4.1), which is likely caused by higher terrestrial OM influx to these locations closer to the lake shore.

Instead, the significant negative correlation between $\delta^{13}C_{OM}$ and $\delta^{15}N$ (r=-0.53; Table 4.1) in well-varved intervals suggests that the depleted $\delta^{13}C_{OM}$ ratios are mainly caused by microbial carbon cycling in phases of well varve preservation (*e.g.* Finlay and Kendall, 2007; Heyng et al., 2012). The oxygen deficient water column facilitates the bacterial decomposition of OM, which may have produced highly ^{13}C-depleted biogenic methane and CO_2 in Lake Tiefer See (Hollander and Smith, 2001; Whiticar, 1999). In result, chemoautrophic and methanotrophic microbial communities might

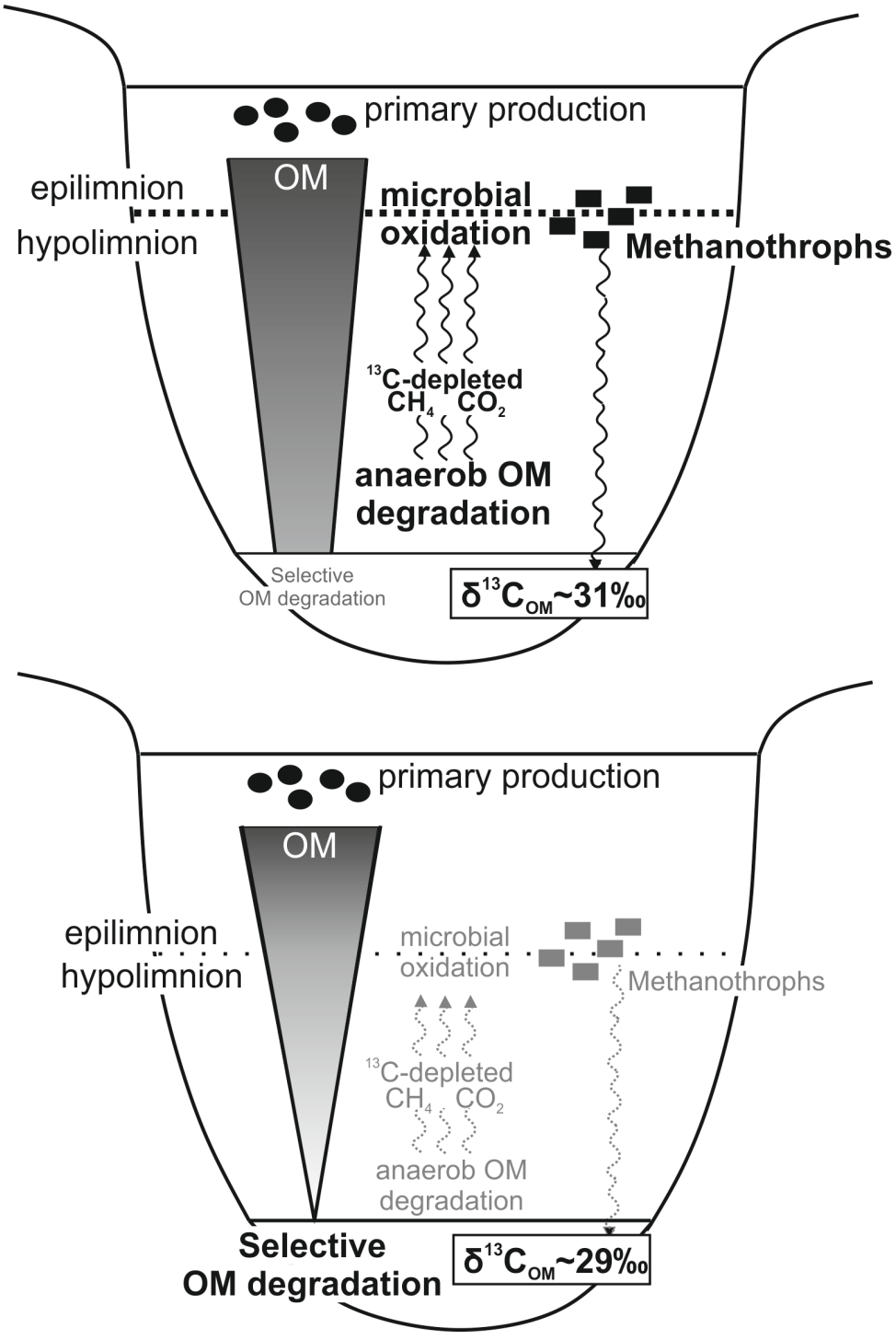

Figure 4.6: Lake model reflecting the control on $\delta^{13}C_{OM}$ in dominantly anoxic (top) and dominantly oxygenated (bottom) bottom water conditions. During anoxic bottom water conditions microbial carbon cycling induces the deposition of more depleted $\delta^{13}C_{OM}$ values. Selective degradation of OM is probably the dominant control in more oxygenated bottom waters inducing enrichment of $\delta^{13}C_{OM}$ in sedimentary OM.

have expanded at the oxic-anoxic boundary of the lake, incorporating this methane and CO_2. The biomass produced by these microbial communities is expected to be depleted of ^{13}C relative to photosynthetically produced organic matter by up to 15‰ by chemoautrophic (Conway et al., 1994; Degans, 1969) and 30‰ by methanotrophic microbes (Summons et al., 1994). Anoxic conditions further favour the presence of anaerobic nitrate-reducing bacteria (Finlay and Kendall, 2007). Enhanced bacterial denitrification results in enrichment of $\delta^{15}N$ values in OM (Finlay and Kendall, 2007; Heyng et al., 2012) and likely has induced the positive shift of $\delta^{15}N$ isotopes simultaneously to the decrease of $\delta^{13}C_{OM}$ ratios. The interpretation of microbial activity as a major source for depleted $\delta^{13}C_{OM}$ values in well-varved intervals, however, has to be further proven, because so far the presence of these microbial communities has not been analysed in Lake Tiefer See, yet.

In contrast to the well-varved sections deeper in the sediment profile, the recent well-varved interval (*i.e.* since AD 1924) indicates no significant correlation between $\delta^{13}C_{OM}$ and $\delta^{15}N$ values (red triangles in Figure 4.3). This suggests that $\delta^{13}C_{OM}$ or/and $\delta^{15}N$ ratios were controlled by different processes during the last century. The $\delta^{13}C_{OM}$ values display a negative shift by ~2‰ at the recent transition to well-varved sediment at AD 1924, which is similar to previous negative shifts observed at poorly-/non-varved and well-varved transitions. Therefore, we assume that microbial carbon cycling also controls $\delta^{13}C_{OM}$ values in the recent well-varved interval. Interestingly, the recent well-varved interval concurs with strongly increased lake productivity. That the $\delta^{13}C_{OM}$ ratio reflects microbial carbon cycling despite of the increased productivity suggests overprinting of the productivity signature by microbial carbon cycling (Hollander and Smith, 2001). While the $\delta^{13}C_{OM}$ ratio is likely influenced by the same processes in the recent well-varved and older well-varved intervals, the $\delta^{15}N$ values are influenced by different processes. The $\delta^{15}N$ ratios indicate a continuously rising trend by about 4.5‰ since AD 1800. A continuous enrichment of $\delta^{15}N$ ratios during the past ~300 years has been previously be explained by increasing input of manure into lakes (Teranes and Bernasconi, 2000). Manure and domestic sewage indicate $\delta^{15}N$ values of 5–25 ‰ (Talbot, 2001). Increasing agriculture in the catchment of Lake Tiefer See and the use of manure likely caused the gradual $\delta^{15}N$ enrichment in Lake Tiefer See.

In addition to microbial carbon cycling one might speculate that also early diagenetic processes have contributed to the $\delta^{13}C_{OM}$ signal in Lake Tiefer See sediments. An indication for this assumption is the coincidence of more enriched $\delta^{13}C_{OM}$ values (~30‰) and the occurrence of Ca-rhodochrosite in well-varved intervals from 6030–5400 cal. a BP and from 2100–1000 cal. a BP. The early diagenetic formation

of Ca-rhodochrosite is presumably linked to phases of lower redox potentials at the sediment-water interface during the stratification period (Dräger et al., 2016; Robbins and Callender, 1975; Stevens et al., 2000). These conditions might have enabled anaerobic microbial activity, producing HCO_3^- ions (Sawlan and Murray, 1983). During this process the lighter ^{12}C might have been preferably re-mineralized from the organic matter pool, leading to more enriched $\delta^{13}C_{OM}$ ratios in the residual sedimentary OM. However, this hypothesis remains speculative and needs to be further investigated and proven.

4.5.2 $\delta^{13}C_{OM}$ in poorly- and non-varved sediment intervals

$\delta^{13}C_{OM}$ values in poorly- and non-varved sediments are more enriched by ~2‰ compared to well-varved intervals. Poor and no varve preservation in Lake Tiefer See has been related to increased lake circulation phases and more oxygenated bottom water conditions. Absent or shorter anoxic phases may have caused reduced production of methane and CO_2, leading to a lower contribution of ^{13}C-depleted microbial biomass to sedimentary OM and to the observed enrichment of $\delta^{13}C_{OM}$ in poorly- and non-varved intervals (Figure 4.6). The assumption of reduced microbial processes in Lake Tiefer See in poorly- and non-varved intervals is supported by a weak positive relation (r=0.38) between $\delta^{13}C_{OM}$ and $\delta^{15}N$ instead of a negative correlation in poorly- and non-varved intervals. A positive relation between $\delta^{13}C_{OM}$ and $\delta^{15}N$ has been previously interpreted to be caused when both isotope ratios are controlled by lake productivity. The $\delta^{15}N$ values are comparable to $\delta^{13}C_{OM}$ ratios enriched during higher primary productivity phases. However, productivity changes only explain ~15% of the $\delta^{13}C_{OM}$ variability in poorly- and non-varved intervals of Lake Tiefer See, suggesting that $\delta^{13}C_{OM}$ is dominantly influenced through other factors.

The strong negative correlation between $\delta^{13}C_{OM}$ and TOC (r=-0.78; Table 4.1) in poorly- and non-varved intervals indicates that organic matter degradation might have influenced $\delta^{13}C_{OM}$ during phases of lower varve preservation. TOC contents are mainly considered as indicator for OM degradation in Lake Tiefer See (Dräger et al., 2016), which is more intense during more oxygenated bottom waters (Aller, 1994; Hedges and Keil, 1995). Rising $\delta^{13}C_{OM}$ ratios together with enhanced OM degradation has been related to selective decomposition of OM (*e.g.* Hedges et al., 1999; Lehmann et al., 2002; Mollenhauer and Eglinton, 2007), which assumes the preferential degradation of autochthonous OM over allochthonous OM, because the latter is chemically more stable and bound to mineral components (*e.g.* Canuel and Martens, 1996; Cranwell, 1981). In result, the proportions of autochthonous and allochthonous compo-

nents change during the degradation process (Mollenhauer and Eglinton, 2007). Thus, the observed shift in $\delta^{13}C_{OM}$ towards more enriched values might reflect the isotopic signature of allochthonous OM (-25.5 – -28‰; Figure 4.5), which relatively increased compared to autochthonous components in the residual bulk OM (Figure 4.2).

Results from the surface cores support the interpretation that OM degradation contributed to the enrichment of $\delta^{13}C_{OM}$ values in poorly- and non-varved intervals. A comparison of the surface sediment cores from different water depths revealed that the onset of varve preservation did not occur synchronously in the lake basin, but was time-transgressive depending on the water depth. In the deepest part of the lake basin at 62 m water depth the deposition of well-varved sediment commenced at AD 1924, whereas at 35 m water depth varve preservation started 55 varve years later (Figure 4.4). This difference reflects the gradual upward extension of anoxic bottom water conditions within the water column during the last century (Groß-Schmölders et al., 2015). For the time interval of 55 years, during which well-varved sediment was deposited at the deepest part and non-varved sediment at 35 m water depth, different $\delta^{13}C_{OM}$ ratios were measured in both cores; depleted $\delta^{13}C_OM$ in the deep core (on average -30.5‰) and enriched ^{13}COM (on average -29‰) in the shallower core. The $\delta^{13}C_OM$ differences in surface cores from the same time interval cannot be explained by processes within the water column, because that would result in the same values at all water depths. Sediment trap data indicate that the isotopic signal of $\delta^{13}C_{OM}$ is identical in the entire water column (on average -31‰), suggesting that the currently formed OM exhibits the same $\delta^{13}C_{OM}$ as OM in the well-varved intervals. Therefore, this difference in $\delta^{13}C_{OM}$ values between the short cores is most likely related to processes altering the $\delta^{13}C_{OM}$ ratio after deposition in the non-varved sediment intervals. A possible reason might be increased selective OM degradation due to more oxic conditions in the shallower part of the lake that led to an enrichment of the $\delta^{13}C_{OM}$ values.

Evaluating the entire ~6000 years long sediment profile of Lake Tiefer See, we find that $\delta^{13}C_{OM}$ is controlled by different factors, which vary in time. In well-varved intervals, microbial activity is an important factor causing more depleted $\delta^{13}C_{OM}$, whereas in non- and poorly-varved intervals increased OM degradation induced a positive $\delta^{13}C_{OM}$ shift.

4.6 Conclusion

We confirm previous studies that $\delta^{13}C_{OM}$ in lake sediment records is controlled by different factors. These factors, however, may not only vary between records from dif-

ferent lake environments, but can also vary in time within one individual record like at Lake Tiefer See. These variations are caused by changes in lake conditions, in case of Tiefer See the prevailing oxygen regime. In more anoxic conditions, microbial processes appear to be the controlling factor for $\delta^{13}C_{OM}$, while selective OM degradation becomes an important factor at more oxygenated conditions. Our study demonstrates that variations in the main controlling factors of $\delta^{13}C_{OM}$ can be distinguished with an in-depth multi-proxy approach including complementary analyses like, stable isotope geochemistry, bulk geochemistry and sediment facies analyses. In conclusion, if integrated in a comprehensive multi-proxy approach, $\delta^{13}C_{OM}$ can be an important proxy for reconstructing past lake environments.

Acknowledgments

We would like to thank all technicians and the coring team of GFZ-section 5.2 that assisted in the field and lab (G. Arnold, D. Berger, B. Brademann, S. Lauterbach, P. Meier, F. Ott, S. Pinkerneil, R. Schedel, R. Weißbach). We further acknowledge M. Köhler (MK-factory) for assistence during coring. This study is a contribution of the Virtual Institute of Integrated CLimate and Landscape Evolution Analysis -ICLEA- of the Helmholtz Association (grant number VH-VI-415). It is further a contribution to the climate initiative REKLIM Topic 8 "Abrupt climate change derived from proxy data" and uses infrastructure of the TERrestrial ENvironmental Observatory (TERENO), both of the Helmholtz Association. Geochemical data files for the investigated Lake Tiefer See sediment intervals are stored at the PANGAEA data library.

5 Spontaneous self-combustion of organic-rich lateglacial lake sediments after freeze-drying

Nadine Dräger*[a] , Achim Brauer[a], Brian Brademann[a], Rik Tjallingii[a], Michał Słowiński[b], Mirosław Błaszkiewicz[b], Norbert Schlaak[c]

[a] GFZ German Research Centre for Geosciences, Section 5.2 Climate Dynamics and Landscape Evolution, Telegrafenberg C, D-14473 Potsdam, Germany

[b] Department of Environmental Resources and Geohazards, Institute of Geography and Spatial Organization, Polish Academy of Sciences, Kopernika 19, 87-100 Toruń, Poland

[c] State Authority of Mining, Geology and Resources Brandenburg, Inselstrasse 26, D-03046 Cottbus, Germany

* Corresponding author

Abstract

We report and investigate for the first time spontaneous self-combustion of freeze-dried lacustrine sediments immediately after ventilation of the vacuum freeze dryer chamber. The smouldering and flameless combustion lasted for approximately 10–20 min and reached temperatures of 357°C. Self-combustion mainly occurred in aluminium boxes containing sediment bars taken for thin section preparation. About 40% of these samples were affected, most of them originated from the basal approximately 3 m thick finely laminated lateglacial sediment interval. The combustion process caused disintegration of siderite to iron oxides (hematite and magnetite) and burning of organic matter to pyrogenic carbon leading to a lowering of total inorganic and organic carbon contents to 1%. The total sulphur content of one combusted bulk sample did not change, but the alteration of sulphur contents in different sediment components suggests a redistribution of sulphur within the sediment. We assume that the self-combustion process was initiated by exothermic oxidation reactions, which were favoured by a combination of factors including the presence of abundant fine-grained iron sulphides in the organic-rich sediments. Self-combustion could be prevented by ventilating the vacuum chamber after freeze-drying with N_2.

Keywords

Spontaneous self-combustion – Freeze-drying – Iron sulphides – Laminated sediment – Thin section

5.1 Introduction

Freeze-drying is a commonly applied method in lake sediment research to dry samples for conservation issues, for geochemical analyses and for resin impregnation required for thin section preparation (Brauer and Casanova, 2001; Last and Smol, 2001; Lotter and Lemcke, 1999). To our knowledge, there have been no reports about self-combustion of organic-rich lake sediments during or after the freeze-drying procedure so far.

Smouldering combustion is a slow, low-temperature and flameless burning of porous fuels and the most persistent type of combustion phenomena (Ohlemiller, 1985, 1986; Rein, 2009). Smouldering combustions are usually observed during wildfires of soils and peatlands as well as during subsurface fires in coal mines and seams, which can burn even for centuries (Rein, 2009; Ohlemiller, 1985). Heat input, heat loss, availability of oxygen and the number and abundance of reactive centres are the limiting factors that determine ignition and propagation of a smouldering reaction (Misra and Singh, 1994; Ohlemiller, 1985; Torero and Fernandez-Pello, 1996; Frandsen, 1997). The presence of a solid matrix furthermore facilitates the reaction by providing (1) a large surface area per volume ratio enhancing surface reactions, (2) thermal insulation reducing heat loss, and (3) permeability enabling oxygen transport to the reaction sites (Ohlemiller, 1985).

In spite of the large amount of information about such processes generated during the past decades, the exact mechanisms of spontaneous combustion are still not completely understood (Banerjee, 1981; Misra and Singh, 1994). Heat can spontaneously be generated by a few natural exothermic reactions including exothermic oxidation of fine-grained iron sulphide minerals (Rosenblum and Spira, 1995; Payant et al., 2012), which is the most assumed cause of ignition and it is a common phenomenon in coal combustion.

This paper describes a case of spontaneous ignition of organic-rich lateglacial sediment samples after freeze-drying in the lab and investigates the geochemical and petrological fingerprint of the combustion process.

5.1.1 Study site

The Wukenfurche palaeolake (N 52° 46.61', E 13° 35.77'; 61 m NN) is located approximately 20 km northeast of Berlin and south of the Pomeranian terminal moraine of the Weichselian glaciation and is part of the Eberswalde ice-marginal valley system (Figure 5.1a). While the northern part of the 1.1 km long SW–NE oriented and narrow (~100 m wide) valley is still water filled (Lake Kleiner Wukensee; 5 m maximum water depth), the southern part was filled up by sediments during the Holocene and is a swampy area today (Schlaak, 1993). The coring location is situated in an 80 m narrow and 140 m long sub-basin of the Wukenfurche palaeolake (Figure 5.1b).

5.2 Material and Methods

Two parallel sediment sequences within a distance of 0.5 m (WUK14 A and WUK14 B) have been obtained in 2014 from the presently swampy area using a Węckowski Corer (Więckowski, 1959). The core location at the deepest point of the sub-basin is close to the position of a previous core (WU5; Schlaak, 1993). Cores were split, imaged and described in the lab. A continuous composite profile has been compiled by correlating macroscopically visible 'marker' layers in both core sequences. Detailed analyses presented here focused on the approximately 3 m thick finely laminated sequence (14.3–11.35 m composite depth) in the basal part of the sediment profile.

The preparation of thin sections followed the method described by (Brauer and Casanova, 2001). Sediment bars (10 x 2 x 1 cm) were cut out of the fresh sediment surface and stored in self-folded open aluminium boxes (aluminium thickness: 180 μm; box size: 10.1 x 2.5 x 2 cm). These samples were shock-frozen in liquid nitrogen and freeze-dried in a vacuum chamber at room temperature for two days. For the first set of samples the vacuum chamber of the freeze drier was ventilated with air (air-ventilated) following the commonly applied procedure. In order to investigate the causes for self-combustion, we repeated the procedure but used nitrogen instead of air for ventilation (N_2-ventilated). Therefore, we simply connected the ventilation valve with a flexible tube linked to a nitrogen source. Subsequently, the dried bars were impregnated with Araldite® resin in vacuum, hardened for two days and further prepared to thin sections. Thin sections produced from air-ventilated sediment bars comprise almost the entire laminated sequence in both sediment profiles (WUK14-A 14.22–11.35 m; WUK14-B 14.3–11.5 m). Thin sections from N_2-ventilated sediment bars were prepared from profile WUK14-B 14.3–13.7 m and 11.45–10.8 m depth.

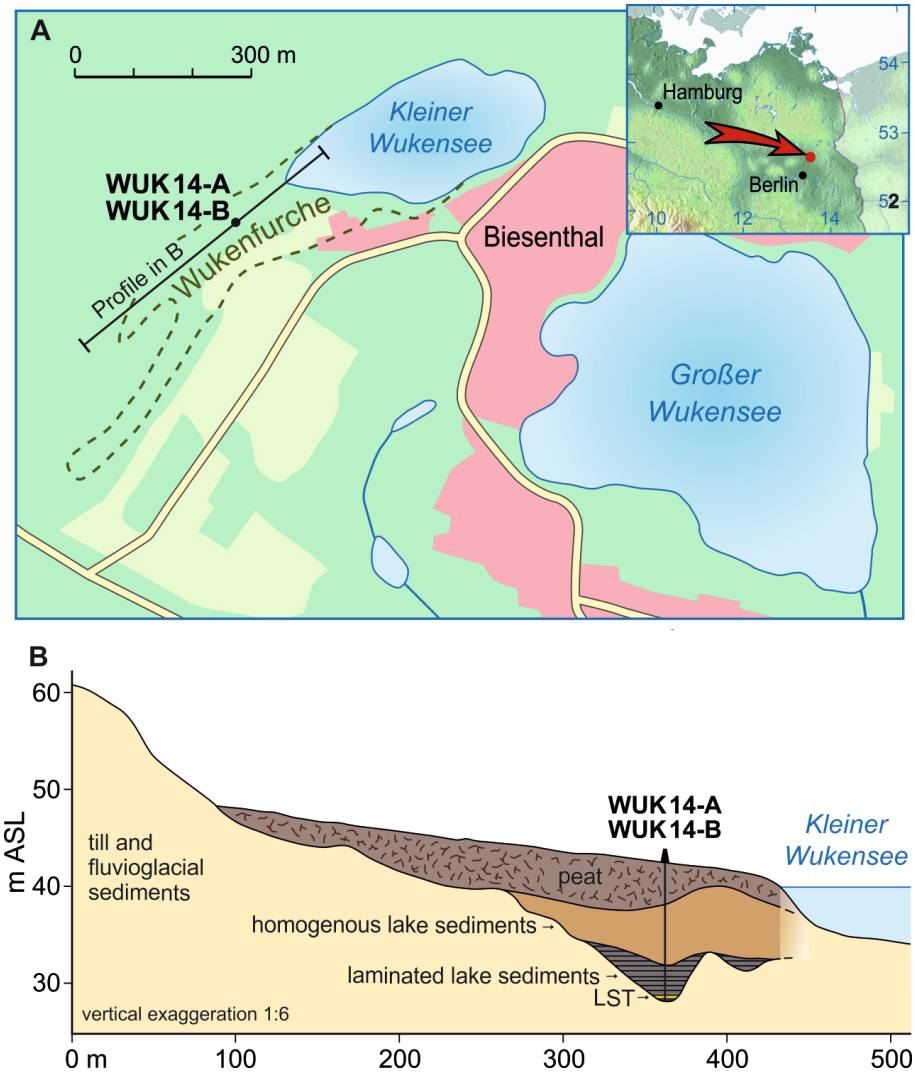

Figure 5.1: (a) Geographic setting of the study area palaeolake Wukenfurche in NE Germany and detailed map of the coring positions including characteristics of the surface catchment area and (b) a SW–NE profile through the Wukenfurche basin illustrating the general sediment succession in the narrow sub-basin with the coring location (after Schlaak, 1993).

From two parallel air- and N_2-ventilated sediment bars (WUK14-B 13.95–13.9 m depth) additional thick sections (100–150 μm sediment thickness) were prepared, carbon coated and analysed with a microprobe (JEOL JXA-8230). Operating conditions used 15 kV voltage, a 10 nA beam current, 5 μm beam size and exposure times of 10 to 20 s per element. Analysed elements were Si, S, Ca and Fe. The carbon coating induced a well-defined peak height of C, which is considered as the 'zero' baseline for the C content in the samples. We infer that a sample contained C if the measured C-peak height exceeded this baseline.

Samples for bulk geochemical analysis (TOC, TC and TS) were obtained every 1 cm from the fresh sediment surface comprising a volume of 2 cm^3 per sample (bulk samples). All samples were stored in plastic tins (plastic thickness: 1 mm, diameter: 2.3 mm, height: 3.6 mm). 83 of these samples were frozen for one day, subsequently freeze-dried in a vacuum chamber for two days and air-ventilated after the drying process. For 17 of these 83 samples a parallel set of samples was freeze-dried but the vacuum chamber was ventilated with N_2. Additionally, for 7 of the 83 samples a parallel set of samples stored in open aluminium boxes (aluminium thickness: 180 μm; box size: 7 x 4 x 4 cm) was air dried at 35°C in an oven.

All freeze-dried (air- and N_2-ventilated) and air-dried samples were ground and analysed for total organic carbon (TOC) and total inorganic carbon (TIC) contents with an elemental analyser (EA3000-CHNS Eurovector). Total sulphur contents (TS) were measured from four freeze-dried (air-ventilated) and parallel air dried samples with an automated LECO CS-800. 12 additional samples (3 from each sediment unit) were air dried and analysed with a scanning electron microscope (SEM, Carl Zeiss SMT Ultra 55). X-ray diffractometer (XRD) analyses of the same powdered samples used for measurements of TS contents was conducted with a PANalytical Empyrean diffractometer with Cu Kα radiation, automatic divergent and anti-scatter slits and a PIXcel3D detector.

The relative variations of Fe and S were measured directly at the split core surface using an ITRAX μ-X-ray fluorescence (μ-XRF) core scanner (10 s, 30 kV and 30 mA) at 200 μm resolution. The obtained element intensities of Fe and S are expressed as counts per seconds. We convert element intensities to log-ratios and centred-log-ratios (CLR), which minimize the influence of matrix and absorption effects and are linearly related to log-ratios of element concentrations (Tjallingii et al., 2007; Weltje and Tjallingii, 2008).

The temperature of two combusting sediment bars was measured at a distance of about 50 cm with a thermal image camera (Testo 882; measuring range 20–550°C) on the sample surface.

5.3 Results

5.3.1 Stratigraphy and lithology

The basal part of the 14.6 m long sediment profile is formed by glacial sands (14.6–14.4 m) covered by a 10 cm peat interval (14.4–14.3 m). Lacustrine sedimentation starts at 14.3 m sediment depth (Figure 5.3). The basal 3 m thick sequence of pelagic lake sed-

iments appeared black immediately after core opening, but after surface oxidation reddish and dark brown mm-scale laminae became visible. Based on the sediment colour after surface oxidation and distinctness of the lamination, four sediment units were differentiated: unit I (14.3–13.7 m) exhibiting distinct red and black alternating laminae, unit II (13.7–12.3 m) characterized by distinct brown and black alternating laminae, unit III (12.3–11.35 m) showing faint red and black alternating laminae and unit IV (11.35–4.35 m) consisting of olive-grey homogenous sediment. In the uppermost part, the lacustrine sediment sequence is covered by a 4.35 m thick peat horizon.

A visible volcanic ash layer 6 cm above the onset of lacustrine deposits corresponds to the Laacher See Tephra (LST, 12880 varve a BP; Brauer et al., 1999), indicating an onset of lake sedimentation in the Allerød. A rough count of the laminae on core pictures yielded approximately 2900 couplets for the entire laminated interval, which corresponds to the number of laminae counted by (Schlaak, 1993) in the previous core WU5. Assuming an annual origin, the laminated sediment sequence would cover the period from the Allerød until the early Holocene.

5.3.2 Micro-XRF element scanning

The ln(S/Fe) ratio and the CLR transformed Fe_{CLR} (Figure 5.3) were calculated from the intensity data obtained by μ-XRF core scanning (Weltje et al. 2015). The ln(S/Fe) ratio reflects relative variations of the iron sulphide content, whereas Fe_{CLR} represents the relative amount of all Fe-containing phases in the sediment. Higher ln(S/Fe) ratios occur at the base of unit I and in unit III. In contrast, Fe_{CLR} values are relatively constant throughout the core. Slightly lower values are only observed in unit II between 13.6 and 12.5 m depth.

5.3.3 Effects of different drying methods

Sediment bars for thin section preparation

Ventilation of the vacuum chamber after freeze-drying with air as commonly applied caused an immediate heating of 28 sediment bars (40% of all samples) resulting in self-combustion associated with sulphur gas release, burned smell and sediment colour change into dark red. For two samples a surface temperature of at least 357°C was measured with a thermal image camera (Figure 5.2). The temperature of the combusted sediment bars remained too high to be touched for another approximately 10 to 20 minutes. The propagation of the combustion front through the sediment bar from one end to the other occurred not evenly but rather pulsating. The other 42 sediment bars

(60% of all samples) showed a normal behaviour and changed from black (fresh sediment) to greenish-grey colours (dry sediment) (Figure 5.4A).

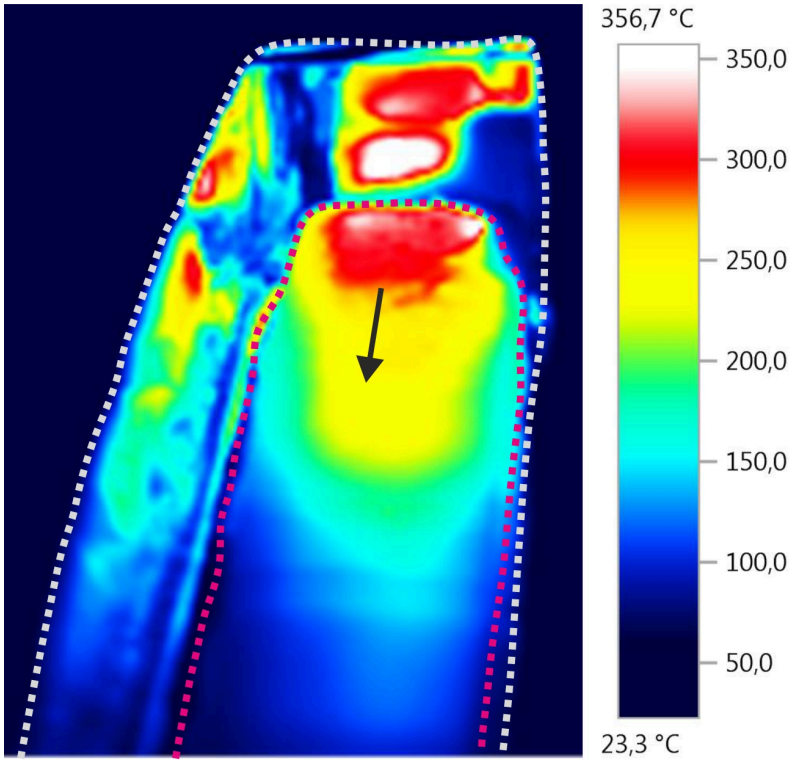

Figure 5.2: Thermal image of a combusting sediment bar stored in an aluminium box.Red and white dotted lines show the margins of the sediment bar and aluminium box, respectively. The image was taken at the beginning of the combustion process. The arrow highlights the direction of movement of the combustion front (video of the combustion on http://www.iclea.de/en/outcome).

Most of the self-combusted samples (26 of the 28 combusted samples) originate from sediment units I and II (Figure 5.3). All sampled sediment bars in unit I self-combusted. From the lower part of unit II below 12.8 m depth, 13 sediment bars (35% of all unit II samples) burned. From units III and IV only one sediment bar each combusted (WUK14-A 11.9–12.0 m depth, WUK-A 11.2–11.3 m depth). About half of the burned sediment samples (8 of 15 combusted samples) from units II, III and IV self-combusted only in one core sequence, but not in the lithological parallel interval (Figure 5.3).

No self-combustion occurred after ventilating the vacuum chamber with N_2 after freeze-drying.

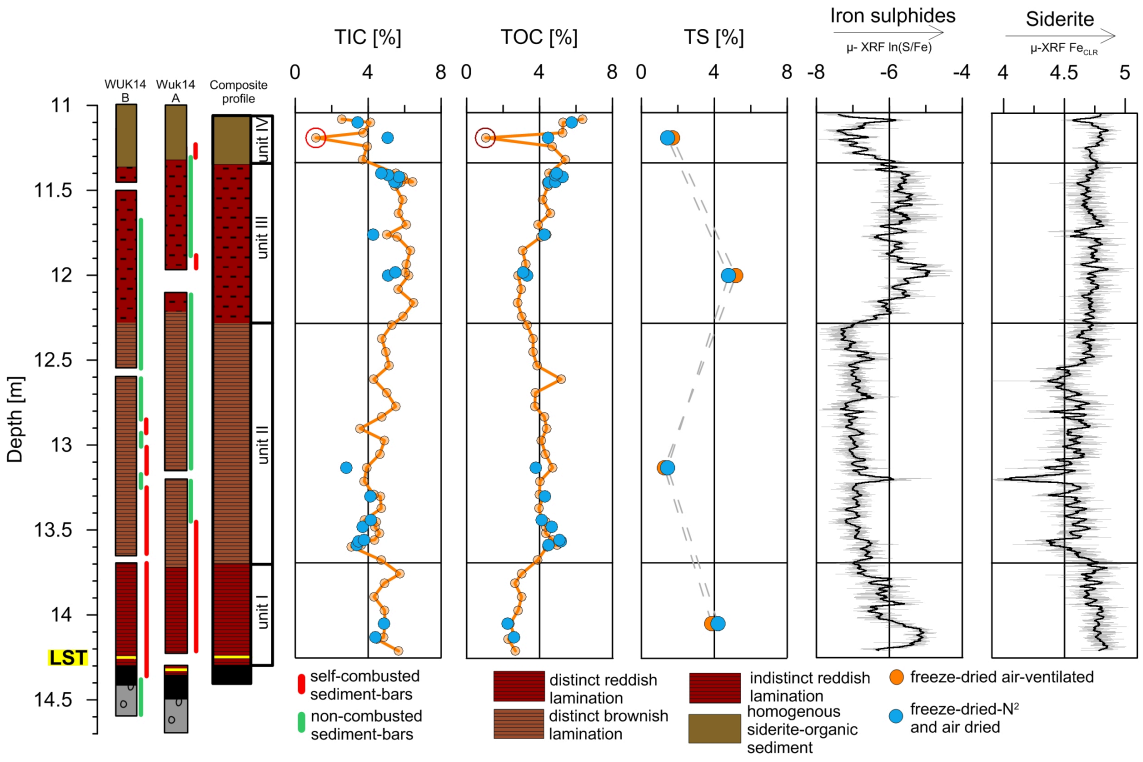

Figure 5.3: Schematic profiles of the individual sediment cores WUK14-A and WUK14-B and of the composite profile. Results of geochemical analysis: total inorganic carbon contents (TIC), total organic carboncontents (TOC),total sulphur contents (TS) and ln(S/Fe) ratios and Fe_{CLR} obtained from μ-XRF data. Solid horizontal lines indicate boundaries of the sediment units I–IV. The red circle around the lowest TIC and TOC values at 11.2 m depth indicates the only self-combusted bulk-sample.

Bulk samples

Only one out of 500 bulk samples (obtained from 11.2 m depth) self-combusted after air-ventilation. The combustion turned this sample into dark red and produced temperatures high enough to melt the plastic sample box. A parallel sample did not self-combust after ventilating the vacuum chamber of the freeze dryer with N_2.

5.3.4 Thin section and SEM analyses

Thin section analyses revealed that non-combusted sediments of units I, II and III consist of alternating layers of siderite, amorphous organic-rich matter and calcite (Figure 5.4D). Siderite ($FeCO_3$) forms at or below the sediment water interface by the reaction of Fe^{2+} with $CO_3{}^{2-}$ in anoxic conditions (Postma, 1981; Bahrig, 1988; Brauer and Negendank, 1993). In siderite layers, two types of siderite grains are differentiated: (i) 2–10 μm sized spherical grains with cross-shaped extinctions under cross polarized light and (ii) micritic crystals typically arranged in aggregates and in coatings. The yellow-

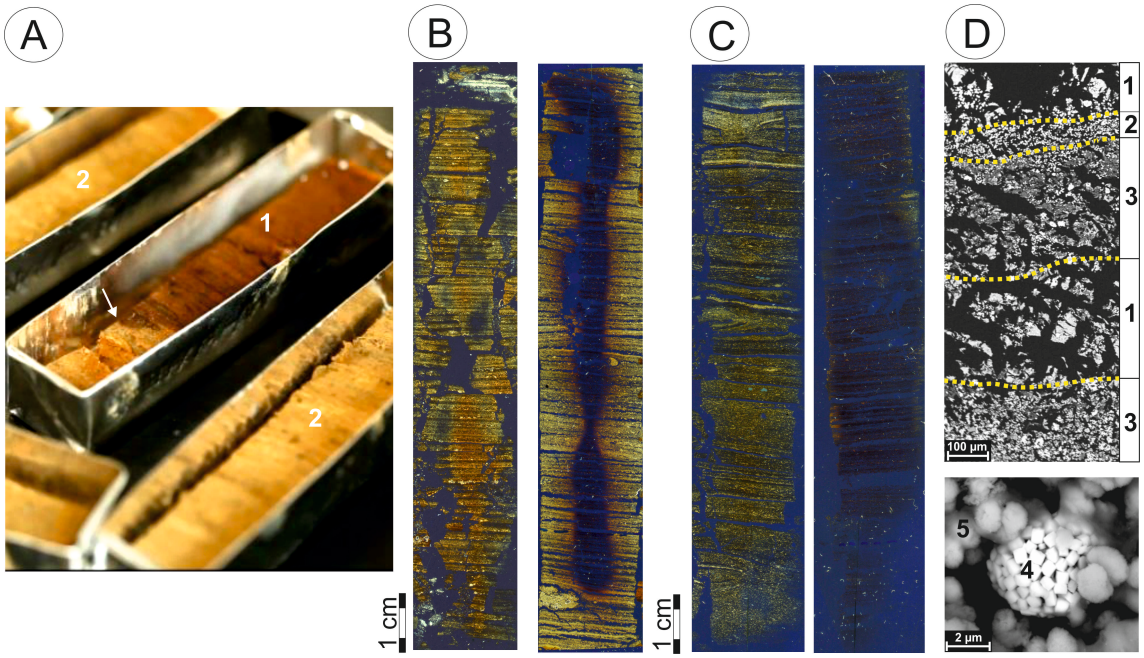

Figure 5.4: (a) Image of a combusting sediment bar (1) and non-combusting sediment bars nearby (2). The position of the combustion front is indicated by an arrow. (b) Thin section scans (cross-polarized light) of non-combusted (left) and self-combusted (right) sediment bars from unit I. The central dark part of the combusted sediment bar is caused by the disintegration of siderite to isotropic iron oxides. (c) Thin section scans (cross-polarized light) of non-combusted (left) and self-combusted (right) sediment bars from unit II. Siderite is disintegrated in the entire combusted sediment bar to isotropic iron oxides. (d) Top BSE-image obtained from a non-combusted thick section from unit I: (1) dense amorphous matter layer with siderite, (2) siderite layer and (3) amorphous organic matter layer with siderite; bottom SEM image of a pyrite framboid (4) and spherical siderite grains (5).

brownish amorphous organic-rich matter represents the background sedimentation and forms discrete layers only when siderite and calcite contents are reduced. In thin sections these amorphous matter layers appear homogenous, but additional backscatter electron (BSE) images obtained by microprobe analyses reveal that the amorphous matter layers consist of two different types of material, which are characterized by different densities: (i) low-density organic matter and (ii) higher density Fe- and Si-rich amorphous matter (see the section on microprobe analysis below). Thin section analyses alone did not enable to differentiate between both amorphous matter types. Calcite layers consist of fragments of the calcifying littoral algae Chara spp. (Haas, 1994), which are transported from the littoral zone into the profundal most likely at the end of the growing season. Most of these fragments are encrusted by micritic siderite indicating an early diagenetic origin of this siderite type.

Spherical and micritic siderite are the dominant components in unit I (mean thickness 0.75 mm) and are intercalated with amorphous matter layers (mean thick-

ness 0.3 mm). Thin Chara layers occur irregularly with mean thicknesses of 0.1 mm. Framboids of iron sulphides (mainly pyrite) are incorporated in all layer types and occasionally form discrete layers between 14.2 and 14 m sediment depth (mean thickness 0.1 mm).

In unit II the abundance of siderite is markedly reduced supporting results obtained from μ-XRF scanning and the micritic siderite type dominates (mean sub-layer thickness 0.5 mm). Chara layers with a mean thickness of 0.7 mm often incorporating scattered quartz grains are regularly formed leading to the distinct appearance of the lamination. Iron sulphide framboids and amorphous matter layers (mean thickness 0.3 mm) only occur irregularly.

In unit III the lamination is less distinct due to only sporadic occurrence of discrete amorphous and Chara sub-layers. The abundance of siderite is comparable to unit I. Chara fragments are still abundant, but arranged as lenses. Iron sulphide layers appear more regular as compared to unit I with up to 0.5 mm thickness as also shown by increased ln(S/Fe) ratios.

The proportion of components in the homogenous unit IV is comparable to unit II characterized by a reduced content of siderite but increased amount of Chara fragments and quartz grains.

Thin-section analyses of self-combusted samples reveal that the burning mainly transformed siderite, characterized by golden colours under polarized light, to isotropic crystals and amorphous matter to an opaque appearance. However, transformation of these sediment components occurred differently in the individual sediment units. While in units I and III siderite was transformed only in the inner part of sediment bars (Figure 5.4B), in units II and IV siderite was transformed in the entire sample (Figure 5.4C). Amorphous matter was usually transformed in units I and III in the entire sample, whereas in units II and IV only some of the amorphous matter layers were transformed into an opaque appearance. Chara fragments were not altered during the combustion and are completely preserved.

5.3.5 Carbon and sulphur content

In non-combusted bulk samples total inorganic carbon (TIC) contents fluctuate around 5 wt.% with slightly higher contents in units I and III of up to 6 wt.% (Figure 5.3). Total organic carbon (TOC) contents are lower (~2.5 wt.%) in unit I and in the lower part of unit III (12.3–11.8 m depth) and increased to ~4 wt.% in unit II and the upper part of unit III (11.8–11.35 m depth). Highest TOC contents of up to 6 wt.% are reached in unit IV (Figure 5.3).

The four air-dried samples analysed for sulphur contents (one for each unit; Figure 5.3) show higher contents of 4 wt.% and 5 wt.% at 14.1 m (unit I) and 12 m depth (unit III), respectively and lower contents of ~1.5 wt.% at 13.1 m (unit II) and 11.2 m depth (unit IV).

Only one sample from unit IV (11.2 m depth; red circled point in Figure 5.3) was self-combusted. After combustion, the TIC and TOC contents of this sample decreased to ~1 wt.% compared to the non-combusted N_2-ventilated sample (5 wt.% and 4.2 wt.%, respectively; Figure 5.3), whereas the TS content did not significantly change through the combustion.

5.3.6 XRD analysis

XRD spectra of non-combusted bulk samples confirmed siderite as a major component in all sediment units. Units II, III and IV additionally contain calcite and subordinated quartz. In the self-combusted bulk sample in unit IV (11.2 m depth) the siderite peak disappeared and was replaced by peaks of hematite and magnetite.

5.3.7 Microprobe analysis

A comparison of non-combusted and self-combusted sediment bars from 13.95–13.9 m sediment depth (unit I) through microprobe analyses on thick sections yields changes of elemental compositions of the different sediment components (Table 5.1). In the non-combusted sample siderite grains reveal high Fe contents (52 ± 5.7 wt.%) and subordinated Ca contents (6.6 ± 0.9 wt.%) and S contents (0.6 ± 0.3 wt.%). The backscatter electron (BSE) image indicates that the amorphous matter identified in the non-combusted thick sections can be divided into two types according to density differences (Figure 5.4D). The lower density amorphous matter (dark grey in BSE image) contained Fe (23.5 wt.%), Si (17.2 wt.%), S (0.8 wt.%), Ca (0.8 wt.%) and C. Since the C-peak exceeded the signal produced by the carbon coating alone, we infer organic matter as the additional C source in the sample. The higher density amorphous matter (lighter grey in BSE) is dominated by higher Fe (44 ± 2.4 wt.%), Si (29 ± 2.1 wt.%) and S (4.8 ± 0.2 wt.%) values.

In self-combusted samples Fe and S contents of the disintegrated siderite grains increased to 61.9 ± 7.6 wt.% and 5.7 ± 1.3 wt.%, respectively, whereas the C-peak was reduced to the level of the carbon coating suggesting an entire loss of C during siderite disintegration. The combusted lower density organic matter exhibits an increase of Fe

to values of 34.6 ± 0.1 wt.% and a slight increase of S to 2.2 ± 0.1 wt.%. In the denser amorphous matter only the S content decreased by about 50% to 2.4 ± 0.2 wt.%.

Table 5.1: Content of SiO_2,SO_3, CaO and FeO in siderite crystals, organic matter and amorphous matter in non-combusted and self-combusted thin section obtained with microprobe analysis

	Non-combusted sediment bar					Self-combusted sediment bar				
		Sio_2 (wt.%)	So_3 (wt.%)	CaO (wt.%)	Feo (wt.%)		SiO_2 (wt.%)	SO_3 (wt.%)	CaO (wt.%)	FeO (wt.%)
Siderite	n=8	0.4±0.6	**0.6±0.3**	6.6±0.9	**52±57**	n=9	0.4±0.5	**5.7±1.3**	9.2±2.5	**61.9±7.6**
Low density amorphous matter	n=1	17.2	**0.8**	0.8	**23.5**	n=2	13.3±1.7	**2.2±0.1**	1.3±0	**34.6±0.1**
High density amorphous matter	n=3	29±2.1	*4.8±0.2*	1.7±0.1	44±2.4	n=3	29.9±0.3	*2.4±0.2*	2.3±0	45.5±1.4

Increased and decreased contents in a specific component of the self-combusted sample are underlined with bold and italics, respectively

5.4 Discussion

We observed for the first time a flameless and smouldering self-combustion of lake sediments after freeze-drying. Here we describe the consequences of the combustion for sediment properties and discuss possible trigger mechanisms for the initiation of the self-combustion process based on a combination of thin section, geochemical and mineralogical analyses.

5.4.1 Consequences of combustion for sediment properties

As proven by XRD analyses, siderite crystals were transferred into isotropic iron oxide minerals (hematite Fe_2O_3 and magnetite Fe_3O_4) during the combustion process. The disintegration is supported by the decrease of the TIC content in the combusted bulk sample. At high temperatures siderite degrades to iron oxide (FeO), which is further oxidized by CO_2 to hematite and magnetite (Bailey et al. 1998). Disintegration temperatures of siderite crystals range from about 400–420°C in lake sediments (Brauer and Negendank, 1993) and between 370°C and 530°C with maximum rate at 430°C in Lower Jurassic brackish-marine deposits (Maes et al., 2000). The maximum temperature of 357°C from the Wukenfurche sediments that we measured during the combustion process is slightly below these values. One possible explanation might be the fact

that we measured the combustion temperature only at the sample surface. Interestingly, in units II and IV siderite disintegrated in the entire sediment bar, while in units I and III siderite was only disintegrated in the central part of the sample (Figure 5.4B, C). This suggests that in unit I and III samples the combustion temperature at the sample margins was not sufficiently high to entirely disintegrate siderite. The coincidence of only central disintegrated siderite and lower TOC contents (~2.5 wt.%) in units I and III sediments and entirely disintegrated siderite in units II and IV with elevated TOC values of ~4–6 wt.% indicates a possible relation between the TOC content and degree of temperature at the sample margins.

In contrast to siderite, Chara fragments are not affected by the combustion process and are not disintegrated, likely because of the considerably higher disintegration temperature <800°C of calcite (Dean, 1974).

Organic matter was transformed by the burning into pyrogenic char (also called 'pyrogenic carbon' or 'black carbon') (Hammes et al., 2007; Santín et al., 2015) identified as opaque components in thin sections. The transformation into pyrogenic char is provoked by the release of volatiles and pyrolysates due to the high temperatures (Huang et al., 2014) and implies an incomplete combustion process, which is typical for smouldering fires lacking ignition (Ohlemiller, 1985, 1986; Rein, 2009). An incomplete combustion is further supported by remaining TOC contents of 1 wt.% after the combustion (Figure 5.3).

Interestingly, the total sulphur content in the bulk sample did not change after burning as one might have expected. Instead, the S content of different sediment components changed, thereby suggesting a redistribution of S within the sediment. The loss of S in the dense amorphous matter by ~2.5 wt.% was balanced by increased S contents in the original siderite and organic matter by ~5 wt.% and ~1.5 wt.%, respectively. However, this might not be a generally valid finding since we could observe this material-dependent change in S contents only in one sample, because no other bulk sample was affected by self-combustion.

5.4.2 Mechanisms for self-combustion

Sediment heating only in air-ventilated samples suggests the initiation of self-combustion by oxidation reactions. Exothermic oxidation of iron sulphides is an associated common cause for self-heating and has been observed in iron sulphide bearing coal and numerous mines and milling operations (Li and Parr, 1926; Rosenblum and Spira, 1995; Ninteman, 1978; Payant et al., 2012). Mariner et al. (2008) reported self-ignition of pyrite in organic shales caused by a landslide, leading to air penetration to pyrite

nodules. Although pyrite is common in lake sediments according to our knowledge no case of self-combustion after freeze-drying has been reported so far.

The presence of iron sulphides in the Wukenfurche sediments, however, cannot be the only trigger for self-combustion, because some of the non-combusted sediment samples in unit III contain up to 0.5 mm thick iron sulphide layers, but did not burn. One additional factor could be the size of iron sulphides since very fine-grained framboids have a higher surface area offering larger contact surfaces for oxidation reaction. Such small grain-sized pyrite particles might have been overlooked because they are not detectable with the methods applied in this study (Morse et al., 1987). An indication for the presence of very fine grained iron sulphides is the concentration of S in the dense amorphous matter before burning. The high Fe content in the dense amorphous matter of ~45% in relation to S (~5 %) and TIC contents (~5%) suggest that only a fraction of Fe is bound in iron sulphides and siderite. One might suspect that the remaining iron is present in fine grained and/or amorphous Fe phases, which might have reacted exothermically with oxygen. However, this hypothesis has to be tested in further investigations.

Additional factors possibly supporting the self-combustion process are the high permeability and porosity of the dry sediment caused by the high water content (~70%). Both features provide both improved thermal insulation and oxygen transport to the reaction centres.

Furthermore, we assume that also the self-sustaining of the combustion process is linked to multiple factors. The propagation of combustion in the sediment even over non-combustible carbonate layers might have been supported by the existence of discrete organic layers and the constant background of organic matter. We assume this from the observed pulsating propagation of the combustion through the sample, caused by the regular slowdown of the burning in Chara layers. The self-sustaining of the combustion might have been additionally favoured by the high abundance of siderite crystals since siderite has a low thermal conductivity (κ=3; Midttømme, 1998; Horai, 1971). One might speculate that this caused reduced heat loss and, therefore, heat accumulation in the sediment further favouring the burning process. However, it remains puzzling why the same sediment interval self-combusted in one core but not in the parallel core. This illustrates that the ultimate trigger for self-combustion likely is a complex interaction of multiple factors.

Most of the described properties of Wukenfurche sediments have been also observed in other sediment records, however, not in the combination as found in the Wukenfurche sediments. Therefore, we assume that the self-combustion of sediments

after freeze-drying has been triggered by a combination of multiple factors including mainly the presence of abundant and very fine-grained iron sulphides as well as the occurrence of discrete amorphous organic layers and high sediment porosity.

5.5 Conclusion

We observed spontaneous combustion of laminated lateglacial lake sediments from the Wukenfurche palaeolake. The self-ignition was caused by exothermic oxidation reactions occurring immediately after air-ventilation of the vacuum chamber after freeze-drying. A comparable reaction of lake sediments has not been described before. We propose a combination of multiple factors including the presence of abundant fine-grained iron sulphides and of discrete amorphous organic layers as cause for this effect. Self-combustion of lake sediments can be prevented by ventilation of the freeze drier vacuum chamber after drying with N_2 instead of air.

Acknowledgements

This study is a contribution to the Virtual Institute of Integrated Climate and Landscape Evolution (ICLEA; www.iclea.de) of the Helmholtz Association (Grant Number VH-VI-415) and is supported by Helmholtz infrastructure of the Terrestrial Environmental Observatory (TERENO) North-eastern Germany. We thank Sebastian Tyszkowski (Polish Academy of Science), Mateusz Kramkowski (GFZ Potsdam) and Slawomir Kowalski (LBGR Brandenburg) for their help with coring and field work. Gabriele Arnold and Dieter Berger (both at GFZ Potsdam) prepared thin sections. We also thank Anja Schleicher for XRD analysis, Oona Appelt for microprobe analysis and Andreas Hendrich for graphical support (all at GFZ Potsdam). We also thank two anonymous reviewers for their constructive comments and suggestions that significantly improved this paper.

6 Synthesis

The primary scientific objective of this doctoral thesis is to reconstruct the climate and environmental variability in NE Germany by investigating annually laminated lake sediments. For this purpose, two varved sediment archives are analysed at high resolution: Lake Tiefer See and Palaeolake Wukenfurche. Detailed microfacies and geochemical analyses (aim I.) are conducted on both sediment archives, in order to establish the lithostratigraphic framework and to provide a base for understanding and interpretation of the proxy data. The aims II., III. and IV. were pursued for the last 6000 years of the Lake Tiefer See sediment record. The first part of the synthesis chapter of the doctoral thesis (Chapter 6.1) provides the main results and conclusions with respect to the aims of the doctoral thesis. Chapter 6.2 examines the contribution of this work to the ICLEA objectives and discusses preliminary results of the regional comparison between Lake Tiefer See and Lake Czechowskie sediment records. Chapter 6.3 highlights ongoing and planned investigations on both sedimentary archives and potential future analyses.

6.1 Main results and conclusions

Aim I.) Conducting high resolution sediment microfacies and geochemical analyses of Tiefer See and Wukenfurche sediment cores.

Detailed microfacies and geochemical analyses of the Lake Tiefer See and Palaeolake Wukenfurche sediment cores are presented in Chapter 2 and Chapter 5, respectively. The following presents the main results and conclusions for the respective study sites.

Lake Tiefer See

Chapter 2 introduces the sedimentology of the 10.8 m long sediment profile of Lake Tiefer See. In this manuscript, high resolution analyses focuses on the upper 7.7 m long and continuous part of the sediment record. Basic information about the lower 3 m of the sediment column are provided in Chapter 2.4.1. A key aspect of this manuscript is the understanding of the highly variable sedimentology from multi-centennial down to decadal and annual time-scales. Most variablity is displayed by the varve preservation and enabled to subdivide the sediment column into well-varved, poorly- and non-varved sediment intervals (Chapter 2.4.3):

i.) *Well-varved sediments* are characterized by well identifiable varve sub-layers, high organic matter contents and high abundance of diagenetic minerals (i.e. vivianite and Ca-rhodochrosite). Furthermore, three different varve types are differentiated: organic varves, calcite varves and Ca-rhodochrosite varves.

ii.) *Poorly-varved sediments* comprise of mixed sediment with frequently intercalated preserved varves and planktonic diatom layers, intermediate organic matter contents and an increased proportion of minerogenic and plant detritus and littoral microfossils.

iii.) *Non-varved sediments* consist of extensively mixed sediment, low organic matter contents and an increased proportion of minerogenic and plant detritus and littoral microfossils.

The combination of microfacies and geochemical analyses (i.e. bulk carbon geochemistry and μ-XRF scanning) enables to relate the deposition of these microfacies types to the prevailing oxygen regime in the bottom waters of the lake (Chapter 2.5.1). Low-energy hypoxic to anoxic conditions in the hypolimnion favor the formation of varves, whereas dominantly oxygenated conditions in the lower water column cause the deposition of non-varved sediment. Poorly-varved intervals likely indicate an intermediate state of bottom water oxygen contents.

The different varve types (*i.e.* organic varves, calcite varves and Ca-rhodochrosite varves, Chapter 2.4.3) indicate a decadal- to annual-scale variability in well-varved intervals. Rarely more than 20 successive varves are characterized by the same varve type. Chapter 2.5.1 presents a first idea of relating the formation of the different varve types to the prevailing redox potential at the sediment water interface. However, the proposed scenario is at this stage highly speculative and requires further investigations.

In conclusion, the combination of rather subjective microfacies analysis in thin sections with high resolution geochemical analyses is a valuable tool to characterize sedimentological changes in great detail. In the case of the Lake Tiefer See sediments, this methodology allows to relate the varve preservation to changes of the oxygen regime in the hypolimnion of the lake. Furthermore, the analyses indicates that Lake Tiefer See sediments display a high variability on multi-centennial to annual time scales. In particular, the frequent alternation of intervals characterized by different varve preservation is rarely observed in sediment archives and, therefore, imply a exceptional sensitivity of the oxygen regime to external forcing mechanisms.

Palaeolake Wukenfurche

Chapter 5 presents a 14.6 m long sediment profile of the Wukenfurche palaeolake. This manuscript mainly focuses on the description and investigation of spontaneous self-combustion of freeze-dried sediment samples after ventilation of the freeze dryer. This reaction was observed for the first time in a palaeolimniological study. The smouldering and flameless combustion of the sediment reached temperatures of about 360°C and lasted for a duration of 10-20 minutes. In order to identify the processes causing the sediment reaction, the microfacies and geochemistry of the sediment are studied in detail. The results presented in Chapter 5.3 suggest that the self-combustion was initiated by oxidation reactions, which are probably favored by a combination of multiple factors including the presence of abundant fine grained iron sulphides and of discrete amorphous organic layers.

This study further provides a base for future analyses at the Wukenfurche palaeolake. The presence of the Laacher See tephra at the onset of the finely laminated sediment interval provides an invaluable time marker for anchoring a chronology. A rough count of the lamination revealed about 2900 layer couplets for the entire laminated interval. Assuming an annual origin of these couplets, the laminated interval probably covers the period from the late Allerød to the early Holocene. The rhythmic deposition of alternating siderite, amorphous organic-rich matter and calcite layers might indicate an annual cycle behind the deposition, which has not been proven, yet. In addition, microfacies and geochemical analysis allows to define distinct intervals of varying geochemical composition and varve composition, which may reflect changes of climate and environmental conditions.

Aim II.) Performing a reliable chronology for the Tiefer See sediment record using different independent dating methods

Independent and reliable chronologies are important for palaeoclimate and -environmental reconstructions, as they enable to compare to different records and to trace potential lead and lags of regional climate response (Brauer et al., 2014). The application of different dating methods (*i.e.*, varve counting, tephrochronology and radiocarbon dating) allows establishing a robust chronology for the upper continuous 7.7 m of the sediment profile. Full details are presented in both Chapter 2.4.2 and in Chapter 3. As a summary, the final chronology consists of two parts, which are separated by a 70 c m thick non-varved sediment unit (unit II, Table 1.2):

ii.) *From 0 to 5.04 m of depth.* The timescale of this interval is developed by down-core varve counting and sedimentation rate estimates given a total of 3100 ± 130 years at 5.04 m of depth. Radiocarbon dates and the Glen Garry and Askja AD 1875 tephras confirm the varve-based chronology within the uncertainties.

i.) *7.7 - 5.71 m depth.* This interval comprises a floating varve chronology, which is anchored to calendar timescales using the HEKLA-4 tephra at 4293±43 cal. a BP (6.06 m depth; Chapter 3.4.1). The resulting timescale covers an interval of 2080 ± 40 varves from 3950 ± 45 to 6030 ± 85 cal. a BP. Radiocarbon dating supports the floating varve chronology.

The age-depth model of the non-varved unit II (5.71 - 5.04 m depth) is determined from linear interpolation between the ages estimated for the top and bottom of this interval. The counting error of the varve chronologies are variable along the sediment profile due to the intercalation of several poorly- and non-varved intervals and amount to ±85 years at 7.7 m depth.

In conclusion, the well-defined chronology of Lake Tiefer See sediments provides a valuable chronological framework for the comparison of the Lake Tiefer See data set with other records. Furthermore, the finding of multiple tephra layers contains the potential for detailed synchronization studies.

Aim III.) Establishing microfacies and geochemical proxies as indicators for climate and environmental changes at Tiefer See.

Combined microfacies and high-resolution geochemical analyses has been used for better understanding of the depositional process in Lake Tiefer See and to establish proxies for climate and environmental changes. Detailed information is shown in both Chapter 2 and Chapter 4. Chapter 2 examines the main processes driving the highly variable sediment deposition and the related oxygen regime in Lake Tiefer See during the last ~6000 years. Controlling factors of the $\delta^{13}C_{OM}$ ratio of sedimentary organic matter are investigated in Chapter 4, as well as their relationship with the anoxia fluctuations and productivity changes in Lake Tiefer See, as a complement of the work presented in Chapter 2.

Varve preservation as proxy for lake circulation

Preservation of annually layers is the most distinct sedimentological characteristic in the Lake Tiefer See sediment record for the last ~6000 years. Several geochemical indi-

cators correspond to the quality of varves, suggesting that alternations in varve preservation reflect distinct changes in the lake system.

As aforementioned, the varve preservation at Lake Tiefer See depends on bottom water anoxia. The oxygen regime in lakes is mainly a function of lake productivity and lake circulation (Demaison and Moore, 1980; Niessen et al., 1992). Preservation of varves during the last century has been mainly ascribed to increased productivity caused by human-induced lake eutrophication (Kienel et al., 2013). Higher lake productivity causes enhanced organic matter flux to the bottom waters and, thereby, the formation of anoxic conditions. Deeper in the sediment profile (*i.e.* before the 20^{th} century), varve formation was favored by reduced lake circulation as indicated by results presented in Chapter 2. During phases of lower lake circulation, oxygen transport decreased and stronger anoxic conditions developed, which promote varve preservation. Instead, intensified lake circulation induces an increase in oxygen transport to the bottom waters resulting in more oxygenated conditions, which are not favorable for varve preservation.

The combination of high-resolution microfacies and geochemical analyses allows to identify lake circulation as the main driver of sediment variability in Lake Tiefer See. Intensity of the lake circulation mainly causes the striking alternation of well-varved and poorl-/non-varved sediments, except for the last century where human induced eutrophication is the most important factor for varve preservation. Consequently, the varve quality is considered as a proxy for the lake circulation at Lake Tiefer See before the 20^{th} centure.

Varying control on $\delta^{13}C_{OM}$

Proxy calibration and verification is one main objective in ICLEA. Therefore, proxy data need to be tested if they can be interpreted the same way throughout the entire sedimentary column (i.e. proxy stationarity). The $\delta^{13}C_{OM}$ is considered to be particularly sensitive to changes in lake productivity (e.g. Brenner et al., 1999; Stuiver, 1975), but also to changes in the oxygen regime in the lake hypolimnion (e.g. Hollander and Smith, 2001; Kohzu et al., 2011). As both factors change in Lake Tiefer See during the last ~6000 years, Chapter 4 examines the main control on $\delta^{13}C$ in sedimentary organic matter. In particular, this study applies a novel concept, which integrates the multi-proxy data set from the long sediment record as well as results from spatially distributed surface sediment cores and from lake monitoring. This comprehensive study has only been possible because of the novel bridging time scale concept within ICLEA.

Results obtained from the long sediment core indicate a close correspondence between the $\delta^{13}C_{OM}$ ratio and the varve preservation during the past ~6000 years. Depleted isotope values are associated with well-varved intervals and enriched values with poorly- and non-varved sections. The comparison of the $\delta^{13}C_{OM}$ ratios with the geochemical data set indicates that the variations are presumably caused by a combination of microbial carbon cycling and selective organic matter degradation in Lake Tiefer See. In particular, the relative influence of microbial carbon cycling and selective organic matter degradation as controlling factors on the $\delta^{13}C_{OM}$ values changes over time. Which of the two factors controls the $\delta^{13}C_{OM}$ ratios depends on the prevailing oxygen regime in the bottom waters of Lake Tiefer See. During anoxic conditions, microbial carbon cycling appears to be the controlling factor for $\delta^{13}C_{OM}$ and causes more depleted values in well-varved sediment intervals. In contrast, selective organic matter degradation becomes an important factor during the prevalence of more oxygenated conditions inducing the enrichment of $\delta^{13}C_{OM}$ ratios.

In conclusion, the results imply that the factors controlling $\delta^{13}C_{OM}$ at Lake Tiefer See vary in time in relation to the lake circulation regime. An interesting aspect is that $\delta^{13}C_{OM}$ is, despite of the strong increase of lake productivity, also in the recent well-varved interval influenced by microbial carbon cycling similarly to the older well-varved sediment sections. This observation might has implications for calibrations studies and for testing the above mentioned hypotheses (e.g. microbial carbon cycling).

Aim IV.) Tracing the effects of climate variability and human activity on sediment deposition at Tiefer See.

Varve formation and preservation at Lake Tiefer See during the past ~6000 years are particularly sensitive to changes in lake circulation, causing distinct alternations of varved and poorly-/non-varved intervals. As lake circulation is mainly influenced by wind stress and lake stratification, which is a function of temperature and seasonality, changes of lake circulation may reflect changes of climate conditions in the past. Furthermore, lake circulation may also be influenced by local factors. As for example, a reduced wind shelter induced by anthropogenic deforestation might lead to increased sensitivity of lake circulation to wind stress (Bierstedt et al., 2015b; Boehrer and Schultze, 2008; Stevens et al., 2000). This means, that also human impact may induce changes in lake circulation.

The main result of the lake-circulation reconstruction from varve preservation at Lake Tiefer See is a trend towards increased lake circulation after ~4000 cal. a BP, which

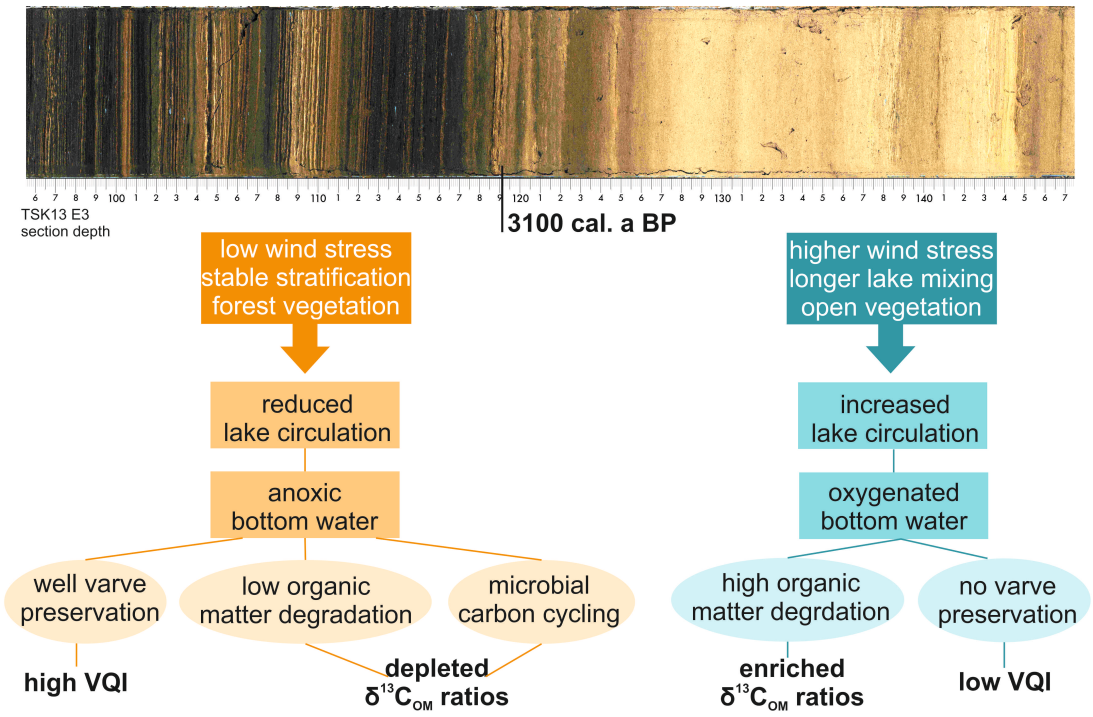

Figure 6.1: Top: sediment section between 4.80 and 5.30 m sediment depth showing the transition between unit II and unit III at ~3100 cal. a BP. Bottom: Overview of processes related to well-varved and non-varved sediment intervals in Lake Tiefer See.

is superimposed by decadal to centennial episodes of increased lake circulation. The long-term trend is indicated by longer and more frequently occurring non- and poorly-varved intervals after ~4000 cal. a BP. Similar trends towards less stable lake stratification and stronger lake circulation after ~5000 cal. a BP have been previously reported from other lakes in Central Europe (e.g. Pędziszewska et al., 2015; Finsinger et al., 2014; Eusterhues et al., 2005). This suggests a common forcing mechanism. A possible explanation might be related to gradual changes in Northern Hemisphere orbital forcing (Laskar, 1990; Laskar et al., 2004), leading to colder summer and warmer winter temperatures and increased windiness in Central Europe (e.g. Wanner et al., 2008; Orme et al., 2016). Cooler summers and warmer winters cause a reduced stability of lake stratification and, thus, enhance the susceptibility to wind-driven lake circulation. The general increased wind stress may has additionally intensified lake circulation.

The superimposed short-term phases of intensified lake circulation generally coincide with increased vegetation openness in the catchment of Lake Tiefer See, suggesting anthropogenic deforestation as an important factor for lake circulation at Lake Tiefer See since ~4000 cal. a BP. However, increased circulation periods at ~2850 cal. a BP, AD 330–510 and AD 1200–1900 also concur with centennial-scale intervals of

colder, moister and winder climate conditions (2.8 ka event e.g. van Geel (1978); 'Dark Ages' e.g. Büntgen et al. (2011); 'Little Ice Age' e.g. Pfister et al. (1998)), suggesting that climate change might has additionally increased lake circulation. The coincidence of climate change and human impact makes it difficult to evaluate the contribution of each factor on the lake circulation. A further complicating factor is the lack of an independent proxy for changes of the wind stress at Lake Tiefer See.

An intriguing finding of this study presented in Chapter 2, is that major phases of non-varved sediment at Lake Tiefer See coincide with periods of bioturbated sediments in the Baltic Sea. The striking correspondence further supports the influence of regional climate change on lake circulation at Lake Tiefer See and suggests a common driver. Bioturbated sediment deposition in the Baltic Sea has been related to enhanced river inflow and windier conditions (Andrén et al., 2000; Jilbert et al., 2015; Ning et al., 2016; Zillén et al., 2008). However, further investigations are necessary to verify and explain this observation.

In conclusion, the driver for variability in lake circulation is most likely a combination of long-term and short-term climate changes as well as anthropogenic deforestation during settlement periods. However, the relative importance of climate and human influences in the respective periods of increased lake circulation remains difficult to disentangle partly due to the lack of independent wind proxies at Lake Tiefer See. In this respect, the comparison of Lake Tiefer See and Lake Czechowskie might represents a great potential to disentangle the influence of climate change and human impact on lake circulation in more detail.

6.2 Contribution to the ICLEA project

This doctoral thesis mainly contributed to Aim B and Aim C of the ICLEA objectives by providing both, high resolution proxy data and a robust chronology from the Lake Tiefer See sediments. Furthermore, in total 3 common tephra layers were identified in the sedimentary archives of Lakes Tiefer See and Czechowskie during the early Holocene and the sub-recent period allowing a detailed synchronization of both sediment records for these time slices. Another important finding for the ICLEA objective Aim A, is the identification of different trigger mechanisms for varve preservation at present and in the past. This is particularly useful for calibration studies, as considering these differences may prevent erroneous transfer functions.

The results presented in this doctoral thesis particularly demonstrate the potential of Lake Tiefer See sediments for palaeoclimate and -environmental reconstruc-

tions. However, detailed interpretations about climate changes during the past ~6000 years remained challenging. Comparing the results to the counterpart on the ICLEA-transect, Lake Czechowskie, potentially allows an improved evaluation of the dominant drivers for lake system change at Lake Tiefer See. In this respect, preliminary results comparing the Lake Tiefer See and Lake Czechowskie sediment records are outlined in the following section.

The comparison of results from Lakes Tiefer See and Lake Czechwoskie indicates two main similarities between both records. The first includes that both records show a long term trend of increasing lake circulation during the past ~6000 years. While at Lake Tiefer See this trend is displayed by an increasing occurrence of periods with enhanced lake circulation after ~4000 cal a BP, the trend at Lake Czechowskie is more gradually culminating in a distinct rise in varve thickness and annual variability after ~2800 cal. a BP (Ott et al., 2015). The thickening of varves is related to intensified lake productivity, which is probably caused by enhanced lake circulation in Lake Czechowskie (Ott et al., 2013). Interestingly, the same process (i.e. increased lake circulation) induced different responses in both lakes: oxygenated conditions at Lake Tiefer See and increased productivity at Lake Czechowskie. These different responses may be related to different local properties. On the other hand, they may also be related to different regional manifestation of climate, which implies that the drivers of lake circulation, such as wind stress, are stronger at Lake Tiefer See as compared to Lake Czechowskie. This idea might be supported by a number of continuously varved sediment records reported from N Poland (Tylmann et al., 2013b), while in N Germany an entirely varved record especially for the Late Holocene has not been found yet. However, this rather speculative hypothesis has to be further investigated in more detail *e.g.* with modeling studies and integration of more lake records.

Another similarity indicated by both records is related to simultaneously increased lake circulation after ~2800 cal. a BP. At Lake Czechowskie varve thickness rises in three distinct centennial-scale intervals after ~2800 cal. a BP (Ott et al., 2013), which coincide with phases of poorly- and non-preserved varves at Lake Tiefer See at ~2800 cal. a BP, at ~1400 cal. a BP and at ~750 cal. a BP. This implies that during three distinct centennial-scale periods lake circulation was increased in both lakes. In contrast to lake Tiefer See, the latter two periods of increased lake circulation at Lake Czechowskie are considered to be not concurrent with increased human impact in the catchment. For the first phase, pollen analyses has not been conducted yet. Nevertheless, these coincidences of distinct periods of increased lake circulation in both lakes suggest a over-regional climate trigger. Interestingly, all three phases coincide with known periods of

cooler, wetter and windier climate corresponding to the 2.8 ka event (Martin-Puertas et al., 2012b; Van Geel et al., 1996), 'Dark Ages' and 'Little Ice Age' (Büntgen et al., 2011).

In conclusion, the comparison of Lakes Tiefer See and Czechowskie highlights the importance of climate changes for three distinct periods of increased lake circulation at Lake Tiefer See. Furthermore, detailed investigations are necessary to verify the finding and to explain the observed similarities. Nevertheless, these first results emphasize the huge potential of regional integration of proxy records and the great value of the work conducted within the ICLEA project.

6.3 Future prospects

The high resolution records presented in this doctoral thesis, offers a huge potential for further high resolution studies. At Lake Tiefer See of probably most interest is to obtain an entirely continuous sediment profile. Preliminary results of the sediment between both sediment gaps indicate almost completely varved sediment, which might cover the Early Holocene until ~9000 cal. a BP. Furthermore, this sediment shows a lower variability as compared to the upper part of the profile. To identify the triggers causing this difference would be an interesting point for future studies. Furthermore, it would be possible to compare the entire Holocene development of Lake Tiefer See and Lake Czechowskie, giving more detailed insight into the climate history of the N central European Lowlands. Another interesting aspect is to study distinct time slices. For examples, the almost completely varved sediment interval between ~6000 and 4000 cal. a BP shows a high annual- to decadal scale variability and might contain interesting high-frequency palaeoclimate and -environmental information. As these interval are presented by calcite varves, stable isotope studies on the calcite may further contribute to detailed climate reconstructions (Leng and Marshall, 2004; Mangili et al., 2007). Testing the presence of microbial processes today and in the past might be a further future study. As also today microbial processes seem to influence carbon cycling in Lake Tiefer See, they might provide another tool for proxy calibration.

At palaeolake Wukenfurche, further studies will include the detailed analysis of the lamination to test if they represent varves. A further potential of the lake Wukenfurche sediments is the continuous deposition of siderite and calcite in the sediment. If both components could be separated, stable isotope analysis on calcite and siderite could be integrated in a multi isotope comparison given inside in, for example, redox path ways and temperature changes (Leng and Marshall, 2004).

Bibliography

a.a. Sommerville, Hansom, J., Sanderson, D., and Housley, R. (2003). Optically stimulated luminescence dating of large storm events in Northern Scotland. *Quaternary Science Reviews*, 22(10-13):1085–1092. 2.7

Aarnes, I., Bjune, A. E., Birks, H. H., Balascio, N. L., Bakke, J., and Blaauw, M. (2012). Vegetation responses to rapid climatic changes during the last deglaciation 13,500-8,000 years ago on southwest Andoya, arctic Norway. *Vegetation History and Archaeobotany*, 21(1):17–35. 3.4.1

Abbott, P. M. and Davies, S. M. (2012). Volcanism and the Greenland ice-cores: The tephra record. *Earth-Science Reviews*, 115(3):173–191. 3.4.1

Aller, R. C. (1994). Bioturbation and remineralization of sedimentary organic matter: effects of redox oscillation. *Chemical Geology*, 114(3-4):331–345. 4.5.2

Amann, B., Lobsiger, S., Fischer, D., Tylmann, W., Bonk, A., Filipiak, J., and Grosjean, M. (2014). Spring temperature variability and eutrophication history inferred from sedimentary pigments in the varved sediments of Lake Żabińskie, north-eastern Poland, AD 1907-2008. *Global and Planetary Change*, 123:86–96. 1.1

Andersson, S., Rosqvist, G., Leng, M. j., Wastegård, S., and Blaauw, M. (2010). Late Holocene climate change in central Sweden inferred from lacustrine stable isotope data. *Journal of Quaternary Science*, 25(8):1305–1316. 3.4

Andrén, E., Andrén, T., and Kunzendorf, H. (2000). Holocene history of the Baltic Sea as a background for assessing records of human impact in the sediments of the Gotland Basin. *The Holocene*, 10(6):687–702. 2.5.3, 6.1

Andrews, J. T., Geirsdóttir, A., Hardardóttir, J., Principato, S., Grönvold, K., Kristjansdóttir, G. B., Helgadóttir, G., Drexler, J., and Sveinbjörnsdóttir, A. (2002). Distribution, sediment magnetism and geochemistry of the Saksunarvatn (10 180 +- 60 cal. yr BP) tephra in marine, lake, and terrestrial sediments, northwest Iceland. *Journal of Quaternary Science*, 17(8):731–745. 3.4.1

Bahrig, B. (1988). Palaeo-environment information from deep water siderite (Lake of Laach, West Germany). *Geological Society, London, Special Publications*, 40(1):153–158. 5.3.4

Banerjee, S. C. (1981). *Spontaneous combustion of coal and mine fires*. Balkema, Rotterdam. 5.1

Barber, K., Langdon, P., and Blundell, A. (2008). Dating the Glen Garry tephra: a widespread late-Holocene marker horizon in the peatlands of northern Britain. *The Holocene*, 18(1):31–43. 2.4.2, 3.4, 3.4.1

Bateman, M. and Godby, S. (2004). Late-Holocene inland dune activity in the UK: a case study from Breckland, East Anglia. *The Holocene*, 4(2004):579–588. 2.7

Batterbee, R., Anderson, N. J., Bennion, H., and Simpson, G. (2012). Combining limnological and palaeolimnological data to disentangle the effects of nutrient pollution and climate change on lake ecosystems: problems and potential. *Freshwater Biology*, 57(10):2091–2106. 1.1

Behl, R. J. and Kennett, J. P. (1995). Brief interstadial events in the Santa Barbara basin, NE Pacific during the past 60 kyr. *Nature*, 379:243–246. 2.1, 2.3.2

Behre, K. E. (1988). The role of man in European vegetation history. In Huntley, B. and Webb, T., editors, *Handbook of Vegetation Science*, pages 633–672. Springer, Netherlands. 1.1

Bergman, J., Wastegård, S., Hammarlund, D., Wohlfarth, B., and Roberts, S. J. (2004). Holocene tephra horizons at Klocka Bog, west-central Sweden: Aspects of reproducibility in subarctic peat deposits. *Journal of Quaternary Science*, 19(3):241–249. 3.4, 3.4.1, 3.7

Beug, H.-J. (2004). *Leitfaden der Pollenbestimmung für Mitteleuropa und angrenzende Gebiete*. München: Verlag Dr. Friedrich Pfeil. 2.3.5

Bierstedt, S. E., Hünicke, B., and Zorita, E. (2015a). Variability of wind direction statistics of mean and extreme wind events over the Baltic Sea region. *Tellus A*, 67. 2.2

Bierstedt, S. E., Hünicke, B., Zorita, E., Wagner, S., and Gómez-Navarro, J. J. (2015b). Variability of daily winter wind speed distribution over Northern Europe during the past millennium in regional and global climate simulations. *Climate of the Past Discussions*, 11(2):1479–1518. 2.5.2, 6.1

Birks, H. H. and Birks, H. J. B. (2006). Multi-proxy studies in palaeolimnology. *Vegetation History and Archaeobotany*, 15(4):235–251. 1.1

Birks, H. H., Gulliksen, S., Haflidason, H., Mangerud, J., and Possnert, G. (1996). New Radiocarbon Dates for the Vedde Ash and the Saksunarvatn Ash from Western Norway. *Quaternary Research*, 45(2):119–127. 3.4.1, 3.4

Björck, S. and Clemmensen, L. B. (2004). Aeolian sediment in raised bog deposits, Halland, SW Sweden: a new proxy record of Holocene winte storminess variation in southern Scandinavia? *The Holocene*, 5:677–688. 2.7

Błaszkiewicz, M. (2011). Timing of the final disappearance of permafrost in the central European Lowland, as reconstructed from the evolution of lakes in N Poland. *Geological Quarterly*, 55(4):361–374. 3.2

Błaszkiewicz, M., Piotrowski, J. A., Brauer, A., Gierszewski, P., Kordowski, J., Kramkowski, M., Lamparski, P., Lorenz, S., Noryśkiewicz, A. M., Ott, F., Słowiński, M., and Tyszkowski, S. (2015). Climatic and morphological controls on diachronous postglacial lake and river valley evolution in the area of Last Glaciation, northern Poland. *Quaternary Science Reviews*, 109:13–27. 1.2, 3.2

Boehrer, B. and Schultze, M. (2008). Stratification of lakes. *Reviews of Geophysics*, 46(2006):1–27. 2.5.2, 6.1

Bonk, A., Tylmann, W., Goslar, T., Wacnik, A., and Grosjean, M. (2015). Comparing Varve Counting And 14C-Ams Chronologies In The Sediments Of Lake Żabińskie, Northeastern Poland: Implications For Accurate 14C Dating Of Lake Sediments. *Geochronometria*, 42:159–171. 2.1

Boygle, J. (1998). A little goes a long way: Discovery of a new mid-Holocene tephra in Sweden. *Boreas*, 27(3):195–199. 3.4, 3.4.1

Bramham-Law, C. W. F., Theuerkauf, M., Lane, C. S., and Mangerud, J. (2013). New findings regarding the Saksunarvatn Ash in Germany. *Journal of Quaternary Science*, 28(3):248–257. 3.1, 3.4.1, 3.4, 3.4.4

Brauer, A. (2004). Annually laminated lake sediments and their palaeoclimatic relevance. In *The Climate in Historical Times*, pages 109–127. Springer. 2.1, 2.5.1

Brauer, A. and Casanova, J. (2001). Chronology and depositional processes of the laminated sediment record from Lac d'Annecy, French Alps. *Journal of Paleolimnology*, 25:163–177. 1.5, 2.3.1, 4.3.2, 5.1, 5.2

Brauer, A., Endres, C., and Negendank, J. F. W. (1999). Lateglacial calendar year chronology based on annually laminated sediments from Lake Meerfelder Maar, Germany. *Quaternary International*, 61:17–25. 2.1, 2.4.1, 3.1, 5.3.1

Brauer, A., Hajdas, I., Blockley, S. P. E., Bronk Ramsey, C., Christl, M., Ivy-Ochs, S., Moseley, G. E., Nowaczyk, N. N., Rasmussen, S. O., Roberts, H. M., Spötl, C., Staff, R. A., and Svensson, A. (2014). The importance of independent chronology in integrating records of past climate change for the 60-8ka INTIMATE time interval. *Quaternary Science Reviews*, 106:47–66. 1.1, 6.1

Brauer, A., Haug, G. H., Dulski, P., Sigman, D. M., and Negendank, J. F. W. (2008). An abrupt wind shift in western Europe at the onset of the Younger Dryas cold period. *Nature Geoscience*, 1(8):520–523. 1.1

Brauer, A. and Negendank, J. F. (1993). Paleoenvironmental reconstruction of the late- and postglacial sedimentary record of lake Weinfelder Maar. *Lecture Notes in Earth Sciences*, 49(Paleolimnology of European Maar Lakes):223–235. 5.3.4, 5.4.1

Brenner, M., Whitmore, T. J., Curtis, J. H., Hodell, D. A., and Schelske, C. L. (1999). Stable isotope (δ13C and δ15N) signatures of sedimented organic matter as indicators of historic lake trophic state. *Journal of Paleolimnology*, 22:205–221. 4.1, 4.5.1, 6.1

Briffa, K. R., Bartholin, T. S., Eckstein, D., Jones, P. D., Karlén, W., Schweingruber, F. H., and Zetterberg, P. (1990). A 1,400-year tree-ring record of summer temperatures in Fennoscandia. *Nature*, 346:434–439. 1.1

Bronk Ramsey, C. (2008). Deposition models for chronological records. *Quaternary Science Reviews*, 27(1-2):42–60. 2.1, 2.3.3, 2.3

Bronk Ramsey, C. (2009). Bayesian Analysis of Radiocarbon Dates. *Radiocarbon*, 51(1):337–360. 2.1, 2.3.3, 2.3

Bronk Ramsey, C., Albert, P. G., Blockley, S. P., Hardiman, M., Housley, R. A., Lane, C. S., Lee, S., Matthews, I. P., Smith, V. C., and Lowe, J. J. (2015). Improved age estimates for key Late Quaternary European tephra horizons in the RESET lattice. *Quaternary Science Reviews*, 118:18–32. 2.4.1, 3.4.1

Bronk Ramsey, C. and Lee, S. (2013). Recent and Planned Developments of the Program OxCal. *Radiocarbon*, 55(2):720–730. 2.3.3

Büntgen, U., Tegel, W., Nicolussi, K., McCormick, M., Frank, D., Trouet, V., Kaplan, J. O., Herzig, F., Heussner, K.-U., Wanner, H., Luterbacher, J., and Esper, J. (2011). 2500 Years of European Climate. *Science*, 331:578–582. 1.1, 2.4.5, 2.5.3, 6.1, 6.2

Burke, I. T., Grigorov, I., and Kemp, A. E. S. (2002). Microfabric study of diatomaceous and lithogenic deposition in laminated sediments from the Gotland Deep, Baltic Sea. *Marine Geology*, 183(1-4):89–105. 2.4.3.1

Calvert, S. E. and Price, N. B. (1970). Composition of manganese nodules and manganese carbonates from Loch Fyne, Scotland. *Contributions to Mineralogy and Petrology*, 29(3):215–233. 2.4.3.1

Canuel, E. A. and Martens, C. S. (1996). Reactivity of recently deposited organic matter: Degradation of lipid compounds near the sediment-water interface. *Geochimica et Cosmochimica Acta*, 60(10):1793–1806. 4.1, 4.5.2

Carey, R., Houghton, B., and Thordarson, T. (2009). Tephra dispersal and eruption dynamics of wet and dry phases of the 1875 eruption of Askja Volcano, Iceland. *Bulletin of Volcanologyll*, 48:109–125. 3.4.1, 3.4.4

Carpenter, S. R. (2005). Eutrophication of aquatic ecosystems: bistability and soil phosphorus. *Proceedings of the National Academy of Sciences of the United States of America*, 102(29):1000–10005. 2.1

Chambers, F. M., Daniell, J. R., Hunt, J. B., Molloy, K., and O'Connell, M. (2004). Tephrostratigraphy of An Loch Mór, Inis Oírr, western Ireland: implications for Holocene tephrochronology in the northeastern Atlantic region. *The Holocene*, 14(5):703–720. 3.4, 3.4.1, 3.7

Cheung, M.-C., Zong, Y., Wang, N., Aitchison, J. C., and Zheng, Z. (2015). δ13Corg and n-alkane evidence for changing wetland conditions during a stable mid-late Holocene climate in the central Tibetan Plateau. *Palaeogeography, Palaeoclimatology, Palaeoecology*, 438:203–212. 4.1

Clemmensen, L. B., Murray, A., Heinemeier, J., and de Jong, R. (2009). The evolution of Holocene coastal dunefields, Jutland, Denmark: A record of climate change over the past 5000 years. *Geomorphology*, 105(3-4):303–313. 2.7

Conway, N. M., Kennicutt, M., and Van Dover, C. L. (1994). table isotopes in the study of marine chemosynthetic-based food webs. In Lajtha, K. and Michener, R. H., edi-

tors, *Stable Isotopes in Ecology and Environmental Science*, chapter 8, pages 158–186. Blackwell Scientific. 4.5.1

Cranwell, P. (1981). Diagenesis of free and bound lipids in terrestrial detritus deposited in a lacustrine sediment. *Organic Geochemistry*, 3(3):79–89. 4.5.2

Czymzik, M., Dreibrodt, S., Feeser, I., Adolphi, F., and Brauer, A. (2016). Mid-Holocene humid periods reconstructed from calcite varves of the Lake Woserin sediment record (north-eastern Germany). *The Holocene*, pages 1–12. 2.1

Czymzik, M., Muscheler, R., Brauer, A., Adolphi, F., Ott, F., Kienel, U., Dräger, N., Słowiński, M., Aldahan, A., and Possnert, G. (2015). Solar cycles and depositional processes in annual 10Be from two varved lake sediment records. *Earth and Planetary Science Letters*, 428:44–51. 2.1

Dansgaard, W., Johnsen, S. J., Clausen, H. B., Dahl-Jensen, D., Gundestrup, N. S., Hammer, C. U., Hvidberg, C. S., Steffensen, J. P., Sveinbjörnsdóttir, Á. E., Jouzel, J., and Bond, G. C. (1993). Evidence for general instability of past climate from a 250-kyr ice-core record. *Nature*, 364:218–220. 1.1

Davies, S. M., Abbott, P. M., Pearce, N. J. G., Wastegård, S., and Blockley, S. P. E. (2012). Integrating the INTIMATE records using tephrochronology: Rising to the challenge. *Quaternary Science Reviews*, 36:11–27. 3.4.1, 3.5, 3.4.4

Davies, S. M., Elmquist, M., Bergmann, J., Wohlfarth, B., and Hammarlund, D. (2007). Cryptotephra sedimentation processes within two lacustrine sequences from west central Sweden. *Holocene*, 17:1–13. 3.4, 3.4.1

Davies, S. M., Wastegård, S., and Wohlfarth, B. (2003). Extending the limits of the Borrobol Tephra to Scandinavia and detection of new early Holocene tephras. *Quaternary Research*, 59(3):345–352. 2.4.1, 3.4.1, 3.4.1, 3.4, 3.7

de Jong, R., Björck, S., Björkman, L., and Clemmensen, L. B. (2006). Storminess variation during the last 6500 years as reconstructed from an ombrotrophic peat bog in Halland, southwest Sweden. *Journal of Quaternary Science*, 21(8):905–919. 2.7

Dean, W. E. (1993). *Elk Lake, Minnesota: Evidence for Rapid Climate Change in the North-Central United States*, volume 276 of *Geological Society of America Special Papers*. Geological Society of America. 2.4.3.1

Dean, W. E. (1999). The carbon cycle and biogeochemical dynamics in lake sediments. *Journal of Paleolimnology*, 21(4):375–393. 2.5.1

Dean, W. E. J. (1974). Determination of carbonate and organic matter in calcareous sediments and sedimentary rocks by loss on ignition: Comparison with other methods. *Journal of Sedimentary Petrology*, 44(I):242–248. 5.4.1

Dearing, J. A. (2006). Climate-human-environment interactions: resolving our past. *Climate of the Past Discussions*, 2(4):563–604. 1.1

Degans, E. (1969). Biogeochemistry of stable carbon isotopes. In Eglinton, E. and Murphy, M., editors, *Organic geochemistry*, pages 304–329. Springer Berlin Heidelberg. 4.5.1

Demaison, G. J. and Moore, G. T. (1980). Anoxic environment and oil source bed genesis. *Organic Geochemistry*, 2:9–31. 2.5.1, 6.1

Demory, F., Oberhänsli, H., Nowaczyk, N. R., Gottschalk, M., Wirth, R., and Naumann, R. (2005). Detrital input and early diagenesis in sediments from Lake Baikal revealed by rock magnetism. *Global and Planetary Change*, 46:145–166. 2.4.4.2

Deplazes, G., Lückge, A., Peterson, L. C., Timmermann, A., Hamann, Y., Hughen, K. A., Röhl, U., Laj, C., Cane, M. A., Sigman, D. M., and Haug, G. H. (2013). Links between tropical rainfall and North Atlantic climate during the last glacial period. *Nature Geoscience*, 6(2):1–5. 2.3.2

Dörfler, W., Feeser, I., van den Bogaard, C., Dreibrodt, S., Erlenkeuser, H., Kleinmann, A., Merkt, J., and Wiethold, J. (2012). A high-quality annually laminated sequence from Lake Belau, Northern Germany: Revised chronology and its implications for palynological and tephrochronological studies. *The Holocene*, 22(12):1413–1426. 2.1, 2.4.2, 3.1, 3.4, 3.4.1, 3.4.1, 3.7

Dräger, N., Brauer, A., Brademann, B., Tjallingii, R., Słowiński, M., Błaszkiewicz, M., and Schlaak, N. (2016). Spontaneous self-combustion of organic-rich lateglacial lake sediments after freeze-drying. *Journal of Paleolimnology*, 55(2):185–194. 2.4.1, 4.1, 4.3.1, 4.2, 4.5.1, 4.5.1, 4.5.2

Dräger, N., Wulf, S., Kienel, U., Dulski, P., Ott, F., Słowiński, M., Theuerkauf, M., and Brauer, A. (2014). High-resolution microfacies analysis and tephrochronology of varved sediments from Lake Tiefer See (NE Germany). *Geophysical Research Abstracts*, 2014:EGU2014–2411. 3.1, 3.2, 3.3.1.1

Dreibrodt, S. and Wiethold, J. (2015). Lake Belau and its catchment (northern Germany): A key archive of environmental history in northern central Europe since the onset of agriculture. *The Holocene*, 25(2):296–322. 1.1, 2.1

Dugmore, A. J., Larsen, G. r., and Newton, A. J. (1995a). Seven tephra isochrones in Scotland. *The Holocene*, 5(3):257–266. 2.4.2, 3.4, 3.4.1

Dugmore, A. J., Shore, J., Cook, G., Newton, A., Edwards, K., and Larsen, G. (1995b). The radiocarbon dating of Icelandic tephra layers in Britain and Iceland. *Radiocarbon*, 37:379–388. 3.4.1, 3.4.1

Eiríksson, J., Knudsen, K. L., Haflidason, H., and Heinemeier, J. (2000). Chronology of late Holocene climatic events in the northern North Atlantic based on AMS 14C dates and tephra markers from the volcano Hekla, Iceland. *Journal of Quaternary Science*, 15(6):573–580. 3.4

Emerson, S. and Hedges, J. I. (1988). Areab , time scale years d plutonium b Seibold c % dw , indicates percent dry weight ; cmb 3 indicates sediment . The difference was calculated assuming a dry sediment. *Palaeogeography, Palaeoclimatology, Palaeoecology*, 3(5):621–634. 4.1

Enters, D., Kirilova, E., Lotter, A. F., Parplies, J., Jahn, S., Kuhn, G., and Zolitschka, B. (2010). Climate change and human impact at Sacrower See (NE Germany) during the past 13,000 years: a geochemical record. *Journal of Paleolimnology*, 43:719–737. 3.1

Eusterhues, K., Heinrichs, H., and Schneider, J. (2005). Geochemical response on redox fluctuations in Holocene lake sediments, Lake Steisslingen, Southern Germany. *Chemical Geology*, 222(1-2):1–22. 2.5.3, 6.1

Fægri, K. and Iversen, J. (1989). *Textbook of Pollen Analysis*. Chichester: Wiley. 2.3.5

Feeser, I., Do rfler, W., Czymzik, M., and Dreibrodt, S. (2016). A mid-Holocene annually laminated sediment sequence from Lake Woserin: The role of climate and environmental change for cultural development during the Neolithic in Northern Germany. *The Holocene*. 1.1, 2.1

Feurdean, A., Persoiu, A., Tantau, I., Stevens, T., Magyari, E., Onac, B., Marković, S., Andrič, M., Connor, S., Farca, S., Gałka, M., Gaudeny, T., Hoek, W., Kolaczek, P., Kuneš, P., Lamentowicz, M., Marinova, E., Michczyńska, D., Persoiu, I., Płóciennik, M., Słowiński, M., Stancikaite, M., Sumegi, P., Svensson, A., Tamas, T., Timar, A., Tonkov, S.,

Toth, M., Veski, S., Willis, K., and Zernitskaya, V. (2014). Climate variability and associated vegetation response throughout Central and Eastern Europe (CEE) between 60 and 8 ka. *Quaternary Science Reviews*, 106:206–224. 3.5

Finlay, J. C. and Kendall, C. (2007). Stable Isotopes tracing of temporal and spatial variability in organic matter sources to freshwater ecosystems. *Stable Isotopes in Ecology and Environmental Science*, pages 283–333. 4.5.1

Finsinger, W., Fonville, T., Kirilova, E., Lami, A., Guilizzoni, P., and Lotter, A. F. (2014). A long-term multi-proxy record of varved sediments highlights climate-induced mixing-regime shift in a large hard-water lake ˜5000 years ago. *Journal of Limnology*, 73(2). 2.5.3, 6.1

Flößner, D. (2000). *Die Haplopoda und Cladocera (ohne Bosminidae) Mitteleuropas*. Backhuys Publishers, Leiden. 2.3.6

Francus, P., Bradley, R. S., Abbott, M. B., Patridge, W., and Keiming, F. (2002). Paleoclimate studies of minerogenic sediments using annually resolved textural parameters. *Geophysical Research Letters*, 29(20):1998–2001. 1.1

Frandsen, W. H. (1997). Ignition probability of organic soils. *Canadian Journal of Forest Research*, 27(9):1471–1477. 5.1

Froggatt, P. C. and Lowe, D. J. (1990). A review of late Quaternary silicic and some other tephra formations from New Zealand: their stratigraphy, nomenclature, distribution, volume, and age. *New Zealand Journal of Geology and Geophysics*, 33:89–109. 2.4.2, 3.4.1

Gaillard, M. J., Sugita, S., Bunting, J., Dearing, J., and Bittmann, F. (2008). Human impact on terrestrial ecosystems, pollen calibration and quantitative reconstruction of past land-cover. *Vegetation History and Archaeobotany*, 17(5):415–418. 1.1

Germer, S., Kaiser, K., Bens, O., and Hüttl, R. F. (2011). Water balance changes and responses of ecosystems and society in the berlin-brandenburg region - A review. *Erde*, 142(1-2):65–95. 1.2

Gilbertson, D. D., Schwenninger, J.-L., Kemp, R. A., and Rhodes, E. J. (1999). Sand-drift and Soil Formation Along an Exposed North Atlantic Coastline: 14,000 Years of Diverse Geomorphological, Climatic and Human Impacts. *Journal of Archaeological Science*, 26:439–469. 2.7

Gill, A. E. (1982). *Atmosphere-ocean dynamics*. Academic press, 1982, vol. 30 edition. 2.5.3

Goossens, H., Düren, R., de Leeuw, J., and Schenck, P. (1989). Lipids and their mode of occurrence in bacteria and sediments-II. Lipids in the sediment of a stratified, freshwater lake. *Organic Geochemistry*, 14(1):27–41. 4.1

Goslar, T., Kuc, T., Ralska-Jasiewiczowa, M., Różanski, K., Arnold, M., Bard, E., van Geel, B., Pazdur, M. F., Szeroczyńska, K., Wicik, B., Więckowski, K., and Walanus, A. (1993). High-Resolution Lacustrine Record of the Late-Glacial Holocene Transition in Central-Europe. *Quaternary Science Reviews*, Vol 12(Iss 5):287–294. 3.1, 3.5

Goslar, T., Ralska-Jasiewiczowa, M., Van Geel, B., Łacka, B., Szeroczyńska, K., Chróst, L., and Walanus, A. (1999). Anthropogenic changes in the sediment composition of Lake Gosciaz (central Poland), during the last 330 yrs. *Journal of Paleolimnology*, 22(2):171–185. 3.1, 3.5

Grönvold, K. and Jóhannesson, H. (1984). Eruption in Grímsvötn 1983; course of events and chemical studies of the tephra. *Jökull*, 34:1–8. 3.4

Grönvold, K., Óskarsson, N., Johnsen, S. J., Clausen, H. B., Hammer, C. U., Bond, G., and Bard, E. (1995). Ash layers from Iceland in the Greenland GRIP ice core correlated with oceanic and land sediments. *Earth and Planetary Science Letters*, 135(1-4):149–155. 3.4.1

Groß-Schmölders, M., Dräger, N., Kienel, U., and Brauer, A. (2015). Development of anoxia during the last 90 years in Lake Tiefer See, NE Germany. *EGU General Assembly*. 4.5.2

Gudmundsdóttir, E. R., Eiríksson, J., and Larsen, G. (2011). Identification and definition of primary and reworked tephra in Late Glacial and Holocene marine shelf sediments off North Iceland. *Journal of Quaternary Science*, 26(6):589–602. 3.4, 3.4.1

Haas, J. (1994). First identification key for charophyte oospores from central Europe. *European journal of phycology*. 5.3.4

Haflidason, H., Sejrup, H. P., and Jones, G. A. (1990). Tephra-, bio- and lithostratigraphy of an AMS dated core from the Norway basin, southern Norwegian Sea. *Geonytt*, 17:52. 3.4.1

Hammes, K., Schmidt, M. W. I., Smernik, R. J., Currie, L. A., Ball, W. P., Nguyen, T. H., Louchouarn, P., Houel, S., Gustafsson, Ö., Elmquist, M., Cornelissen, G., Skjemstad, J. O., Masiello, C. A., Song, J., Peng, P., Mitra, S., Dunn, J. C., Hatcher, P. G., Hockaday, W. C., Smith, D. M., Hartkopf-Fröder, C., Böhmer, A., Lüer, B., Huebert, B. J., Amelung, W., Brodowski, S., Huang, L., Zhang, W., Gschwend, P. M., Flores-Cervantes, D. X., Largeau, C., Rouzaud, J. N., Rumpel, C., Guggenberger, G., Kaiser, K., Rodionov, A., Gonzalez-Vila, F. J., Gonzalez-Perez, J. S., de la Rosa, J. M., Manning, D. A. C., López-Capél, E., and Ding, L. (2007). Comparison of quantification methods to measure fire-derived (black-elemental) carbon in soils and sediments using reference materials from soil, water, sediment and the atmosphere. *Global Biogeochemical Cycles*, 21(3). 5.4.1

Harms, E. (1998). *Volatile composition and syn-eruptive degassing of the Laacher See phonolite magma (12,900 years BP)*. Phd thesis, Chrstian-Albrecht-University Kiel. 2.2

Harms, E. and Schmincke, H.-U. (2000). Volatile composition of the phonolitic Laacher See magma (12,900 yr BP): implications for syn-eruptive degassing of S, F, Cl and H2O. *Contributions to Mineralogy and Petrology*, 138(1):84–98. 2.2

Hartnett, H. E., Keil, R. G., Hedges, J. I., and Devol, A. H. (1998). Influence of oxygen exposure time on organic carbon preservation in continental margin sediments. *Nature*, 391:572–575. 2.5.1

Hedges, J. I., Hu, F. S., Devol, A. H., Hartnett, H. E., Tsamakis, E., and Keil, R. G. (1999). Sedimentary organic matter preservation: A test for selective degradation under oxic conditions. *American Journal of Science*, 299(7-9):529–555. 4.1, 4.5.2

Hedges, J. I. and Keil, R. G. (1995). Sedimentary organic matter preservation: an assessment and speculative synthesis. *Marine Chemistry*, 49(2-3):81–115. 4.5.2

Heyng, A. M., Mayr, C., Lücke, A., Striewski, B., Wastegård, S., and Wissel, H. (2012). Environmental changes in northern New Zealand since the Middle Holocene inferred from stable isotope records (δ15N, δ13C) of Lake Pupuke. *Journal of Paleolimnology*, 48(2):351–366. 4.1, 4.5.1

Hodell, D. A. and Schelske, C. L. (1998). Production, sedimentation, and isotopic composition of organic matter in Lake Ontario. *Limnology and Oceanography*, 43(2):200–214. 4.1

Hollander, D. J. and Smith, M. A. (2001). Microbially mediated carbon cycling as a control on the δ13C of sedimentary carbon in eutrophic Lake Mendota (USA): new models for interpreting isotopic excursions in the sedimentary record. *Geochimica et Cosmochimica Acta*, 65(23):4321–4337. 4.1, 4.5.1, 6.1

Holzhauser, H., Magny, M., and Zumbühl, H. J. (2005). Glacier and lake-level variations in west-central Europe over the last 3500 years. *The Holocene*, 15(6):789–801. 2.5.3

Horai, K. (1971). Thermal Conductivity of Rock-Forming Minerals. *Journal of Geophysical Research*, 76(5):1278–1307. 5.4.2

Housley, R. A., MacLeod, A., Armitage, S. J., Kabacinski, J., and Gamble, C. S. (2013a). The potential of cryptotephra and OSL dating for refining the chronology of open-air archaeological windblown sand sites: a case study from Mirkowice 33, northwest Poland. *Quaternary Geochronology*, 20:99–108. 3.1, 3.4.1

Housley, R. A., MacLeod, A., Nalepka, D., Jurochnik, A., Masojć, M., Davies, L., Lincoln, P. C., Bronk Ramsey, C., Gamble, C. S., and Lowe, J. J. (2013b). Tephrostratigraphy of a Lateglacial lake sediment sequence at We{ogonek}gliny, southwest Poland. *Quaternary Science Reviews*, 77:4–18. 3.1, 3.4.1, 3.4

Huang, K.-F., Oppo, D. W., and Curry, W. B. (2014). Decreased influence of Antarctic intermediate water in the tropical Atlantic during North Atlantic cold events. *Earth and Planetary Science Letters*, 389:200–208. 5.4.1

Hunt, J. B. and Hillt, P. G. (1996). an Inter-Laboratory Comparison of the Electron Probe Microanalysis of Glass Geochemistry. *Quaternary International*, 6182(95):229–241. 2.3.3, 3.3.2

Ingalls, A. E., Aller, R. C., Lee, C., and Wakeham, S. G. (2004). Organic matter diagenesis in shallow water carbonate sediments. *Geochimica et Cosmochimica Acta*, 68(21):4363–4379. 4.1

Jennings, a., Thordarson, T., Zalzal, K., Stoner, J., Hayward, C., Geirsdottir, a., and Miller, G. (2014). Holocene tephra from Iceland and Alaska in SE Greenland Shelf Sediments. *Geological Society, London, Special Publications*, 398(1):157–193. 3.4.1

Jenny, J.-P., Francus, P., Normandeau, A., Lapointe, F., Perga, M.-E., Ojala, A. E. K., Schimmelmann, A., and Zolitschka, B. (2016). Global spread of hypoxia in freshwater ecosystems during the last three centuries is caused by rising local human pressure. *Global change biology*, 22:1481–1489. 2.1

Jilbert, T., Conley, D. J., Gustafsson, B. G., Funkey, C. P., and Slomp, C. P. (2015). Glacio-isostatic control on hypoxia in a high-latitude shelf basin. *Geology*, 43(5):427–430. 2.5.3, 6.1

Jóhannesdóttir, G., Thordarson, T., Geirsdóttir, A., and Larsen, G. (2005). The widespread ˜10 ka Saksunarvatn tephra: a product of three large basaltic phreato-plinian eruptions? *Geophysical Research Abstracts*, 7. 3.4.1

Jóhansen, J. (1985). Studies in the Vegetation History of the Faroe and Shetland Islands. *Føroya FróÃ°skaparfelag, Tórshavn, Faroe Islands*. 3.4.1

Johnson, S. J., Clausen, H. B., Dansgaard, W., Fuhrer, K., Gundestrup, N., Hammer, C. U., Iversen, P., Jouzel, J., Stauffer, B., and Steffensen, J. (1992). Irregular glacial interstadials recorded in a new Greenland ice core. *Nature*, 359:311–313. 1.1

Jouve, G., Francus, P., Lamoureux, S., Provencher-Nolet, L., Hahn, A., Haberzettl, T., Fortin, D., and Nuttin, L. (2013). Microsedimentological characterization using image analysis and μ-XRF as indicators of sedimentary processes and climate changes during Lateglacial at Laguna Potrok Aike, Santa Cruz, Argentina. *Quaternary Science Reviews*, 71:191–204. 2.4.3.1, 2.4.4.2

Juvigné, E., Bastin, B., Delibras, G., Evin, G., Gewelt, M., Gilot, E., and Streel, M. (1996). A comprehensive pollen- and tephra-based chronostratigraphic model for the Late Glacial and Holocene period in the french Massif Central. *Quaternary International*, 34-36:113–120. 2.2

Juvigné, E. H., Kozarski, S., and Nowaczyk, B. (1995). The occurrence of laacher see tephra in Pomerania, NW Poland. *Boreas*, 24:225–231. 2.2, 3.1

Kaiser, K., Lorenz, S., Germer, S., Juschus, O., Küster, M., Libra, J., Bens, O., and Hüttl, R. F. (2012). Late Quaternary evolution of rivers, lakes and peatlands in northeast Germany reflecting past climatic and human impact - an overview. *Quaternary Science Journal*, 61(2):103–132. 3.2

Kalis, A. J., Merkt, J., and Wunderlich, J. (2003). Environmental changes during the Holocene climatic optimum in central Europe - Human impact and natural causes. *Quaternary Science Reviews*, 22(1):33–79. 1.1

Kaplan, J. O., Krumhardt, K. M., and Zimmermann, N. (2009). The prehistoric and preindustrial deforestation of Europe. *Quaternary Science Reviews*, 28(27-28):3016–3034. 1.1

Kelts, K. and Hsü, K. (1978). Freshwater carbonate sedimentation. In Lerman, A., editor, *Lakes: chemistry, geology and physics*, pages 295–323. Springer, Berlin. 2.4.3.1, 2.5.1

Kienel, U., Dulski, P., Ott, F., Lorenz, S., and Brauer, A. (2013). Recently induced anoxia leading to the preservation of seasonal laminae in two NE-German lakes. *Journal of paleolimnology*, 50(4):535–544. 1.2, 1.3, 2.1, 2.2, 2.2, 2.4.3.1, 2.5.1, 3.2, 3.3.1.1, 3.4.1, 4.2, 4.5.1, 6.1

Kinder, M., Tylmann, W., Enters, D., Piotrowska, N., Poręba, G., and Zolitschka, B. (2013). Construction and validation of calendar-year time scale for annually laminated sediments - an example from Lake Szurpiły (NE Poland). *GFF*, 135:248–257. 3.5

Kohzu, A., Imai, A., Ohkouchi, N., Fukushima, T., Kamiya, K., Komatsu, K., Tomioka, N., Kawasaki, N., Miura, S., and Satou, T. (2011). Direct evidence for the alteration of 13 C natural abundances during early diagenesis in Lake Kasumigaura, Japan. *Geochemistry, Geophysics, Geosystems*, 12(10):n/a–n/a. 4.1, 6.1

Koschel, R. (1990). Pelagic calcite precipitation and trophic state of hardwater lakes. *Arch. Hydrobiol. Beih. Ergebn. Limnol.*, 33:713–722. 2.4.3.1

Koschel, R., Benndorf, J., Proft, G., and Recknagel, F. (1983). Calcite precipitation as a natural control mechanism of eutrophication. *Archiv Fur Hydrobiologie*, 98:380–408. 2.4.3.1

Koschel, R., Proft, G., and Raidt, R. (1987). Autochtone Kalkf˜illung in Hartwasserseen der Mecklenburger Seenplatte. *Limnologica*, 19:317–338. 2.4.3.1

Koutsodendris, A., Brauer, A., Zacharias, I., Putyrskaya, V., Klemt, E., Sangiorgi, F., and Pross, J. (2015). Ecosystem response to human- and climate-induced environmental stress on an anoxic coastal lagoon (Etoliko, Greece) since 1930 AD. *Journal of Paleolimnology*, 53(3):255–270. 1.1

Kuehn, S. C., Froese, D. G., and Shane, P. A. R. (2011). The INTAV intercomparison of electron-beam microanalysis of glass by tephrochronology laboratories: Results and recommendations. *Quaternary International*, 246(1-2):19–47. 2.3.3, 3.3.2

Kylander, M. E., Lind, E. M., Wastegard, S., and Lowemark, L. (2012). Recommendations for using XRF core scanning as a tool in tephrochronology. *The Holocene*, 22(3):371–375. 3.4.1

Lamb, A. L., Leng, M. J., Mohammed, M. U., and Lamb, H. F. (2004). Holocene climate and vegetation change in the Main Ethiopian Rift Valley, inferred from the composition (C/N and δ13C) of lacustrine organic matter. *Quaternary Science Reviews*, 23(7-8):881–891. 4.1

Lamb, H. H. (1979). Climatic variation and changes in the wind and ocean circulation: The Little Ice Age in the northeast Atlantic. *Quaternary Research*, 11(1):1–20. 2.5.3

Lamy, F., Kilian, R., Arz, H. W., Francois, J.-P., Kaiser, J., Prange, M., and Steinke, T. (2010). Holocene changes in the position and intensity of the southern westerly wind belt. *Nature Geoscience*, 3(10):695–699. 2.5.3

Landesamt für Umwelt, N. (2000). Geologische Karte von Mecklenburg-Vorpommern 1:500000. *Landesamt für Umwelt, Naturschutz und Geologie Mecklenburg Vorpommern, Güstrow*. 1.2, 1.3, 2.2, 4.2

Lane, C. S., Blockley, S. P. E., Bronk Ramsey, C., and Lotter, A. F. (2011). Tephrochronology and absolute centennial scale synchronisation of European and Greenland records for the last glacial to interglacial transition: A case study of Soppensee and NGRIP. *Quaternary International*, 246(1-2):145–156. 2.2, 3.4.1, 3.4, 3.7

Lane, C. S., Brauer, A., Blockley, S. P. E., and Dulski, P. (2013). Volcanic ash reveals time-transgressive abrupt climate change during the Younger Dryas. *Geology*, 41(12):1251–1254. 1.1, 3.4.4

Lane, C. S., De Klerk, P., and Cullen, V. L. (2012). A tephrochronology for the Lateglacial palynological record of the Endinger Bruch (Vorpommern, north-east Germany). *Journal of Quaternary Science*, 27(2):141–149. 2.4.1, 2.2, 3.1, 3.4.1, 3.4.1, 3.4

Larsen, G. (1982). Gjóskutímatal Jökuldals og nágrennis. In Thórarinsdóttir, H., Óskarsson, Ó. H., Steinthórsson, S., and Einarsson, T., editors, *Eldur er í NorÃ°ri*, pages 51–65. Sögufélag, Reykjavík. 3.4

Larsen, G. (1984). Recent volcanic history of the Veidivötn fissure swarm, southern Iceland - an approach to volcanic risk assessment. *Journal of Volcanology and Geothermal Research*, 22(1-2):33–58. 3.4.1

Larsen, G., Dugmore, A., and Newton, A. (1999). Geochemistry of historical-age silicic tephras in Iceland. *The Holocene*, 9(4):463–471. 3.4, 3.4.1, 3.4.1

Larsen, G., Eiríksson, J., Knudsen, K. L., and Heinemeier, J. (2002). Correlation of late Holocene terrestrial and marine tephra markers, north Iceland: Implications for reservoir age changes. *Polar Research*, 21(2):283–290. 3.4, 3.4.1, 3.4.1

Larsen, G. and Thorarinsson, S. (1977). H4 and other acid Hekla tephra layers. *Jökull*, 27:28–46. 3.4.1

Larsen, J. J. and Noe-Nygaard, N. (2014). Lateglacial and early Holocene tephrostratigraphy and sedimentology of the Store Slotseng basin, SW Denmark: A multi-proxy study. *Boreas*, 43(2):349–361. 3.4.1

Laskar, J. (1990). The chaotic motion of the solar system: A numerical estimate of the size of the chaotic zones. *Icarus*, 88(2):266–291. 2.5.3, 6.1

Laskar, J., Robutel, P., Joutel, F., Gastineau, M., Correia, a. C. M., and Levrard, B. (2004). A long-term numerical solution for the insolation quantities of the Earth. *Astronomy and Astrophysics*, 428(1):261–285. 2.5.3, 6.1

Last, W. M. and Smol, J. P. (2001). *Tracking Environmental Change Using Lake Sediments*. Springer, Dordrecht. 5.1

Lawson, I., Swindles, G., Plunkett, G., and Greenberg, D. (2012). The spatial distribution of Holocene cryptotephras in north-west Europe since 7 ka: implications for understanding ash fall events from Icelandic eruptions. *Quaternary Science Reviews*, 41:57–66. 3.5

Lehmann, M. F., Bernasconi, S. M., Barbieri, A., and McKenzie, J. a. (2002). Preservation of organic matter and alteration of its carbon and nitrogen isotope composition during simulated and in situ early sedimentary diagenesis. *Geochimica et Cosmochimica Acta*, 66(20):3573–3584. 4.5.2

Lehmann, M. F., Bernasconi, S. M., Barbieri, A., Simona, M., and McKenzie, J. A. (2004). Interannual variation of the isotopic composition of sedimenting organic carbon and nitrogen in Lake Lugano: A long-term sediment trap study. *Limnology and Oceanography*, 49(3):839–849. 4.1

Leng, M. J. and Marshall, J. D. (2004). Palaeoclimate interpretation of stable isotope data from lake sediment archives. *Quaternary Science Reviews*, 23(7-8):811–831. 6.3

Li, S. H. and Parr, S. W. (1926). The Oxidation of Pyrites as a Factor in the Spontaneous Combustion of Coal1. *Industrial & Engineering Chemistry*, 18(12):1299–1304. 5.4.2

Lilja, C., Lind, E. M., Morén, B., and Wastegård, S. (2013). A Lateglacial-early Holocene tephrochronology for SW Sweden. *Boreas*, 42(3):544–554. 3.4.1, 3.4.1, 3.4

Lind, E. M. and Wastegård, S. (2011). Tephra horizons contemporary with short early Holocene climate fluctuations: New results from the Faroe Islands. *Quaternary International*, 246(1-2):157–167. 3.4.1, 3.4.1, 3.4.1, 3.4, 3.4.1

Lind, E. M., Wastegård, S., and Larsen, J. J. (2013). A Late Younger Dryas-Early Holocene tephrostratigraphy for Fosen, Central Norway. *Journal of Quaternary Science*, 28(8):803–811. 3.4.1

Lohne, O. S., Mangerud, J., and Birks, H. H. (2013). Precise 14C ages of the Vedde and Saksunarvatn ashes and the Younger Dryas boundaries from western Norway and their comparison with the Greenland Ice Core (GICC05) chronology. *Journal of Quaternary Science*, 28(5):490–500. 3.4.1, 3.7

Lohne, Ø. S., Mangerud, J., and Birks, H. H. (2014). IntCal13 calibrated ages of the Vedde and Saksunarvatn ashes and the Younger Dryas boundaries from Kråkenes, western Norway. *Journal of Quaternary Science*, 29(5):506–507. 2.4.1

Lotter, A. F. and Lemcke, G. (1999). Methods for preparing and counting biochemical varves. *Boreas*, 28(2):243–252. 5.1

Lotter, A. F. and Lemcke, G. (2008). Methods for preparing and counting biochemical varves. *Boreas*, 28(2):243–252. 2.4.3.1

Lowe, D. J. (2011). Tephrochronology and its application: A review. *Quaternary Geochronology*, 6(2):107–153. 3.1

Lücke, A., Schleser, G. H., Zolitschka, B., and Negendank, J. F. (2003). A Lateglacial and Holocene organic carbon isotope record of lacustrine palaeoproductivity and climatic change derived from varved lake sediments of Lake Holzmaar, Germany. *Quaternary Science Reviews*, 22(5-7):569–580. 4.1

Lüder, B., Kirchner, G., Lücke, A., and Zolitschka, B. (2006). Palaeoenvironmental reconstructions based on geochemical parameters from annually laminated sediments of Sacrower See (northeastern Germany) since the 17th century. *Journal of Paleolimnology*, 35:897 – 912. 2.1, 2.5.1

Luterbacher, J., Werner, J. P., Smerdon, J. E., Fernández-Donado, L., González-Rouco, F. J., Barriopedro, D., Ljungqvist, F. C., Büntgen, U., Zorita, E., Wagner, S., Esper,

J., McCarroll, D., Toreti, A., Frank, D., Jungclaus, J. H., Barriendos, M., Bertolin, C., Bothe, O., Brázdil, R., Camuffo, D., Dobrovolný, P., Gagen, M., García-Bustamante, E., Ge, Q., Gómez-Navarro, J. J., Guiot, J., Hao, Z., Hegerl, G. C., Holmgren, K., Klimenko, V. V., Martín-Chivelet, J., Pfister, C., Roberts, N., Schindler, A., Schurer, A., Solomina, O., von Gunten, L., Wahl, E., Wanner, H., Wetter, O., Xoplaki, E., Yuan, N., Zanchettin, D., Zhang, H., and Zerefos, C. (2016). European summer temperatures since Roman times. *Environmental Research Letters*, 11(2):024001. 1.1

Maes, I. I., Gryglewicz, G., Yperman, J., Franco, D. V., D'Haes, J., D'Olieslaeger, M., and Van Poucke, L. C. (2000). Effect of siderite in coal on reductive pyrolytic analyses. *Fuel*, 79(15):1873–1881. 5.4.1

Magee, M. R., Wu, C. H., Robertson, D. M., Lathrop, R. C., and Hamilton, D. P. (2016). Trends and abrupt changes in 104-years of ice cover and water temperature in a dimictic lake in response to air temperature , wind speed , and water clarity drivers. *Hydrology and Earth System Sciences*, 20:1681–1702. 2.5.2

Mangerud, J., Furnes, H., and Jóhansen, J. (1986). A 9000-year-old ash bed on the Faroe islands. *Quaternary Research*, 26(2):262–265. 3.4.1

Mangili, C., Brauer, A., Plessen, B., and Moscariello, A. (2007). Centennial-scale oscillations in oxygen and carbon isotopes of endogenic calcite from a 15,500 varve year record of the Pi??nico interglacial. *Quaternary Science Reviews*, 26(13-14):1725–1735. 6.3

Mariner, R. H., Minor, S. A., King, A. P., Boles, J. R., Kellogg, K. S., Evans, W. C., Landis, G. A., Hunt, A. G., and Till, C. B. (2008). A landslide in tertiary marine shale with superheated fumaroles, coast ranges, California. *Geology*, 36(12):959–962. 5.4.2

Marks, L. (2012). Timing of the Late Vistulian (Weichselian) glacial phases in Poland. *Quaternary Science Reviews*, 44:81–88. 3.2

Martin-Puertas, C., Brauer, A., Dulski, P., and Brademann, B. (2012a). Testing climateproxy stationarity throughout the Holocene: an example from the varved sediments of Lake Meerfelder Maar (Germany). *Quaternary Science Reviews*, 58:56–65. 1.1, 2.7

Martin-Puertas, C., Matthes, K., Brauer, A., Muscheler, R., Hansen, F., Petrick, C., Aldahan, A., Possnert, G., and van Geel, B. (2012b). Regional atmospheric circulation shifts induced by a grand solar minimum. *Nature Geoscience*, 5(6):397–401. 1.1, 2.1, 2.5.3, 6.2

Masson-Delmotte, V., Schulz, M., A., A.-O., Beer, J., Ganopolski, A., González Rouco, J. F., Jansen, E., Lambeck, K., Luterbacher, J., Naish, T., Osborn, T., Otto-Bliesner, B., Quinn, T., Ramesh, R., Rojas, M., Shao, X., and Timmermann, A. (2013). Information from Paleoclimate Archives. In Stocker, T. F., Qin, D., Plattner, G.-K., Tignor, M., Allen, S. K., Boschung, K., Nauels, A., Xia, Y., Bex, V., and Midgley, P. M., editors, *Climate Change 2013: The Physical Science Basis. Contribution of Working Group I to the Fifth Assessment Report of the Intergovernmental Panel on Climate Change*, pages 383–464. Cambridge University Press, Camebridge, Unites Kingdom an New York, NY, USA. 1.1

Mayewski, P. A., Rohling, E. E., Stager, J. C., Karlén, W., Maasch, K. A., Meeker, L. D., Meyerson, E. A., Gasse, F., van Kreveld, S., Holmgren, K., Lee-Thorp, J., Rosqvist, G., Rack, F., Staubwasser, M., Schneider, R. R., and Steig, E. J. (2004). Holocene climate variability. *Quaternary Research*, 62(3):243–255. 2.5.3

Meara, R. H. (2012). *Geochemical Fingerprinting of Icelandic Silicic Holocene Tephra Layers*. PhD thesis, University of Edinburgh. 3.4

Merkt, J. and Müller, H. (1999). Varve chronology and palynology of the Lateglacial in Northwest Germany from lacustrine sediments of Hamelsee in Lower Saxony. *Quaternary International*, 61(1999):41–59. 3.1, 3.7

Merkt, J., Müller, W., Knabe, W., Müller, P., and Weiser, T. (1993). The early Holocene Saksunarvatn Tephra found in lake sediments in N.W. Germany. *Boreas*, 22:93–100. 3.4.1, 3.7, 3.4.4

Meyers, P. A. (1994). Preservation of elemental and isotopic source identification of sedimentary organic matter. *Chemical Geology*, 114(3-4):289–302. 4.1

Meyers, P. A. and Ishiwatari, R. (1993). Lacustrine organic geochemistry-an overview of indicators of organic matter sources and diagenesis in lake sediments. *Organic Geochemistry*, 20(7):867–900. 2.5.1, 4.1

Meyers, P. A. and Lallier-Vergés, E. (1999). Lacustrine Sedimentary Organic Matter Records of Late Quaternary Paleoclimates. *Journal of Paleolimnology*, 21(3):345–372. 4.1

Midttømme, K. (1998). Thermal Conductivity of Selected Claystones and Mudstones from England. *Clay Minerals*, 33(1):131–145. 5.4.2

Misra, B. K. and Singh, B. D. (1994). Susceptibility to spontaneous combustion of Indian coals and lignites: an organic petrographic autopsy. *International Journal of Coal Geology*, 25(3-4):265–286. 5.1

Mohn, H. (1878). Askeregnen den 29de-30-te Marts 1875. *Forhandlinger I Videnskapsselskabet I Christiania aar 1877*, 10:89–92. 3.4.1, 3.4.4

Mollenhauer, G. and Eglinton, T. I. (2007). Diagenetic and sedimentological controls on the composition of organic matter preserved in California Borderland Basin sediments. *Limnology and Oceanography*, 52(2):558–576. 4.1, 4.5.2

Moore, P. D., Webb, J. A., and Collinson, M. E. (1991). *Pollen Analysis*. London: Blackwell Scientific Publications. 2.3.5

Morse, J., Millero, F., Cornwell, J., and Rickard, D. (1987). The chemistry of the hydrogen sulfide and iron sulfide systems in natural waters. *Earth-Science Reviews*, 24(1):1–42. 5.4.2

Mortensen, A. K., Bigler, M., Grönvold, K., Steffensen, J. P., and Johnsen, S. J. (2005). Volcanic ash layers from the last glacial termination in the NGRIP ice core. *Journal of Quaternary Science*, 20(3):209–219. 3.4.1, 3.4, 3.7

Müller, A. and Voss, M. (1999). The palaeoenvironments of coastal lagoons in the southern Baltic Sea, II. δ13C and δ15N ratios of organic matter - sources and sediments. *Palaeogeography, Palaeoclimatology, Palaeoecology*, 145(1-3):17–32. 4.1, 4.5.1

Neugebauer, I., Brauer, A., Dräger, N., Dulski, P., Wulf, S., Plessen, B., Mingram, J., Herzschuh, U., and Brande, A. (2012). A Younger Dryas varve chronology from the Rehwiese palaeolake record in NE-Germany. *Quaternary Science Reviews*, 36:91–102. 2.1, 2.4.1, 2.2, 2.4.2, 3.1

Neumann, T., Stögbauer, A., Walpersdorf, E., Stüben, D., and Kunzendorf, H. (2002). Stable isotopes in recent sediments of Lake Arendsee, NE Germany: response to eutrophication and remediation measures. *Palaeogeography, Palaeoclimatology, Palaeoecology2*, 178:75–90. 2.1

Niessen, F., Wick, L., Bonani, G., Chondrogianni, C., and Siegenthaler, C. (1992). Aquatic system response to climatic and human changes: Productivity, bottom water oxygen status, and sapropel formation in Lake Lugano over the last 10 000 years. *Aquatic Sciences*, 54(3-4):257–276. 2.5.1, 6.1

Ning, W., Ghosh, A., Jilbert, T., Slomp, C. P., Khan, M., Nyberg, J., Conley, D. J., and Filipsson, H. L. (2016). Evolving coastal character of a Baltic Sea inlet during the Holocene shoreline regression: impact on coastal zone hypoxia. *Journal of Paleolimnology*. 2.5.3, 6.1

Ninteman, D. J. (1978). A literature survey: spontaneous oxidation and combustion of sulfide ores in underground mines. *United States Department of the Interior Bureau of Mines Information Circular, Washington*, 8775. 5.4.2

Nixdorf, E., Hemm, M., and Hoffmann, A. (2004). Dcumentation about the state and the development of the most important German lakes (part 2 Mecklenburg Vorpommern). In Umweltbundesamt, editor, *Abschlussbericht F&E Vorhaben FKZ 299 24 274*. Cottbus: Brandenburg University of Technology Cottbus, Lehrstuhl Gewässerschutz. 2.2, 4.2

Nriagu, J. and Dell, C. (1974). Diagenetic Formation of lron Phosphates in Recent Lake Sediments. *American Mineralogist*, 59:934–946. 2.4.3.1, 2.5.1

Nriagu, J. O. (1972). Stability of vivianite and ion-pair formation in the system fe3(PO4)2-H3PO4H3PO4-H2o. *Geochimica et Cosmochimica Acta*, 36(4):459–470. 2.4.3.1, 2.5.1

Ohlemiller, T. J. (1985). Modelling of smoldering combustion propagation. *Progress in Energy and Combustion Science*, 11(4):277–310. 5.1, 5.4.1

Ohlemiller, T. J. (1986). Smoldering combustion. In Quincy, M. A., editor, *SFPE handbook of fire protection engineering*, pages 171–179. Building and Fire Res. Lab., Natl. Inst. of Stand., Gaithersburg. 5.1, 5.4.1

Óladóttir, B. A., Larsen, G., and Sigmarsson, O. (2011). Holocene volcanic activity at Grímsvötn, Bárdarbunga and Kverkfjöll subglacial centres beneath Vatnajökull, Iceland. *Bulletin of Volcanology*, 73(9):1187–1208. 3.4, 3.4.1, 3.4.1, 3.4.1

Óladóttir, B. A., Sigmarsson, O., Larsen, G., and Thordarson, T. (2008). Katla volcano, Iceland: Magma composition, dynamics and eruption frequency as recorded by Holocene tephra layers. *Bulletin of Volcanology*, 70(4):475–493. 3.4

Oldfield, F., Thompson, R., Crooks, P. R. J., Gedye, S. J., Hall, V. a., Harkness, D. D., Housley, R. a., McCormac, F. G., Newton, a. J., Pilcher, J. R., Renberg, I., and Richardson, N. (1997). Radiocarbon dating of a recent high latitude peat profile: Stor Åmyran, northern Sweden. *The Holocene*, 7(3):283–290. 3.4, 3.4.1

Olsen, J., Anderson, N. J., and Leng, M. J. (2013). Limnological controls on stable isotope records of late-Holocene palaeoenvironment change in SW Greenland: a paired lake study. *Quaternary Science Reviews*, 66:85–95. 1.1

Orme, L. C., Reinhardt, L., Jones, R. T., Charman, D. J., Barkwith, A., and Ellis, M. A. (2016). Aeolian sediment reconstructions from the Scottish Outer Hebrides: Late Holocene storminess and the role of the North Atlantic Oscillation. *Quaternary Science Reviews*, 132:15–25. 2.5.3, 6.1

Orme, L. C., Reinhardt, L., Jones, R. T., Charman, D. J., Croudace, I., Dawson, A., Ellis, M., and Barkwith, A. (2015). Investigating the maximum resolution of Â XRF core scanners: A 1800 year storminess reconstruction from the Outer Hebrides. *The Holocene*. 2.7

O'Sullivan, P. E. (1983). Annually-laminated lake sediments and the study of Quaternary environmental changes - a review. *Quaternary Science Reviews*, 1(4):245–313. 1.1

Ott, F., Brauer, A., Słowiński, M., Dulski, P., Plessen, B., and Błaszkiewicz, M. (2013). Holocene and Late Glacial varved sediments from Czechowskie Lake (Poland). *Geophysical Research Abstracts*, 15:EGU2013–12660. 6.2

Ott, F., Brauer, A., Słowiński, M., Wulf, S., Putyrskaya, V., and Błaszkiewicz, M. (2014). Constructing a precise and robust chronology for the varved sediment record of Lake Czechowskie (Poland). *Geophysical Research Abstracts*, 2014:EGU2014–10328. 3.1, 3.2, 3.3.1.2

Ott, F., Brauer, A., Słowiński, M., Wulf, S., Putyrskaya, V., Plessen, B., and Błaszkiewicz, M. (2015). Varved sediments from Lake Czechowskie (Poland) reveal gradual increase in Atlantic influence during the Holocene. *Geophysical Research Abstracts*, 17:EGU2015–308. 6.2

Ott, F., Wulf, S., Serb, J., Słowiński, M., Obremska, M., Tjallingii, R., Błaszkiewicz, M., and Brauer, A. (2016). Constraining the time span between the early Holocene Hässeldalen and Askja-S Tephras through varve counting in the Lake Czechowskie sediment record , Poland. *Journal of Quaternary Science*. 2.4.1

Payant, R., Rosenblum, F., Nesset, J. E., and Finch, J. A. (2012). The self- heating of sulfides: galvanic effects. *Minerals Engineering*, 26:57–63. 5.1, 5.4.2

Pędziszewska, A., Tylmann, W., Witak, M., Piotrowska, N., Maciejewska, E., and Latałowa, M. (2015). Holocene environmental changes reflected by pollen, diatoms, and geochemistry of annually laminated sediments of Lake Suminko in the Kashubian Lake District (N Poland). *Review of Palaeobotany and Palynology*, 216:55–75. 2.5.3, 6.1

Pfister, C., Schwarz-Zanetti, G., Wegmann, M., and Luterbacher, J. (1998). Winter air temperature variations in western Europe during the Early and High Middle Ages (AD 750-1300). *The Holocene*, 8:535–552. 2.5.3, 6.1

Pilcher, J. R., Bradley, R. S., Francus, P., and Anderson, L. (2005). A Holocene tephra record from the Lofoten islands, arctic Norway. *Boreas*, 34:136–156. 3.4, 3.4.1

Pilcher, J. R., Hall, V. a., and McCormac, F. G. (1996). An outline tephrochronology for the Holocene of the north of Ireland. *October*, 11(6):485–494. 2.4.2, 3.4, 3.4.1, 3.4.1

Polcyn, I. (1996). Application of Cladocera analysis in achaeology. *Circaea, The Journal of the Association for Environmental Archaeology*, 11(2):41–48. 2.4.6, 2.5.1

Postma, D. (1981). Formation of Siderite and Vivianite and the pore-water composition of a recent bog sediment in Denmark. *Chemical Geology*, 31:225–244. 5.3.4

Pyne-O'Donnell, S., Blockley, S. P., Turney, C. S., and Lowe, J. J. (2008). Distal volcanic ash layers in the Lateglacial Interstadial (GI-1): problems of stratigraphic discrimination. *Quaternary Science Reviews*, 27(1):72–84. 3.4

Rach, O., Brauer, a., Wilkes, H., and Sachse, D. (2014). Delayed hydrological response to Greenland cooling at the onset of the Younger Dryas in western Europe. *Nature Geoscience*, 7(1):109–112. 3.4.4

Raible, C. C., Yoshimori, M., Stocker, T. F., and Casty, C. (2007). Extreme midlatitude cyclones and their implications for precipitation and wind speed extremes in simulations of the Maunder Minimum versus present day conditions. *Climate Dynamics*, 28:409–423. 2.5.3

Ranner, P. H., Allen, J. R. M., and Huntley, B. (2005). A new early Holocene cryptotephra from northwest Scotland. *Journal of Quaternary Science*, 20(3):201–208. 3.4

Rasmussen, S. O., Andersen, K. K., Svensson, A. M., Steffensen, J. P., Vinther, B. M., Clausen, H. B., Siggaard-Andersen, M. L., Johnsen, S. J., Larsen, L. B., Dahl-Jensen, D., Bigler, M., Röthlisberger, R., Fischer, H., Goto-Azuma, K., Hansson, M. E., and

Ruth, U. (2006). A new Greenland ice core chronology for the last glacial termination. *Journal of Geophysical Research Atmospheres*, 111(6):1–16. 1.1, 3.4.1, 3.7

Rasmussen, S. O., Bigler, M., Blockley, S. P., Blunier, T., Buchardt, S. L., Clausen, H. B., Cvijanovic, I., Dahl-Jensen, D., Johnsen, S. J., Fischer, H., Gkinis, V., Guillevic, M., Hoek, W. Z., Lowe, J. J., Pedro, J. B., Popp, T., Seierstad, I. K., Steffensen, J. P., Svensson, A. M., Vallelonga, P., Vinther, B. M., Walker, M. J., Wheatley, J. J., and Winstrup, M. (2014). A stratigraphic framework for abrupt climatic changes during the Last Glacial period based on three synchronized Greenland ice-core records: refining and extending the INTIMATE event stratigraphy. *Quaternary Science Reviews*, 106:14–28. 3.7

Reimer, P. J., Bard, E., Bayliss, A., Beck, J. W., Blackwell, P. G., Bronk Ramsey, C., Buck, C. E., Cheng, H., Edwards, R. L., Friedrich, M., Grootes, P., Guilderson, T., Haflidason, H., Hajdas, I., Hatté, C., Heaton, T. J., Hoffmann, D. L., Hogg, A. G., Hughen, K. A., Kaiser, K. F., Kromer, B., Manning, S. W., Niu, M., Reimer, R. W., Richards, D. A., Scott, E. M., Southon, J. R., Staff, R. A., Turney, C. S., and van der Plicht, J. (2013). IntCal13 and Marine13 Radiocarbon Age Calibration Curves 0-50,000 Years cal BP. *Radiocarbon*, 55(4):1869–1887. 2.1, 2.3.3

Rein, G. (2009). Smouldering Combustion Phenomena in Science and Technology. *International Review of Chemical Engineering*, 1:3–18. 5.1, 5.4.1

Riede, F., Bazely, O., Newton, A. J., and Lane, C. S. (2011). A Laacher See-eruption supplement to Tephrabase: Investigating distal tephra fallout dynamics. *Quaternary International*, 246(1-2):134–144. 2.4.1, 2.2, 3.1

Rinterknecht, V., Börner, A., Bourlès, D., and Braucher, R. (2014). Cosmogenic 10Be dating of ice sheet marginal belts in Mecklenburg-Vorpommern, Western Pomerania (northeast Germany). *Quaternary Geochronology*, 19:42–51. 3.2

Robbins, J. A. and Callender, E. (1975). Diagenesis of manganese in lake michigan sediments. *American Journal of Science*, 275:512–533. 2.4.3.1, 2.5.1, 4.5.1

Roden, E. E. and Edmonds, J. W. (1997). Phosphate mobilization in iron-rich anaerobic sediments: Microbial Fe(III) oxide reduction versus iron-sulfide formation. *Archiv Fur Hydrobiologie*, 139(3):347–378. 2.4.3.1, 2.5.1

Rosenblum, F. and Spira, P. (1995). Evaluation of hazards from self- heating of sulphide rock. *Canadian Institute of Mining, Metallurgy and Petroleum*, 94:92–99. 5.1, 5.4.2

Rothe, M., Frederichs, T., Eder, M., Kleeberg, A., and Hupfer, M. (2014). Evidence for vivianite formation and its contribution to long-term phosphorus retention in a recent lake sediment: a novel analytical approach. *Biogeosciences Discussions*, 11(5):7359–7388. 2.4.3.1, 2.5.1

Santín, C., Doerr, S. H., Preston, C. M., and González-Rodríguez, G. (2015). Pyrogenic organic matter production from wildfires: a missing sink in the global carbon cycle. *Global Change Biology*, 21(4):1621–1633. 5.4.1

Sawlan, J. J. and Murray, J. W. (1983). Trace metal remobilization in the interstitial waters of red clay and hemipelagic marine sediments. *Earth and Planetary Science Letters*, 64(2):213–230. 4.5.1

Schelske, C. L. and Hodell, D. A. (1991). Recent changes in productivity and climate of Lake Ontario detected by isotopic analysis of sediments. *Limnology and Oceanography*, 36(5):961–975. 2.5.1

Schlaak, N. (1993). Studie zur Landschaftsgenese im Raum Nordbarnim und Eberswalder Urstromtal. *Berliner Geographische Arbeiten*. 1.3, 5.1.1, 5.2, 5.1, 5.3.1

Self, S. and Sparks, R. S. J. (1978). Characteristics of widespread pyroclastic deposits formed by the interaction of silicic magma and water. *Bulletin Volcanologique*, 41(3):196–212. 3.4.1

Sigurdsson, H. and Sparks, R. S. J. (1978). Rifting episode in north iceland in 1874-1875 and the eruptions of askja and sveinagja. *Bulletin Volcanologique*, 41(3):149–167. 3.4.1

Sigurdsson, H. and Sparks, R. S. J. (1981). Petrology of rhyolitic and mixed magma ejecta from the 1875 eruption of Askja, Iceland. *Journal of Petrology*, 22(1):41–84. 3.4.1

Sigvaldason, G. E. (2002). Volcanic and tectonic processes coinciding with glaciation and crustal rebound: An early Holocene rhyolitic eruption in the Dyngjufjöll volcanic centre and the formation of the Askja caldera, north Iceland. *Bulletin of Volcanology*, 64(3-4):192–205. 3.4.1

Słowiński, M. (2010). Macro fossil reconstruction of preboreal wetland formed on dead ice block: A case study of the borzechowo mire in East Pomerania, Poland. *Studia Quaternaria*, 27:3–10. 3.2

Słowiński, M., Błaszkiewicz, M., Brauer, A., Noryśkiewicz, B., Ott, F., and Tyszkowski, S. (2015). The role of melting dead ice on landscape transformation in the early Holocene in Tuchola Pinewoods, North Poland. *Quaternary International*, 388:64–75. 3.2, 3.4.4

Sorrel, P., Debret, M., Billeaud, I., Jaccard, S. L., McManus, J. F., and Tessier, B. (2012). Persistent non-solar forcing of Holocene storm dynamics in coastal sedimentary archives. *Nature Geoscience*, 5(12):1–5. 2.7

Steinthórsson, S. (1977). Tephra layers in a drill core from the Vatnajökull ice. *Jökull*, 27:2–27. 3.4

Stevens, L. R., Ito, E., and Olson, D. E. L. (2000). Relationship of Mn-carbonates in varved lake-sediments to catchment vegetation in Big Watab Lake, MN, USA. *Journal of Paleolimnology*, 24:199–211. 2.4.3.1, 2.5.1, 2.5.2, 4.5.1, 6.1

Striewski, B., Mayr, C., Flenley, J., Naumann, R., Turner, G., and Lücke, A. (2009). Multi-proxy evidence of late Holocene human-induced environmental changes at Lake Pupuke, Auckland (New Zealand). *Quaternary International*, 202(1-2):69–93. 1.1

Stuiver, M. (1975). Climate versus changes in 13C content of the organic component of lake sediments during the Late Quarternary. *Quaternary Research*, 5(2):251–262. 4.1, 6.1

Sugita, S. (2007). Theory of quantitative reconstruction of vegetation I: pollen from large sites REVEALS regional vegetation composition. *The Holocene*, 2:229–242. 2.3.5

Summons, R. E., Jahnke, L. L., and Roksandic, Z. (1994). Carbon isotopic fractionation in lipids from methanotrophic bacteria: Relevance for interpretation of the geochemical record of biomarkers. *Geochimica et Cosmochimica Acta*, 58(13):2853–2863. 4.5.1

Sverrisdottir, G. (2007). Hybrid magma generation preceding Plinian silicic eruptions at Hekla, Iceland: evidence from mineralogy and chemistry of two zoned deposits. *Geological Magazine*, 144(04):643. 3.4.1

Swierczynski, T., Lauterbach, S., Dulski, P., Delgado, J., Merz, B., and Brauer, A. (2013). Mid- to late Holocene flood frequency changes in the northeastern Alps as recorded in varved sediments of Lake Mondsee (Upper Austria). *Quaternary Science Reviews*, 80:78–90. 2.4.2

Szeroczyńska, K. (1998). Palaeolimnological investigations in Poland based on Cladocera (Crustacea). *Palaeogeography, Palaeoclimatology, Palaeoecology*, 140(1-4):335–345. 2.4.6, 2.5.1

Szeroczyńska, K. and Sarmaja-Korjonen, K. (2007). *Atlas of subfossil Cladocera from Central and Northern Europe*. Świecie: Friends of the Lower Vistula Society, 200. 2.3.6

Talbot, M. R. (2001). Nitrogen Isotopes in Palaeolimnology. In Last, W. M. and Smol, J. P., editors, *Tracking Environmental Change Using Lake Sediments: Physical and Geochemical Methods*, chapter Nitrogen I, pages 401–439. Springer Netherlands, Dordrecht. 4.5.1

Talbot, M. R. and Johannessen, T. (1992). A high resolution palaeoclimatic record for the last 27, 500 years in tropical West Africa from the carbon and nitrogen isotopic composita hiof lacustrine organic matter. *Earth and Planetary Letters, 110, p. 23-37.*, 110:23–37. 4.4.1.2

Talbot, M. R. and Lærdal, T. (2000). The Late Pleistocene - Holocene palaeolimnology of Lake Victoria, East Africa, based upon elemental and isotopic analyses of sedimentary organic matter. *Journal of Paleolimnology*, 23(2):141–164. 4.1

Teranes, J. L. and Bernasconi, S. M. (2000). The record of nitrate utilization and productivity limitation provided by δ 15 N values in lake organic matter-A study of sediment trap and core sediments from Baldeggersee, Switzerland. *Limnology and Oceanography*, 45(4):801–813. 4.5.1

Theuerkauf, M., Couwenberg, J., Kuparinen, A., and Liebscher, V. (2016). A matter of dispersal - REVEALSinR introduces state-of-the-art dispersal models to quantitative vegetation reconstruction. *Vegetation History and Archaeobotany*. 2.3.5

Theuerkauf, M., Dräger, N., Kienel, U., Kuparinen, A., and Brauer, A. (2015). Effects of changes in land management practices on pollen productivity of open vegetation during the last century derived from varved lake sediments. *The Holocene*, 25(5):733–744. 2.1

Thordarson, T., Miller, D. J., Larsen, G., Self, S., and Sigurdsson, H. (2001). New estimates of sulfur degassing and atmospheric mass-loading by the 934 AD Eldgjá eruption, Iceland. *Journal of Volcanology and Geothermal Research*, 108(1):33–54. 3.4

Tisdall, E. W., Mcculloch, R. D., Sanderson, D. C. W., Simpson, I. A., and Woodward, N. L. (2013). Living with sand : A record of landscape change and storminess during the Bronze and Iron Ages Orkney , Scotland. *Quaternary International*, 308-309:205–215. 2.7

Tjallingii, R., Röhl, U., Kölling, M., and Bickert, T. (2007). Influence of water content on X-ray fluorescence core-scanning measurements in soft marine sediments. *Geochemistry Geophysics Geosystems*, 8(2):1–12. 2.3.4, 5.2

Torero, J. L. and Fernandez-Pello, a. C. (1996). Forward smolder of polyurethane foam in a forced air flow. *Combustion and Flame*, 106(1-2):89–109. 5.1

Turney, C. S. M., Harkness, D. D., and Lowe, J. J. (1997). The use of microtephra horizons to correlate Late-glacial lake sediment successions in Scotland. *Journal of Quaternary Science*, 12(6):525–531. 3.4

Turney, C. S. M., van den Burg, K., Wastegård, S., Davies, S. M., Whitehouse, N. J., Pilcher, J. R., and Callaghan, C. (2006). North European last glacial-interglacial transition (LGIT; 15-9 ka) tephrochronology: Extended limits and new events. *Journal of Quaternary Science*, 21(4):335–345. 3.4.1

Tylmann, W., Enters, D., Kinder, M., Moska, P., Ohlendorf, C., Poreba, G., and Zolitschka, B. (2013a). Multiple dating of varved sediments from Lake Łazduny, northern Poland: Toward an improved chronology for the last 150 years. *Quaternary Geochronology*, 15:98–107. 3.5

Tylmann, W., Szpakowska, K., Ohlendorf, C., Woszczyk, M., and Zolitschka, B. (2012). Conditions for deposition of annually laminated sediments in small meromictic lakes: A case study of Lake Suminko (Northern Poland). *Journal of Paleolimnology*, 47:55–70. 2.1

Tylmann, W., Zolitschka, B., Enters, D., and Ohlendorf, C. (2013b). Laminated lake sediments in northeast Poland: Distribution, preconditions for formation and potential for paleoenvironmental investigation. *Journal of Paleolimnology*, 50(4):487–503. 3.5, 6.2

Van Bogaard, C. D. and Schmincke, H. U. (2002). Linking the North Atlantic to central Europe: A high-resolution Holocene tephrochronological record from northern Germany. *Journal of Quaternary Science*, 17(1):3–20. 3.4, 3.4.1, 3.4.1, 3.4.2, 3.7, 3.4.4

Van Den Bogaard, C., Dorfler, W., Glos, R., Nadeau, M. J., Grootes, P. M., and Erlenkeuser, H. (2002). Two tephra layers bracketing late Holocene paleoecological changes in northern Germany. *Quaternary Research*, 57(3):314–324. 3.4.1, 3.4.1

van den Bogaard, C. and Schmincke, H.-U. (1985). Laacher See Tephra: A widespread isochronous late Quaternary tephra layer in central and northern Europe. *Geological Society of America Bulletin*, 96(12):1554–1571. 2.4.1

van Geel, B. (1978). A palaeoecological study of Holocene peat bog sections in Germany and the Netherlands. *Review of Palaeobotany and Palynology*, 25:1–120. 6.1

Van Geel, B., Buurman, J., and Waterbolk, H. T. (1996). Archaeological and palaeoecological indications of an abrupt climate change in The Netherlands, and evidence for climatological teleconnections around 2650 BP. *Journal of Quaternary Science*, 11(6):451–460. 2.5.3, 6.2

Van Loon, A. J., Btaszkiewicz, M., and Degórski, M. (2012). The role of permafrost in shaping the Late Glacial relief of northern Poland. *Geologie en Mijnbouw/Netherlands Journal of Geosciences*, 91(1-2):223–231. 3.2

Vinther, B. M., Clausen, H. B., Johnsen, S. J., Rasmussen, S. O., Andersen, K. K., Buchardt, S. L., Dahl-Jensen, D., Seierstad, I. K., Siggaard-Andersen, M. L., Steffensen, J. P., Svensson, A., Olsen, J., and Heinemeier, J. (2006). A synchronized dating of three Greenland ice cores throughout the Holocene. *Journal of Geophysical Research Atmospheres*, 111(13):1–11. 3.7

Von Rad, U., Schulz, H., Riech, V., Den Dulk, M., Berner, U., and Sirocko, F. (1999). Multiple monsoon-controlled breakdown of oxygen-minimum conditions during the past 30,000 years documented in laminated sediments off Pakistan. *Palaeogeography, Palaeoclimatology, Palaeoecology*, 152(1-2):129–161. 2.3.2

Wanner, H., Beer, J., Butikofer, J., Crowley, T. J., Cubasch, U., Fluckiger, J., Goosse, H., Grosjean, M., Joos, F., Kaplan, J. O., Kuttel, M., Muller, S. A., Prentice, I. C., Solomina, O., Stocker, T. F., Tarasov, P., Wagner, M., Widmann, M., Bütikofer, J., Crowley, T. J., Cubasch, U., Flückiger, J., Goosse, H., Grosjean, M., Joos, F., Kaplan, J. O., Küttel, M., Müller, S. a., Prentice, I. C., Solomina, O., Stocker, T. F., Tarasov, P., Wagner, M., and Widmann, M. (2008). Mid- to Late Holocene climate change: an overview. *Quaternary Science Reviews*, 27(19-20):1791–1828. 2.5.3, 6.1

Wanner, H., Solomina, O., Grosjean, M., Ritz, S. P., and Jetel, M. (2011). Structure and origin of Holocene cold events. *Quaternary Science Reviews*, 30(21-22):3109–3123. 2.5.3

Wastegård, S. (2005). Late Quaternary tephrochronology of Sweden: A review. *Quaternary International*, 130(1):49–62. 3.4, 3.4.1

Wastegård, S. and Davies, S. M. (2009). An overview of distal tephrochronology in northern Europe during the last 1000 years. *Journal of Quaternary Science*, 24(5):500–512. 3.4.1

Waters, C. N., Zalasiewicz, J., Summerhayes, C., Barnosky, A. D., Poirier, C., Ga uszka, A., Cearreta, A., Edgeworth, M., Ellis, E. C., Ellis, M., Jeandel, C., Leinfelder, R., McNeill, J. R., Richter, D. d., Steffen, W., Syvitski, J., Vidas, D., Wagreich, M., Williams, M., Zhisheng, A., Grinevald, J., Odada, E., Oreskes, N., and Wolfe, A. P. (2016). The Anthropocene is functionally and stratigraphically distinct from the Holocene. *Science*, 351(6269):aad2622–aad2622. 1.1

Weltje, G. J. and Tjallingii, R. (2008). Calibration of XRF core scanners for quantitative geochemical logging of sediment cores : Theory and application. *Earth and Planetary Science Letters*, 274:423–438. 2.3.4, 5.2

Wheeler, D., Garcia-Herrera, R., Wilkinson, C. W., and Ward, C. (2010). Atmospheric circulation and storminess derived from Royal Navy logbooks: 1685 to 1750. *Climatic Change*, 101(1):257–280. 2.5.3

Wheeler, D. and Suarez-Dominguez, J. (2006). Climatic reconstructions for the north-east Atlantic region AD 1685-1700: a new source of evidence from naval logbooks. *The Holocene*, 16(1):39–49. 2.5.3

Whiticar, M., Faber, E., and Schoell, M. (1986). Biogenic methane formation in marine and freshwater environments: CO2 reduction vs. acetate fermentation-Isotope evidence. *Geochimica et Cosmochimica Acta*, 50(5):693–709. 4.1

Whiticar, M. J. (1999). Carbon and hydrogen isotope systematics of bacterial formation and oxidation of methane. *Chemical Geology*, 161(1-3):291–314. 4.5.1

Więckowski, K. (1959). Pierwsze próby z sondą rdzeniowa do pobierania monolitów osadów dennych jezior. *Przegląd Geograficzny*, 31:361–366. 5.2

Wilson, P., McGourty, J., and Bateman, M. D. (2004). Mid- to late-Holocene coastal dune event stratigraphy for the north coast of Northern Ireland. *The Holocene*, 14(2004):406–416. 2.7

Wohlfarth, B., Blaauw, M., Davies, S. M., Andersson, M., Wastegård, S., Hormes, A., and Possnert, G. (2006). Constraining the age of Lateglacial and early Holocene pollen zones and tephra horizons in southern Sweden with Bayesian probability methods. *Journal of Quaternary Science*, 21(4):321–334. 2.4.1, 3.4.1, 3.4.1, 3.4.2, 3.7

Wulf, S., Dräger, N., Ott, F., Serb, J., Appelt, O., GuÃ°mundsdóttir, E., van den Bogaard, C., Słowiński, M., Błaszkiewicz, M., and Brauer, A. (2016). Holocene tephrostratigraphy of varved sediment records from Lakes Tiefer See (NE Germany) and Czechowskie (N Poland). *Quaternary Science Reviews*, 132:1–14. 2.3.3, 2.2, 2.4.1, 2.4.2, 2.4.2, 4.3.1

Wulf, S., Dräger, N., Ott, F., Serb, J., and Brauer, A. (2014). Findings of historical Icelandic (Askja AD 1875) tephras in varved lake records from Lake Tiefer See and Lake Czechowskie: a new potential for synchronizing the recent environmental history in NE Germany and N central Poland. *Geophysical Research Abstracts*, 16:EGU2014–9947. 3.4.2

Wulf, S., Ott, F., Słowiński, M., Noryśkiewicz, A. M., Dräger, N., Martin-Puertas, C., Czymzik, M., Neugebauer, I., Dulski, P., Bourne, A. J., Błaszkiewicz, M., and Brauer, A. (2013). Tracing the Laacher See Tephra in the varved sediment record of the Trzechowskie palaeolake in central Northern Poland. *Quaternary Science Reviews*, 76:129–139. 1.1, 2.4.1, 2.2, 3.1, 3.4.4, 3.7

Zahrer, J., Dreibrodt, S., and Brauer, A. (2013). Evidence of the North Atlantic Oscillation in varve composition and diatom assemblages from recent, annually laminated sediments of Lake Belau, northern Germany. *Journal of Paleolimnology*, 50:231–244. 2.1

Zen, E.-a. (1959). Mineralogy and Petrography of Marine Bottom Sediment Samples off the Coast of Peru and Chile. *SEPM Journal of Sedimentary Research*, Vol. 29(4):513–539. 2.4.3.1

Zielinski, G. a., Germani, M. S., Larsen, G., Baillie, M. G., Whitlow, S., Twickler, M. S., and Taylor, K. (1995). Evidence of the Eldgja (Iceland) eruption in the GISP2 Greenland ice core: relationship to eruption processes and climatic conditions in the tenth century. *The Holocene*, 5(2):129–140. 3.4

Zielinski, G. A., Mayewski, P. A., Meeker, L. D., Grönvold, K., Germani, M. S., Whitlow, S., Twickler, M. S., and Taylor, K. (1997). Volcanic aerosol records and tephrochronology of the Summit, Greenland, ice cores. *Journal of Geophysical Research: Oceans*, 102(C12):26625–26640. 3.4.1

Zillén, L., Conley, D. J., Andrén, T., Andrén, E., and Björck, S. (2008). Past occurrences of hypoxia in the Baltic Sea and the role of climate variability, environmental change and human impact. *Earth-Science Reviews*, 91(1-4):77–92. (document), 2.1, 2.7, 2.5.3, 6.1

Zillén, L. M., Wastegård, S., and Snowball, I. F. (2002). Calendar year ages of three mid-Holocene tephra layers identified in varved lake sediments in west central Sweden. *Quaternary Science Reviews*, 21(14-15):1583–1591. 2.4.2, 3.4.1

Zolitschka, B. (1990). Jahreszeitlich geschichtete Seesedimente ausgewählter Eifelmaare. *Doc. Naturae*, 60:1–226. 3.1

Zolitschka, B., Francus, P., Ojala, A. E., and Schimmelmann, A. (2015). Varves in lake sediments - a review. *Quaternary Science Reviews*, 117:1–41. 2.1

Appendix

Supplementary file Chapter 2

Supplement 1: Major element concentrations of volcanic glass shards of tephra sample TSK13_F6_150-153_T in 1115.5 cm composite depth (correlated with the Laacher See Tephra) and secondary glass standard data (Lipari obsidian).

Sample	**SiO_2**	**TiO_2**	**Al_2O_3**	**FeO_t**	**MnO**	**MgO**	**CaO**	**Na_2O**	**K_2O**	**P_2O_5**	**Total**	**Cl**
TSK13_F6_150-153_T	62.41	0.34	21.23	1.28	0.10	0.12	2.37	5.96	6.43	0.06	100.30	0.15
TSK13_F6_150-153_T	61.21	0.51	20.40	2.38	0.27	0.26	1.38	6.83	6.83	0.04	100.10	0.30
TSK13_F6_150-153_T	61.18	0.41	20.82	2.20	0.18	0.17	1.38	6.75	6.92	0.04	100.05	0.31
TSK13_F6_150-153_T	60.66	0.42	19.99	1.85	0.15	0.20	1.64	7.19	6.85	0.04	98.99	0.25
TSK13_F6_150-153_T	61.90	0.47	20.47	2.12	0.24	0.25	1.55	6.50	7.01	0.04	100.55	0.28
TSK13_F6_150-153_T	61.42	0.43	20.76	2.18	0.18	0.26	1.57	6.47	6.96	0.03	100.26	0.27
TSK13_F6_150-153_T	61.33	0.35	20.40	1.42	0.12	0.14	2.58	5.49	6.35	0.01	98.18	0.12
TSK13_F6_150-153_T	61.16	0.55	20.27	2.29	0.20	0.21	1.74	6.64	7.00	0.06	100.11	0.28
TSK13_F6_150-153_T	61.40	0.52	20.77	2.46	0.25	0.18	1.02	6.91	6.95	0.05	100.50	0.37
TSK13_F6_150-153_T	61.89	0.40	19.47	1.56	0.10	0.14	2.03	5.33	6.53	0.06	97.50	0.19
TSK13_F6_150-153_T	61.87	0.49	21.04	2.20	0.19	0.37	2.21	6.21	5.69	0.06	100.34	0.15
TSK13_F6_150-153_T	62.34	0.36	20.34	2.07	0.18	0.15	1.32	6.76	6.79	0.07	100.38	0.33
TSK13_F6_150-153_T	60.65	0.55	20.35	2.84	0.23	0.40	1.97	6.24	6.47	0.01	99.71	0.34
TSK13_F6_150-153_T	59.95	0.43	21.14	2.12	0.23	0.27	2.00	7.67	6.21	0.04	100.05	0.42
TSK13_F6_150-153_T	60.72	0.51	20.74	2.28	0.22	0.24	1.38	7.06	6.68	0.04	99.87	0.32
TSK13_F6_150-153_T	62.93	0.46	20.61	1.38	0.06	0.14	2.32	6.12	6.75	0.03	100.80	0.18
TSK13_F6_150-153_T	62.28	0.48	20.45	2.13	0.23	0.20	1.48	6.60	6.74	0.04	100.62	0.30
TSK13_F6_150-153_T	62.78	0.32	20.51	1.78	0.14	0.13	1.58	6.57	6.82	0.03	100.67	0.24
TSK13_F6_150-153_T	61.15	0.47	20.35	1.83	0.08	0.31	2.69	5.19	5.68	0.05	97.80	0.13
TSK13_F6_150-153_T	61.54	0.51	20.57	1.83	0.09	0.18	2.51	6.21	6.44	0.02	99.90	0.18
TSK13_F6_150-153_T	61.74	0.48	20.61	1.82	0.16	0.18	1.80	6.36	6.85	0.00	100.01	0.22
TSK13_F6_150-153_T	60.77	0.44	20.65	2.20	0.19	0.23	1.65	6.59	6.99	0.06	99.77	0.29
TSK13_F6_150-153_T	60.81	0.48	20.56	2.14	0.17	0.23	1.87	6.20	6.99	0.06	99.52	0.29
TSK13_F6_150-153_T	62.11	0.44	20.16	1.88	0.18	0.22	1.36	6.89	7.34	0.05	100.64	0.24
TSK13_F6_150-153_T	61.26	0.44	20.37	2.19	0.23	0.21	1.48	6.81	7.16	0.05	100.19	0.28
TSK13_F6_150-153_T	60.93	0.50	20.41	2.37	0.21	0.26	1.45	6.94	6.90	0.03	100.00	0.29
TSK13_F6_150-153_T	61.44	0.48	20.81	1.83	0.16	0.22	1.85	6.60	6.53	0.04	99.95	0.17
TSK13_F6_150-153_T	61.95	0.49	20.94	1.89	0.12	0.21	1.83	6.24	5.90	0.04	99.61	0.24
TSK13_F6_150-153_T	60.85	0.44	20.84	1.67	0.12	0.15	1.60	6.70	7.05	0.04	99.46	0.29
TSK13_F6_150-153_T	61.60	0.36	20.37	1.37	0.09	0.11	2.48	5.65	5.74	0.06	97.83	0.11
TSK13_F6_150-153_T	62.08	0.41	20.81	1.89	0.19	0.20	2.06	6.51	6.26	0.04	100.45	0.25
TSK13_F6_150-153_T	62.41	0.42	20.45	2.04	0.18	0.14	2.02	6.76	6.28	0.03	100.72	0.22
TSK13_F6_150-153_T	62.43	0.46	20.39	1.91	0.15	0.13	2.06	6.30	6.59	0.04	100.47	0.26
TSK13_F6_150-153_T	61.48	0.39	20.91	1.87	0.18	0.18	1.73	6.11	7.26	0.03	100.15	0.22
TSK13_F6_150-153_T	61.18	0.48	20.72	2.51	0.24	0.20	1.17	6.40	7.35	0.03	100.29	0.35
TSK13_F6_150-153_T	60.27	0.47	20.83	2.12	0.20	0.27	1.52	6.41	7.15	0.07	99.31	0.27
TSK13_F6_150-153_T	62.15	0.47	20.28	2.34	0.26	0.20	0.84	6.81	7.06	0.04	100.44	0.34
TSK13_F6_150-153_T	61.94	0.37	20.24	1.86	0.17	0.17	1.28	6.94	6.58	0.01	99.55	0.29
TSK13_F6_150-153_T	59.98	0.47	19.39	2.02	0.16	0.25	1.43	5.37	6.38	0.03	95.48	0.34

Lipari obsidian	**SiO_2**	**TiO_2**	**Al_2O_3**	**FeO_t**	**MnO**	**MgO**	**CaO**	**Na_2O**	**K_2O**	**P_2O_5**	**Total**	**Cl**
10 µm-beam	75.79	0.06	12.80	1.44	0.05	0.04	0.72	4.01	5.12	0.01	100.04	0.34
10 µm-beam	76.06	0.07	12.95	1.45	0.06	0.06	0.72	3.73	5.07	0.00	100.17	0.35
15 µm-beam	75.96	0.11	12.87	1.52	0.05	0.04	0.76	3.79	5.17	0.01	100.28	0.38
15 µm-beam	75.53	0.05	13.05	1.51	0.06	0.01	0.73	3.91	5.22	0.00	100.07	0.35
20 µm-beam	75.26	0.08	12.88	1.53	0.04	0.06	0.71	4.00	5.20	0.02	99.78	0.33
20 µm-beam	75.78	0.03	12.80	1.63	0.05	0.04	0.71	3.90	5.16	0.02	100.12	0.33
Hunt and Hill (1996) 12 µm-beam	74.35	n.d.	12.87	1.51	0.07	0.05	0.74	3.93	5.11	n.d.	98.63	n.d.

Lake Tiefer See

Sample:	***TSK11_K3_33-34_T***	**Glass standard:**												
Correlation:	Askja-AD1875	Lipari obsidian	**SiO_2**	**TiO_2**	**Al_2O_3**	**FeO**	**MnO**	**MgO**	**CaO**	**Na_2O**	**K_2O**	**P_2O_5**	**Cl**	**F**	**Total**
Instrument:	JEOL JXA-8230	10 µm-beam	75.14	0.04	12.99	1.41	0.07	0.02	0.73	3.91	5.24	0.00	0.34	0.04	99.94
voltage:	15 kV	20 µm-beam	74.81	0.10	12.60	1.48	0.06	0.00	0.70	3.81	5.11	0.00	0.33	0.04	99.04
beam current:	10 nA														
beam size:	8-10 µm														

Sample:	***TSK11_B1u_137-142_T***	**Glass standard:**												
Correlation:	unknown Grimsvötn	Lipari obsidian	**SiO_2**	**TiO_2**	**Al_2O_3**	**FeO**	**MnO**	**MgO**	**CaO**	**Na_2O**	**K_2O**	**P_2O_5**	**Cl**	**F**	**Total**
Instrument:	JEOL JXA-8230	10 µm-beam	75.27	0.10	12.75	1.51	0.06	0.03	0.74	3.92	4.87	0.01	0.34	0.00	99.59
voltage:	15 kV	15 µm-beam	74.78	0.07	12.73	1.51	0.10	0.04	0.72	3.95	4.94	0.00	0.33	0.00	99.17
beam current:	10 nA	20 µm-beam	74.68	0.09	12.55	1.41	0.03	0.05	0.75	3.88	4.92	0.01	0.34	0.00	98.71
beam size:	8 µm														

Sample:	***TSK11_B2o_84-85_T***	**Glass standard:**												
Correlation:	Glen Garry?	Lipari obsidian	**SiO_2**	**TiO_2**	**Al_2O_3**	**FeO**	**MnO**	**MgO**	**CaO**	**Na_2O**	**K_2O**	**P_2O_5**	**Cl**	**F**	**Total**
Instrument:	JEOL JXA-8230	5 µm-beam	74.55	0.07	13.17	1.46	0.08	0.02	0.74	3.83	5.22	0.00	0.36	0.00	99.50
voltage:	15 kV	10 µm-beam	73.94	0.04	13.05	1.51	0.08	0.05	0.72	3.61	5.26	0.00	0.34	0.07	98.66
beam current:	10 nA	15 µm-beam	74.61	0.10	13.22	1.58	0.02	0.06	0.73	3.99	5.21	0.00	0.36	0.00	99.89
beam size:	8 µm	20 µm-beam	74.41	0.09	12.99	1.51	0.06	0.03	0.73	3.79	5.15	0.00	0.38	0.00	99.14

Sample:	***TSK11_A3_120-125_T***	**Glass standard:**												
Correlation:	Hekla-4	Lipari obsidian	**SiO_2**	**TiO_2**	**Al_2O_3**	**FeO**	**MnO**	**MgO**	**CaO**	**Na_2O**	**K_2O**	**P_2O_5**	**Cl**	**F**	**Total**
Instrument:	JEOL JXA-8230	5 µm-beam	74.55	0.07	13.17	1.46	0.08	0.02	0.74	3.83	5.22	0.00	0.36	0.00	99.50
voltage:	15 kV	10 µm-beam	73.94	0.04	13.05	1.51	0.08	0.05	0.72	3.61	5.26	0.00	0.34	0.07	98.66
beam current:	10 nA	15 µm-beam	74.61	0.10	13.22	1.58	0.02	0.06	0.73	3.99	5.21	0.00	0.36	0.00	99.89
beam size:	5 µm	20 µm-beam	74.41	0.09	12.99	1.51	0.06	0.03	0.73	3.79	5.15	0.00	0.38	0.00	99.14

Sample:	***TSK13_F5_37-43_T***	**Glass standard:**												
Correlation:	Lairg-B	Lipari obsidian	**SiO_2**	**TiO_2**	**Al_2O_3**	**FeO**	**MnO**	**MgO**	**CaO**	**Na_2O**	**K_2O**	**P_2O_5**	**Cl**	**F**	**Total**
Instrument:	JEOL JXA-8230	5 µm-beam	73.46	0.08	13.27	1.42	0.08	0.05	0.64	4.01	5.19	0.00	0.35	0.00	98.55
voltage:	15 kV	10 µm-beam	73.34	0.06	13.33	1.44	0.03	0.05	0.62	4.31	5.11	0.03	0.35	0.00	98.66
beam current:	10 nA	20 µm-beam	72.79	0.09	13.16	1.39	0.11	0.05	0.57	4.39	5.02	0.00	0.38	0.00	97.95
beam size:	8 µm														

Sample:	***TSK13_F6_55_T***	**Glass standard:**												
Correlation:	Saksunarvatn	Lipari obsidian	**SiO_2**	**TiO_2**	**Al_2O_3**	**FeO**	**MnO**	**MgO**	**CaO**	**Na_2O**	**K_2O**	**P_2O_5**	**Cl**	**F**	**Total**
Instrument:	JEOL JXA-8230	10 µm-beam	76.08	0.12	12.81	1.53	0.07	0.05	0.73	3.83	5.04	0.03	0.33	0.00	100.62
voltage:	15 kV	20 µm-beam	75.36	0.07	12.64	1.48	0.08	0.03	0.76	3.96	5.24	0.00	0.33	0.03	99.98
beam current:	10 nA														
beam size:	10 µm														

Sample:	***TSK13_F6_91-92_T***	**Glass standard:**												
Correlation:	Askja-S	Lipari obsidian	**SiO_2**	**TiO_2**	**Al_2O_3**	**FeO**	**MnO**	**MgO**	**CaO**	**Na_2O**	**K_2O**	**P_2O_5**	**Cl**	**F**	**Total**
Instrument:	JEOL JXA-8230	5 µm-beam	74.14	0.10	13.04	2.03	0.11	0.03	0.71	3.80	5.12	0.00	0.31	0.00	99.39
voltage:	15 kV	10 µm-beam	74.58	0.07	13.20	1.66	0.07	0.07	0.78	3.91	5.23	0.01	0.33	0.00	99.90
beam current:	10 nA	15 µm-beam	74.81	0.09	13.02	1.55	0.03	0.02	0.74	4.10	5.30	0.02	0.37	0.00	100.06
beam size:	5 µm	20 µm-beam	74.95	0.09	13.17	1.57	0.08	0.04	0.71	3.88	5.15	0.00	0.35	0.00	99.99

Sample:	***TSK13_F6_99-100_T***	**Glass standard:**												
Correlation:	Hässeldalen	Lipari obsidian	**SiO_2**	**TiO_2**	**Al_2O_3**	**FeO**	**MnO**	**MgO**	**CaO**	**Na_2O**	**K_2O**	**P_2O_5**	**Cl**	**F**	**Total**
Instrument:	JEOL JXA-8230	10 µm-beam	76.06	0.07	12.95	1.45	0.06	0.06	0.72	3.73	5.07	0.00	0.35	0.02	100.53
voltage:	15 kV	15 µm-beam	75.96	0.11	12.87	1.52	0.05	0.04	0.76	3.79	5.17	0.01	0.38	0.00	100.66
beam current:	10 nA	20 µm-beam	75.78	0.03	12.80	1.63	0.05	0.04	0.71	3.90	5.16	0.02	0.33	0.00	100.45
beam size:	8 µm														

Lake Czechowskie

Sample:	***JC12_K2_35-36_T***	**Glass standard:**												
Correlation:	Askja-AD1875	Lipari obsidian	**SiO_2**	**TiO_2**	**Al_2O_3**	**FeO**	**MnO**	**MgO**	**CaO**	**Na_2O**	**K_2O**	**P_2O_5**	**Cl**	**F**	**Total**
Instrument:	JEOL JXA-8230	10 µm-beam	76.06	0.07	12.95	1.45	0.06	0.06	0.72	3.73	5.07	0.00	0.35	0.02	100.53
voltage:	15 kV	15 µm-beam	75.96	0.11	12.87	1.52	0.05	0.04	0.76	3.79	5.17	0.01	0.38	0.00	100.66
beam current:	10 nA	20 µm-beam	75.78	0.03	12.80	1.63	0.05	0.04	0.71	3.90	5.16	0.02	0.33	0.00	100.45
beam size:	8 µm														

Sample:	***JC09_B2_155-158_T***	**Glass standard:**												
	JC09_B2_170-173_T	Lipari obsidian	**SiO_2**	**TiO_2**	**Al_2O_3**	**FeO**	**MnO**	**MgO**	**CaO**	**Na_2O**	**K_2O**	**P_2O_5**	**Cl**	**F**	**Total**
Correlation:	?	5 µm-beam	73.46	0.08	13.27	1.42	0.08	0.05	0.64	4.01	5.19	0.00	0.35	0.00	98.55
Instrument:	JEOL JXA-8230	10 µm-beam	73.34	0.06	13.33	1.44	0.03	0.05	0.62	4.31	5.11	0.03	0.35	0.00	98.66
voltage:	15 kV	20 µm-beam	72.79	0.09	13.16	1.39	0.11	0.05	0.57	4.39	5.02	0.00	0.38	0.00	97.95
beam current:	10 nA														
beam size:	8 µm														

Sample:	***JC12_D6_95-95.5_T***	**Glass standard:**												
Correlation:	Askja-S	Lipari obsidian	**SiO_2**	**TiO_2**	**Al_2O_3**	**FeO**	**MnO**	**MgO**	**CaO**	**Na_2O**	**K_2O**	**P_2O_5**	**Cl**	**F**	**Total**
Instrument:	JEOL JXA-8230	10 µm-beam	73.61	0.09	12.87	1.55	0.06	0.03	0.71	4.02	5.22	0.02	0.37	0.00	98.55
voltage:	15 kV	15 µm-beam	73.53	0.10	12.85	1.61	0.11	0.02	0.72	4.06	5.30	0.00	0.37	0.00	98.66
beam current:	10 nA	20 µm-beam	73.56	0.05	12.78	1.49	0.11	0.05	0.72	4.01	5.26	0.00	0.34	0.00	98.36
beam size:	5-8 µm														

Sample:	***JC12_D6_112-113_T***	**Glass standard:**												
Correlation:	Hässeldalen	Lipari obsidian	**SiO_2**	**TiO_2**	**Al_2O_3**	**FeO**	**MnO**	**MgO**	**CaO**	**Na_2O**	**K_2O**	**P_2O_5**	**Cl**	**F**	**Total**
Instrument:	JEOL JXA-8230	5 µm-beam	74.14	0.10	13.04	2.03	0.11	0.03	0.71	3.80	5.12	0.00	0.31	0.00	99.39
voltage:	15 kV	10 µm-beam	74.58	0.07	13.20	1.66	0.07	0.07	0.78	3.91	5.23	0.01	0.33	0.00	99.90
beam current:	10 nA	15 µm-beam	74.81	0.09	13.02	1.55	0.03	0.02	0.74	4.10	5.30	0.02	0.37	0.00	100.06
beam size:	5 µm	20 µm-beam	74.95	0.09	13.17	1.57	0.08	0.04	0.71	3.88	5.15	0.00	0.35	0.00	99.99

Content of Data CD

thesis.pdf: pdf-file of this doctoral thesis
chapter2.pdf: Data related to Chapter 2
chapter4.pdf: Data related to Chapter 4
chapter5.pdf: Data related to Chapter 5
CV.pdf: curriculum vitae
publication.pdf: list of publications